Development of Biomaterials from Sustainably Produced Macroalgae Feedstocks

A thesis

submitted in fulfilment

of the requirements for the degree

of

Doctor of Philosophy in Chemistry

at

The University of Waikato

by

Nethmie Jayasooriya

THE UNIVERSITY OF
WAIKATO
Te Whare Wānanga o Waikato

2024

Preface

The thesis consists of four chapters, with Chapter 2 already been published in the Journal of Bioresource Technology, Chapter 3 under review in a peer-reviewed journal and 4 is being prepared for peer-review. I conducted the research, laboratory work, data analysis, and writing unless otherwise referenced or acknowledged.

Abstract

Upgrading and maintaining large-scale wastewater treatment plants (WWTPs) is notably expensive, particularly in rural areas of New Zealand. Freshwater macroalgae ponds may offer a cost-effective alternative for wastewater treatment in these areas. These ponds produce significant amounts of residual macroalgae biomass as a by-product of the bioremediation process, which is nutrient-rich and contains valuable biopolymers like cellulose. Utilizing this residual biomass as a substrate for high-value cellulose production is yet to be demonstrated. Therefore, this thesis investigated the potential of utilizing this residual freshwater macroalgae biomass to develop bioproducts (cellulose and biostimulants) aligning with the principles of a circular economy and waste recovery.

The first chapter investigated the dual extraction process of biostimulants and high-purity cellulose from *Oedogonium calcareum* grown in primary effluent. It introduces an economical and effective extraction method utilizing a hot alkali, which also provides disinfection, ensuring that the biomass is free from pathogens, making it safe for further use. The biostimulant extract was found to be comprised of several plant-promoting substances. Subsequently, the residual biomass was used to extract cellulose, and the quality of this Oedogonium-derived cellulose was assessed to determine its characteristics for potential future use in biocomposites.

In the second chapter, a comparative analysis was conducted on cellulose extracted from four macroalgae species, namely *Rhizoclonium sp*., *Zygnema sp.*, *Oedogonium sp.*, and *Stigeoclonium sp*. This research filled a significant gap by providing a detailed characterization of cellulose derived from freshwater macroalgae, which has been less studied compared to cellulose from marine macroalgae. This chapter makes a significant contribution by fully characterizing the physicochemical properties of freshwater macroalgae cellulose, which as a by-product of wastewater treatment, provides an alternative and sustainable source of cellulose with potential future applications in biocomposites.

The final chapter details the development of biocomposite films using poly(3-hydroxybutyrate-co-3-hydroxyvalerate) (PHBV) reinforced with cellulose nanofibers derived from a naturally co-existing mixed algae culture of *Cladophora sp.* and

Rhizoclonium sp. The production and characterization of 2,2,6,6-tetramethyl-1-piperidinyloxy (TEMPO)-oxidized Cellulose NanoFibre (CNF) from these macroalgae was accessed. Additionally, PHBV polymer biocomposite films incorporating either commercially available plant-derived CNF, unmodified algae cellulose, or TEMPO-oxidized CNF were compared. The films were comprehensively characterized, with a focus on their mechanical and thermal properties. The results demonstrated the potential of these biocomposite films for use in applications such as packaging materials, highlighting their environmental and functional benefits.

Overall, this thesis demonstrates significant advancements in the utilization of algae grown in wastewater for the successful extraction of bioproducts. It investigated the efficient recovery and application of macroalgae-derived cellulose and also highlighted the potential of these bio-based materials in enhancing the properties of the PHBV polymer, thus contributing to the development of sustainable biocomposite materials.

Acknowledgements

After spending nearly four years at the University of Waikato pursuing my PhD, I write this with a heart full of emotions and gratitude. This journey has been one of growth, perseverance, and unforgettable memories. It is the people who stood by me that turned this into a rewarding experience, and I want to take this moment to thank them for making my PhD a success.

The past four years were filled with bittersweet moments, and as I look back, I feel deeply grateful for the amazing people I met along the way. To me, what matters most is being a wonderful human being above all while excelling at what you do, and I feel fortunate to have been surrounded by such individuals. While I could write an entire book about them, I will try to keep this brief.

First, I would like to express my deepest gratitude to my supervisors, without whom this achievement would not have been possible. To my chief supervisor, Prof. Christopher Battershill, thank you for your support, expertise, and motivation. I feel incredibly fortunate to have worked with such a respected scholar and a true superstar in academia. Thank you for showing me what it means to be a great professor worth the title- someone who inspires students! Your kindness, attentiveness, and positivity are qualities I want to carry forward in my own life. I want to thank Dr. Rupert Craggs for his immense support throughout my PhD journey. I feel deeply honoured to have worked with such a highly respected and an esteemed scientist in the field. Your expertise and your great character make you a role model for me to follow in my life. As a scientist, you inspired me to be someone like you. I enjoyed all our conversations and always walked away feeling like I had learned so much from you. Thank you for your constant inspiration and motivation, and for being such a wonderful human being! I want to thank Dr. Chanelle Gavin for her immense support in my work. It was such a pleasure working with you, and I really enjoyed our brainstorming sessions together. You were more like a supportive friend—kind, approachable, and always willing to help. I feel so happy and lucky to have worked with such a talented and wonderful academic like you! Finally, I want to thank Dr. Christian Gauss for his guidance and immense support for my work, always being just one email away. Thank you for all your valuable insights, encouragement, and motivation throughout my research. You were so generous with your resources, knowledge, and time, and your passion for science was truly inspiring. I feel incredibly fortunate to have worked with such a great scientist like you!

I want to thank MBIE and NIWA for funding this research and the University of Waikato for the opportunity to conduct my research.

I would also like to thank the Waikato University staff. I thank A. Prof. Marie Magnusson for her valuable insights and support during the first two chapters of my thesis. To Dr. Ari Banderburg, your support during my experiments and our fun conversations in the lab made the experience memorable. Also, thank you for being a good friend during stressful times. I also want to thank research technician Dr. Sophia Rodrigues for her support at the materials science lab in the chemical engineering department. Thank you for training me on the instruments and your support throughout my experiments.

A big thank you to Helen Turner for her support and for taking the time to train me on the SEM, and to Dr. Stella Raynova for training me on TGA. I'm also grateful to lab manager Elizabeth for accommodating me in her lab space for composite preparation and for all her moral support during the last chapters of my thesis. I want to thank former librarian Cheryl Ward for her help as well.

I also want to extend my thanks to the science admin Soli Weiss, for promptly arranging travel and accommodation for my research making life so easier. I want to thank technicians Peter, Chris

and other technicians from the Environmental Research Institute-TGA, as well as the technicians from NIWA-Hamilton for their hard work in providing my algae on time.

I want to extend my huge thanks to Prof Joanne Ellis for helping me out in my PhD concerns and making necessary arrangements to accompany that. I feel grateful for the help I received both from Joanne and Prof Michael Mucalo who helped me continue my PhD.

These dedicated and passionate academics and technicians made my work so much easier, and I am very thankful for their support.

That one thing I was absolutely happy about was getting to know this amazing bunch of my friends at the Uni. I want to thank my two close friends Indi and Harizah, for being beside me, being a huge part of my PhD! Without the two of you, I don't think I would have made it without burning out. Thank you both, for being such amazing supportive friends for life. I also want to thank my very first friend I made here at the uni- Roby. Thank you for your love and support and making me feel at home! Thank you, my dearest friend Jacob, for being such a nice friend that I could always lean on! I will forever remember our game nights and all the fun stuff we did together. Thank you, Alisa and Holly, for sticking with me till the end, we started together and finished together! I am so happy to meet such a wonderful bunch- Emma, Zoe, Beth, Aliesha, Natalie and Tim - you guys made my stint at the uni so worthwhile. Those times and memories we had together will last for a lifetime and I thank you for making my life happy.

And my best friends living thousands of miles apart-my best friend Hasangi, for always being so proud of me and cheering for my achievements since we were 10. Thank you for reminding me of the reasons to keep up and do my best! Thank you Dulanji for all the science talks and making me laugh when I felt down. And I want to thank all my friends (list is too long!) who helped me directly or indirectly encouraging me to do well.

Lastly, I want to thank my loving family! My amazing parents-without whom I won't be here achieving all these. I feel the luckiest and am forever grateful for my parent’s unconditional love and support and also for putting mine and my sister’s education first. Thank you for always supporting me financially and sacrificing so much in your life just to see us happy and successful. I want to thank my amazing sister who has been my cheer leader since birth! I am the luckiest to have you in my life and your love keeps me going! I want to thank my parents-in-law and brother-in-law for their love and support. Last but not least, I want to thank my amazing husband who has been my pillar- encouraging me to be the best version of myself! I can't think of someone else who would sacrifice so much just to support me. What would I have done without you? I feel the luckiest to have you in my life!

Thank you, everyone, so much! I apologize if I missed mentioning anyone here, but I am sending good vibes your way for the littlest thing you did to help me.

Table of Contents

List of Figures

List of Tables

List of Equations

Chapter 1
General Introduction

This thesis, titled "Development of Biomaterials from Sustainably Produced Macroalgae Feedstocks," investigates novel methods of residual wastewater-grown algae biomass utilisation to advance sustainable bio-based material development. As environmental sustainability and efficient resource use become increasingly imperative, the application of bioremediation processes aids in effective wastewater management while providing a renewable source of raw materials for various applications. This introductory section lays the foundation for a detailed study of current challenges and advancements in wastewater treatment, highlighting the role of bioremediation in generating valuable biomass feedstocks. This section further explores the potential of cellulose, particularly focusing on its chemistry, alternative sources such as macroalgal cellulose, and the development and application of nanocellulose. This approach aligns the broad objectives of this thesis with specific research initiatives aimed at advancing sustainable material sciences.

1.1 Bioremediation of municipal wastewater in New Zealand

In urbanized countries worldwide, 265 L of municipal wastewater is produced daily per capita and it is estimated that approximately 60% of municipal wastewater is released untreated into streams, lakes, coastal waters, and rivers (La Barre et al. 2018; Neveux et al. 2016; Warwick et al. 2013). In New Zealand untreated domestic wastewater has highly variable concentrations of organic and inorganic materials: total solids range from 50-800 mg/L; dissolved organic matter elicits biochemical oxygen demand/ BOD_5 ranging from 150-450 mg/L; microorganisms range from 10^4 - 10^5/ 100 mL; nutrients such as nitrogen foe example total N concentration ranges from 7-60 mg/L, and phosphorus (total P) ranges from 3.3-13 mg/L; not to mention large variations in types and concentrations of heavy metals, fats, and oils (Ray 2002). World health organization (WHO) concentration values for the nitrogen and phosphorus content of municipal wastewater are generally in a similar but slightly higher range from 20-85 mgN/L and 5-20 mgP/L, respectively. The large New Zealand agriculture sector (NZ$12.4bn; 7% GDP; 2018) is putting increased risk of eutrophication on adjacent aquatic ecosystems. Therefore, there is an increased

demand for management tools to protect aquatic ecosystems including riparian zone protection and reestablishment, reduced agricultural fertiliser use, and upgrading wastewater treatment plants (Prepas and Charette 2003).

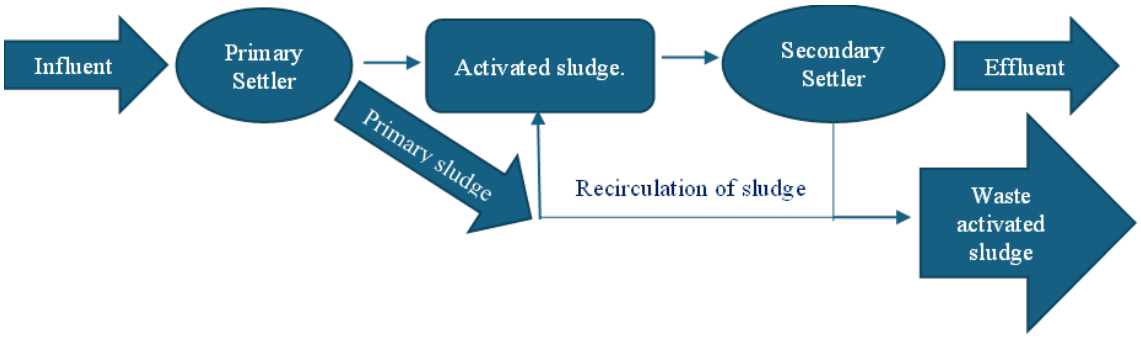

Figure 1.1 : Typical schematic of the core treatment steps in a municipal WWTP.

The general process for wastewater treatment plants (WWTP) includes combinations of physical, biological, and chemical treatments, which can be divided into primary and secondary, and tertiary treatment processes (Figure 1.1) (Segneanu et al. 2013). Small WWTPs typically have fewer treatment steps (i.e. only a primary and secondary treatment) (Environment 2017). Moreover, many NZ WWTPs are now at or over capacity and need significant upgrades to improve effluent quality to meet the national policy statement for freshwater (NPS-FM) (Ray 2002) (NZ government). WWTPs may be upgraded to include combinations of biological treatment with filtration (e.g. membrane bioreactors) and chemical oxidation processes (Rajasulochana and Preethy 2016). However, implementation of these technologies in small to medium-scale WWTPs is costly (Department of Internal Affairs 2018; Environment 2017). For example, the cost of upgrading small-sized WWTPs has been estimated to be $1.19-1.79 million per capita) which is an order of magnitude higher than for medium plants ($0.0144-0.11million per capita) and large plants ($0.018-0.226 million per capita). Therefore, alternative upgrade options for small-sized WWTPs are required to meet current and future effluent guidelines.

Table 1. 1: Relative cost for upgrading WWTPs to meet currently proposed water quality standards (New et al., 2017)

Scale	Population served	Cost to upgrade in ($NZ million)	Relative cost per capita ($NZ million)
Small	less than 501 people	600-900	1.19-1.79
Moderate	5000-10000 people	720-1100	0.0144-0.11
Large	More than 10,000 people	180-260	0.018-0.226
Total cost		1500-2260	-

Bioremediation is the removal of contaminants (i.e. nutrients and heavy metals) using living organisms such as bacteria, algae, and aquatic plants. It provides an alternative option to upgrade WWTPs particularly for nutrient removal and recovery. Bioremediation can be added onto existing systems with relatively small expense, and targeted species selection can allow the cultivation of a valuable biomass using effluent nutrients. One example of bioremediation is at the Rotorua WWTP which includes the irrigation of *Pinus radiata* plantation to scrub excess nutrients from its effluent prior to entering the waterways. However, this approach has had a number of limitations, including product quality issues, specifically affecting the timber quality reducing its commercial value, a large footprint, and is not suitable for many NZ WWTPs. Another approach is the cut and dry farming system where crops are grown using wastewater, frequently cropped and removed in bulk from the site (e.g. cut and carry farming operation in Taupo, New Zealand) (Sunich 2016). This guarantees nutrient removal from water. However, the main drawback is that this method needs large amounts of wastewater irrigated to the land which will eventually alter the salinity and alkalinity of the soil environment (Laurenson et al. 2007). Phycoremediation using intensive cultivation of macroalgae is a novel alternative. Cultivation of macroalgae in the wastewater removes nutrients in the form of algal biomass and these nutrients are therefore removed from the wastewater upon the harvest of the biomass. Regardless of the targeted biomass produced, its production aids in the recovery and reuse of nutrients and aligns with Aotearoa NZ policy to move to a more circular bio-economy (Environment 2017).

The primary focus for species selection for phycoremediation is maximising nutrient removal and biomass productivity under the targeted cultivation conditions (Neveux et al. 2016). A secondary consideration is given to the value-added products that can be developed from the biomass produced. Assuming a similar performance in the primary

function of phycoremediation (i.e. bioremediation), species selection can be deferred to favourable biomass quality for the development of products of higher value. The latter can further aid in offsetting the cost of implementation and operation of phycoremediation infrastructure. Furthermore, macroalgae are well suited to processing in cascading biorefineries that target multiple products from a single batch of biomass adding further value to the implementation of phycoremediation technologies (Lawton et al. 2013).

1.2 Biorefinery Processing and macroalgal products

The biorefinery concept integrates thermochemical, biochemical, and microbial processes in order to produce bio-products such as fuels, materials, chemicals, supplements, and plant biostimulants and fertilizers (Lawton et al. 2017; Ubando et al. 2020). Broadly, biorefineries target value-added products from a range of biomasses including lignocellulosic material, algal biomass, together with food and animal waste products (Ubando et al. 2020). Relevant to the current study, an increasing number of biorefinery processes targeting products from macroalgal biomass grown in the bioremediation of wastewater have been developed (Khammee et al. 2020; Magnusson et al. 2016; Neveux et al. 2013; Postma et al. 2018). These products include biofuels, biostimulants, animal feed, bio sorbents, and soil ameliorants (Table 1. 2) (Foley et al. 2011; Lawton et al. 2017). However, product potential from biomass produced in the bioremediation of municipal wastewater may be limited due to potential contaminants and/or public perception, where socially acceptable products include agricultural products (e.g. biostimulants, animal feeds, and biochar) and highly processed industrial products (e.g. biofuel, biochemicals, and materials).

Table 1. 2: Examples of macroalgal biorefinery products

Species	**Aquatic environment**	**Biorefinery products**	**References**
Ulva lactuca	Marine	Proteins and carbohydrates	(Postma et al. 2018)

U. ohnoi	Marine	Salt, pigment, ulvan, and protein	(Glasson et al. 2017; Magnusson et al. 2016)
Kappaphycus alvarezii	Marine	Carrageenan, pigments and ethanol	(Masarin et al. 2016)
Cladophora	Freshwater and Marine	Plant biostimulants, Chlorophyll and carotenoids	(Zollmann et al. 2019)
Spirogyra	Freshwater	Biofuel	(Eshaq et al. 2010; Ge et al. 2018)
Oedogonium	Freshwater	Biostimulants, biosorbents,	(Neveux et al. 2020)
Rhizoclonium	Freshwater	Bioethanol	(Khammee et al. 2020)

Due to differences in the physicochemical properties of the different types of biomolecules (e.g. salts, small molecules, pigments, polysaccharides, and proteins), and the relatively simple structure (e.g. lack of lignin) of macroalgal biomass compared to many terrestrial plant-based materials, fractionation of their biomolecules can often be achieved using mild extraction conditions. This is an advantage for cascading biorefinery schemes that target multiple products (Error! Reference source not found.) sequentially as the quality of the residual biomass is retained. Pertinent to the work presented in this thesis, there are a number of recent examples illustrating the production of high-value nanocellulose products and composites from residual biomass from the phycocolloid industry (Trivedi et al. 2016). However, to date, there is no information on cascading use in freshwater macroalgae and the potential to further valorise freshwater macroalgal biomass produced in the bioremediation of municipal wastewater to promote this bioremediation strategy. Therefore, the research presented here aims to develop socially acceptable products derived from biomass cultivated in the bioremediation of wastewater and to specifically characterise the physicochemical properties of freshwater macroalgae cellulose, and its potential for use in cellulose-based bio composites. Opportunities are examined below.

Table 1. 3: Percentage composition of macroalgae chemical constituents (Biris-Dorhoi et al., 2020)

Chemical constituent	Composition
Carbohydrates	Up to 60%
proteins	10%–47%
lipids	1%–3%
Minerals	7%–38%

1.3 Cellulose

Over the past few years, the development of sustainable structural materials based on naturally sourced nanomaterial building blocks (sized between 1-100 nm, e.g. nanocelluloses) (Huang et al. 2018) has become an attractive subject in the field of renewable material science due to their physicochemical and mechanical properties (Malmir et al. 2017). Modification of the nanomaterial also allows the possibility for fine-tuning bulk properties of the macroscale materials, such as composites. Composites combine two or more constituents of unique properties to obtain a distinct product (Bhong et al. 2023). For example, carbon fibre-reinforced plastics combine a reinforcement (i.e. carbon fibre is woven into fabric) with a polymer matrix material (resin) to strengthen and improve the bulk properties of the composite material (Koyanagi and Sato 2019). Recently there has been increasing interest in using cellulose in advanced materials such as hydrogels, aerogels, and biodegradable electronics (Kontturi, Laaksonen et al. 2018, Rahmanian, Pirzada et al. 2021, Zhao, Zhu et al. 2021). For instance, hydrogels reinforced with nanocellulose exhibit enhanced strength to external stimuli, making them ideal for 3D bioprinting and biomedical applications, such as tissue engineering and drug delivery systems (John and Zhong 2019). Moreover, cellulose-based aerogels demonstrate high thermal insulation, lightweight, and high porosity characteristics (Gupta, Singh et al. 2018). These aerogels have been used in thermal insulation, packaging, and absorbent materials for environmental cleanup (Lebedev, Suslova et al. 2021). Additionally, nanocellulose has proven to be an excellent substrate for flexible electronics due to their mechanical strength and flexibility. The development of nanocellulose-based composites with conductive metal nanoparticles has recently paved the way for printable, biodegradable electronics (Zhao, Zhu et al. 2021).

1.3.1 Cellulose structure and chemistry

Cellulose is the most abundant biomaterial available on earth and the main component in parenchyma cells in terrestrial plants. Cellulose can be derived from many sources such as terrestrial plants (both hardwood and softwood), bacteria, algae, fungi, and tunicates (Moon et al. 2011).

Cellulose is a semi-crystalline polymer, i.e., the polymer contains both amorphous and crystalline regions (Figure 1. 2). The crystalline region is retained by highly ordered intramolecular hydrogen bonds and Van der Waals interactions between cellulose chains and its tight packing prevents incursion of even the smallest molecules (including acids and bases) that contribute to its hydrolysis (Quiroz-Castañeda and Folch-Mallol 2013). The amorphous region is less tightly packed and more susceptible to hydrolysis by acids, bases, and enzymes (Habibi et al. 2010). This differentiation in the reactivity of amorphous and crystalline regions toward hydrolysis is important as it allows a level of control over the preparation and development of nanocellulose products.

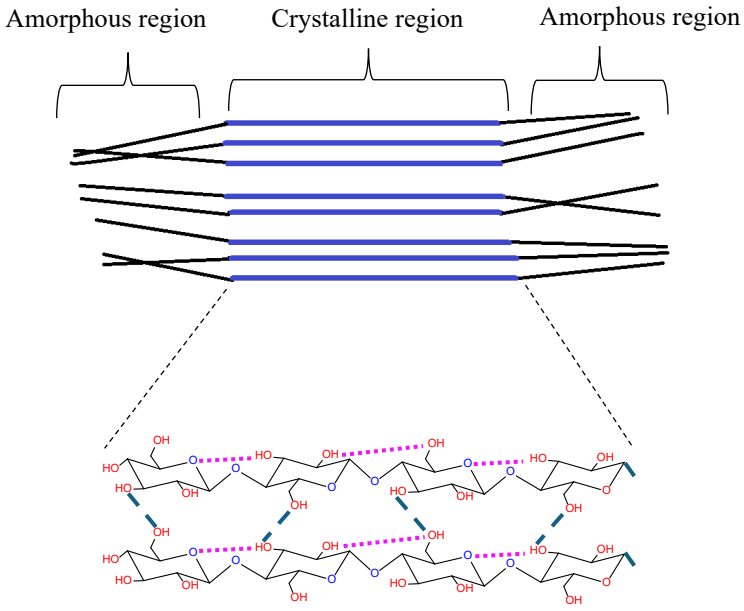

Figure 1. 2: Crystalline and amorphous regions of cellulose. The crystalline structure is retained by the hydrogen bonds and Van der Waals interactions.

The structure of cellulose (Figure 1.3) can be described in three levels; molecular, supramolecular, and morphological (Börjesson and Westman 2015). In this configuration, each β-glucose unit $(C_6H_{12}O_6)_n$; where n ranges from 10,000-15000 depending on the source) has three free hydroxyl (OH) groups. Two of the hydroxyl groups at the C2 and C3 positions are secondary alcohols while the OH group at C6 is a primary alcohol. At the surface of cellulose fibres, these three hydroxyl groups are potential sites for modification, while in the bulk of the cellulose fibres, the C2, C3, and C6 hydroxyls drive the molecular arrangement of β-glucose units within the crystalline regions of the cellulose fibres. For example, intramolecular hydrogen bonds between the O3-H group and the O5 ring oxygen of the adjacent glucopyranose unit are at 180° to each other (Figure 1. 3). The degree of polymerization (Khalil et al.) is determined by the number of cellobiose units present and ranges from 10,000 up to 40,000 *in vivo* depending on the source of cellulose, and ranges from 300 to 1700 after the purification and chemical modification processes used in its isolation (Börjesson and Westman 2015).

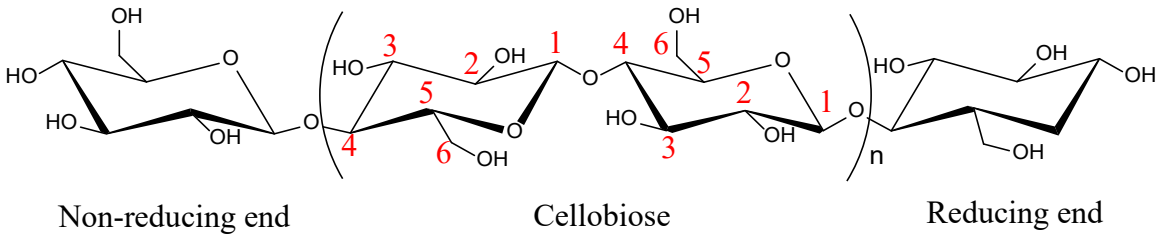

Figure 1. 3: Chemical structure of cellulose showing the non-reducing end, cellobiose unit and the reducing unit.

The supramolecular structure of cellulose varies depending on the source and the method of isolation (Peciulyte et al. 2015). While there are subtle variations between cellulose types, intramolecular (O3—H---O5; O6—H---O2) (Figure 1.4) and intermolecular (O6—H---O3) hydrogen bonding formed between free hydroxyl groups and H-acceptors govern the crystal structure and its stability (Börjesson and Westman 2015). At the morphological level, the functionality or the stiffness of the cellulose polymer is raised due to the intramolecular hydrogen bonds. Intermolecular hydrogen bonds are responsible for forming two-dimensional sheet structures and Van der Waal interactions hold these sheets together giving rise to the three-dimensional structure of cellulose fibrils. These tightly

packed cellulose fibrils within the cell wall provide strength and mechanical resistance to the outer forces of the cell membrane (Tarchevsky and Marchenko 1991).

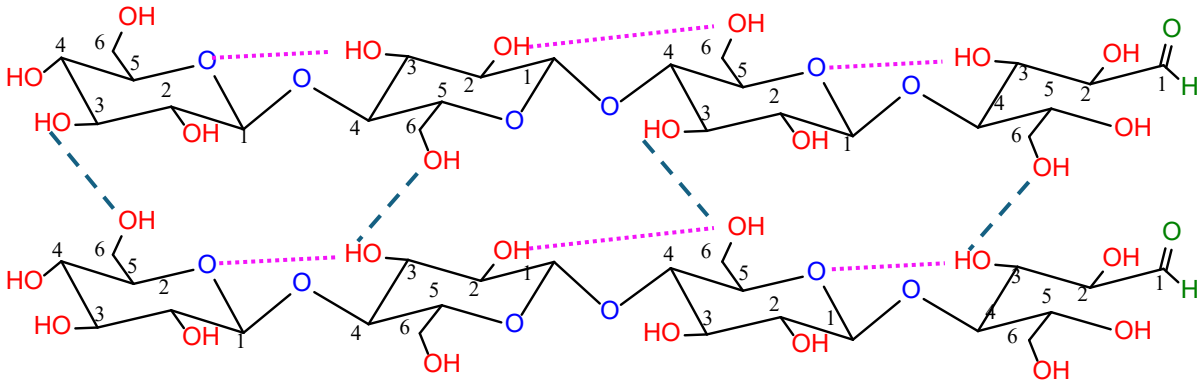

Figure 1. 4: Intramolecular hydrogen-bonding network in cellulose polymer.

1.3.1.1 Classification of Cellulose

Subtle variations in the crystalline structure of cellulose have been identified using X-ray diffraction and solid-state 13C NMR (nuclear magnetic resonance) experiments (Quiroz-Castañeda and Folch-Mallol 2013). These variations result from differences in the hydrogen-bonding network leading to changes in the molecular orientations and material properties. Thus, cellulose is described as exhibiting polymorphism with four different allomorphs being so far identified, including cellulose I, II, III and, IV. Figure 1. 5 shows the relationship between the cellulose polymorphs and their source (Henriksson and Lennholm 2009).

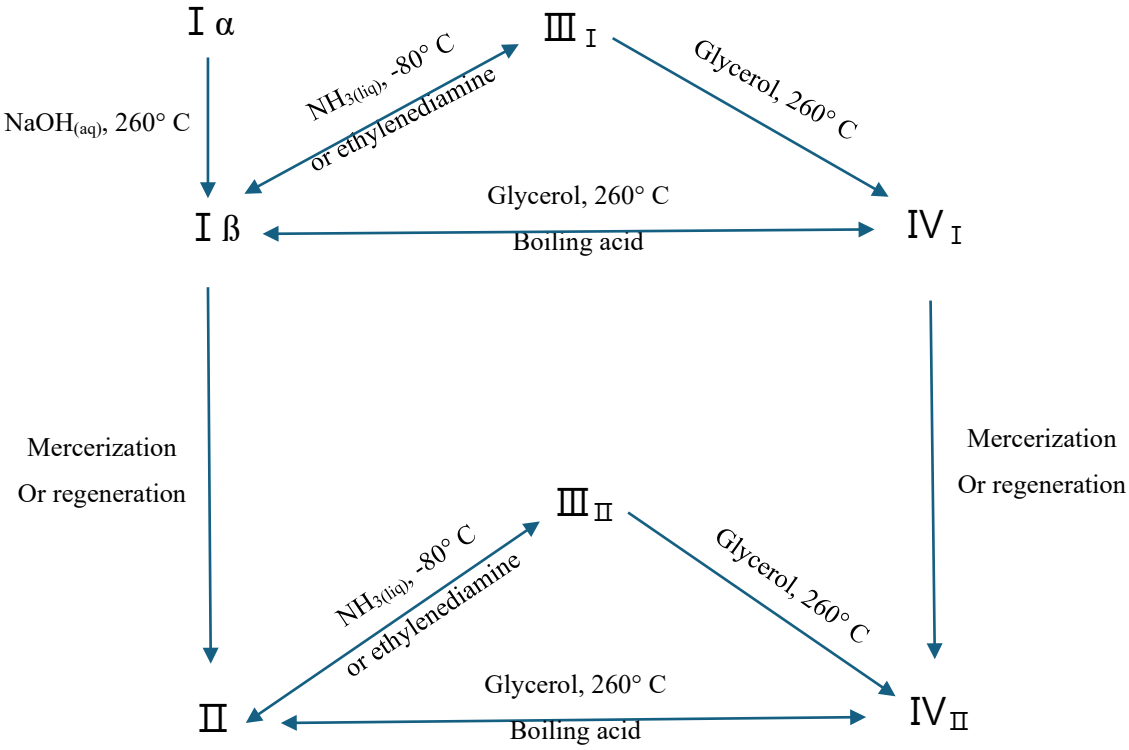

Figure 1. 5: Relationship between different polymorphs of cellulose.

1.3.1.2 Cellulose Ⅰ

Cellulose I, or native cellulose, is the most abundant form of cellulose and the naturally occurring form of cellulose. Structural analysis using cross-polarization magic angle spinning technique (CP-MAS) and X-ray crystallography indicate that cellulose I occurs as two allomorphs; Iα and Iβ. Cellulose Iβ is predominantly found in terrestrial plants and tunicates whereas cellulose Iα is predominant in algae and bacteria (Moon et al. 2011). However, the sources are often mixtures and the ratio of the allomorphs I_α and I_β vary depending on the source of cellulose (Moon et al. 2011). For example, ^{13}C NMR studies of the freshwater macroalgal species *Glaucocytstis* indicate it contains 90% of Iα (Imai et al. 1999) whereas, *Cladophora* species contains 80% of I_α (Wada and Okano 2001).

The crystalline structures of Iα and Iβ vary according to the hydrogen bonding network although both Iα and Iβ chains exist in parallel configurations. In both Iα and Iβ allomorphs, cellulose layers are piled up in parallel to each other while the C6-hydroxyl groups are aligned in tg configuration (Figure 1. 6) (Gong et al. 2017; Habibi et al. 2010).

This orientation ensures the intramolecular hydrogen bonding between the C6-OH and the adjacent C2-OH group (Figure 1. 6).

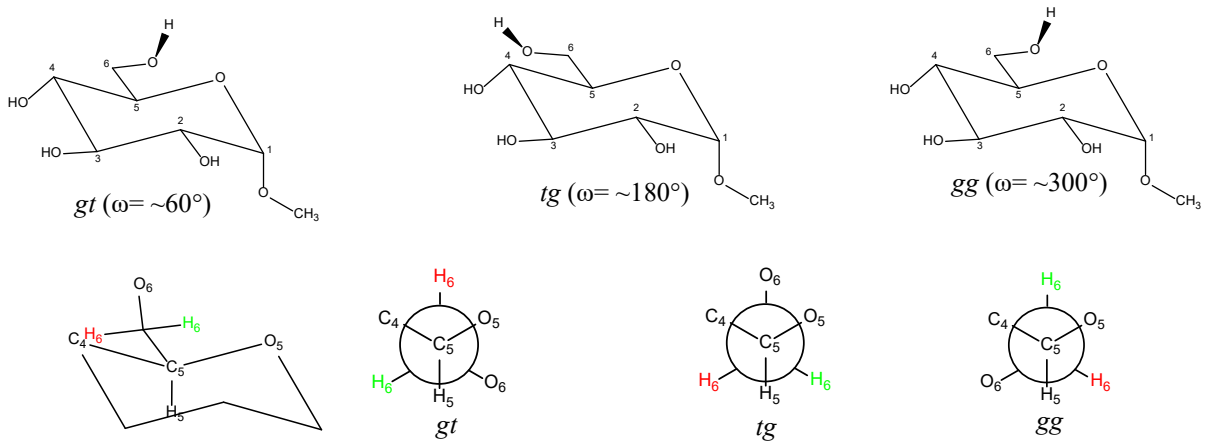

Figure 1. 6: The three probable rotations of hydroxyl group. Image adopted from (Habibi et al., 2010)

The differences between cellulose I_α and I_β give rise to differences in the X-ray crystallographic data with Iα having a triclinic *P*1 unit cell (a = 6.717 Å, b= 5.962 Å, c = 10.400 Å, α= 118.08°, ß = 114.80°, and γ = 80.37°) while I_β has a monoclinic $P2_1$ unit cell (a = 7.784 Å, b= 8.201 Å, c = 10.38 Å, α= ß = 90° and γ = 96.5°) with two cellulose chains (Habibi et al. 2010). Figure 1. 7 demonstrates polymer alignment of monoclinic and triclinic forms of cellulose and the packing of cellulose chains within the monoclinic and triclinic unit cell.

Previous research shows that I_α has high thermal stability (metastable) (Horikawa and Sugiyama 2009) inhibiting the complete conversion of I_α to I_β (Moon et al. 2011). However, partial conversion of cellulose I_α to I_β can be achieved by hydrothermal treatment of I_α at high temperatures (260°C) in NaOH or organic solvents (e.g. glycerol, ethanol or acetone (Figure 5)) (Horikawa and Sugiyama 2009; Moon et al. 2011). Thermal conversion of cellulose I_α to I_β in an inert gas such as helium is also possible (Moon et al. 2011; Wada et al. 2003). It has also been demonstrated that conversion of cellulose I_α to I_β can be achieved with acid-treatments at high temperatures with treatment duration influencing the degree of conversion (Wada et al. 2003). For example, treatment of cellulose (~80% cellulose I_α) isolated from *Cladophora* species with 60% sulfuric acid reduced the content of cellulose I_α to 60% and 40% after 24 and 48 hours at 100°C, respectively (Wada and Okano 2001). The latter point is important in terms of processing

conditions used to prepare nanocellulose products. In this regard, the I_α form is more easily degraded by enzymatic reactions than I_β giving the capacity to use more sustainable processing tools than strong acids for preparing nanocellulose products (Horikawa and Sugiyama 2009).

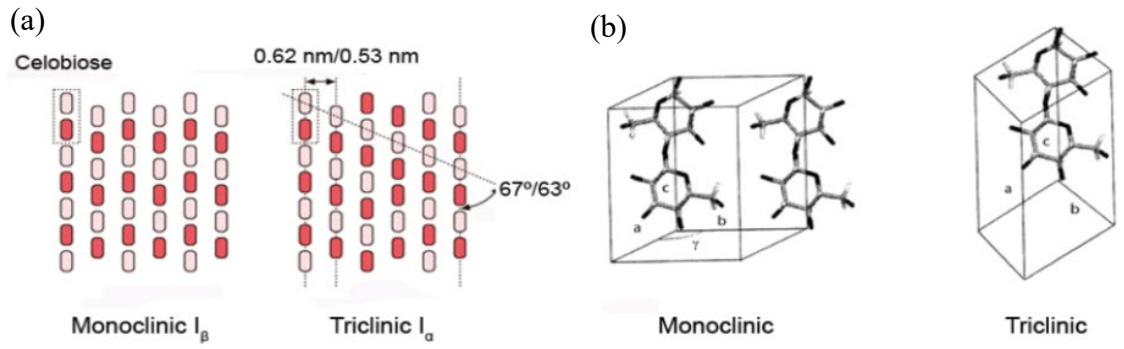

Figure 1. 7: (a) Monoclinic and triclinic forms of cellulose. (b) Mode of cellulose chains packing in monoclinic and triclinic forms. Image from (Quiroz-Castañeda & Folch-Mallol, 2013)

1.3.1.3 Cellulose II

Cellulose II occurs rarely in nature (Habibi et al. 2010) and is mainly prepared from cellulose I. Compared to cellulose I, extracted cellulose II has increased transparency, higher affinity for dyes, and higher tensile strength (Gautam et al. 2010; Habibi et al. 2010). These characteristics are beneficial for applications in textile and materials technologies where consistent product characteristics are important. For example, cellulose II (regenerated cellulose) including viscose and lyocell, is known for its softness, moisture absorption, and breathability, for producing comfortable and breathable garments (Periyasamy and Militky 2020). Moreover, cellulose II is used for the preparation of composite materials such as aerogels, targeting applications in pharmaceutical, bio-medical, and food technologies (Zugenmaier 2008).

The crystal structure of cellulose II has a change in unit cell to the monoclinic $P2_1$ form (a = 8.10 Å, b= 9.03 Å, c = 10.31 Å, α= β = 90°, and γ = 117.10°). The crystal structure data demonstrates that the chemical regeneration of cellulose I lead to a conformational change from *tg* to *gt* (Figure 1. 6) and concurrent changes in the intermolecular H-bonding interactions from O6-H----O3 to O6-H---O2 in cellulose II (Figure 1. 8). Importantly,

while cellulose I converts to cellulose II, the reverse process is not possible as cellulose II is thermodynamically stable (Gubitosi et al.).

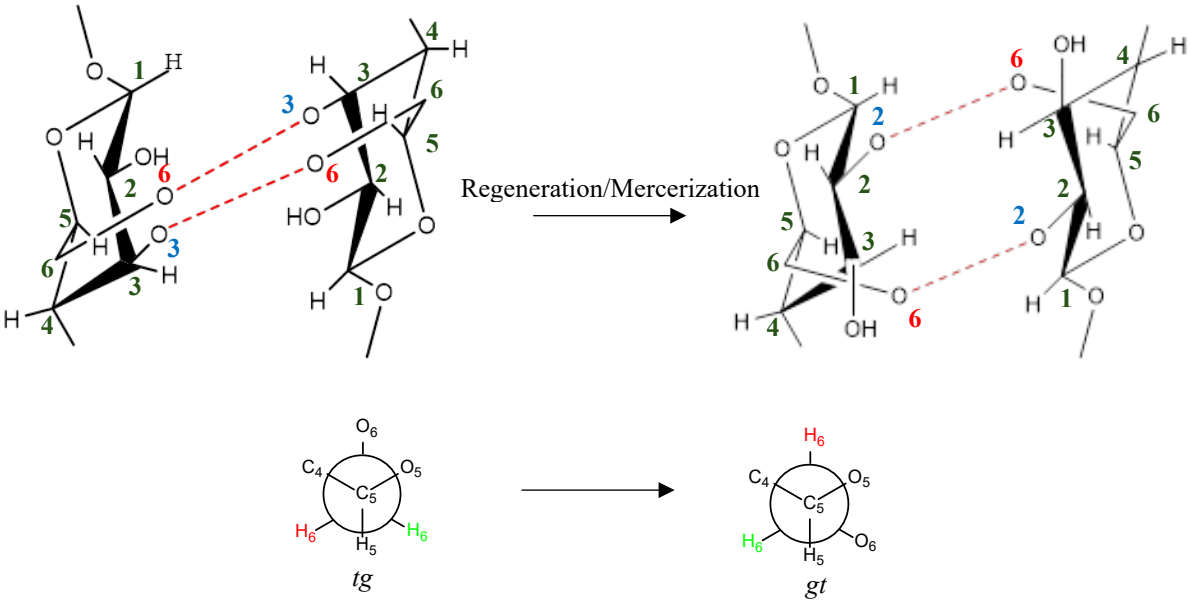

Figure 1. 8: Conversion of cellulose I to cellulose II

Cellulose II can be prepared from cellulose I by either chemical regeneration or mercerization (Ciolacu and Popa 2010). Chemical regeneration involves dissolving cellulose I in a solvent and letting it re-precipitate in the solvent. Several solvent systems can be used for this process, including copper (II) hydroxide solution in ammonia (cuoxam/ Scheweizer's reagent), cupriethylenediamine (cuen), amine/thiocyanate, hydrazine thiocyanate, lithium chloride/N,N-dimethylacetamide and N-methylmorpholine-N-oxide/water solutions. Mercerization converts native cellulose to cellulose II by treatment in concentrated solutions of either NaOH (20-30%) or HNO3 acid (65%) at higher temperatures (60-100 °C) (Faria-Tischer et al. 2015).

1.3.1.4 Cellulose III

Cellulose III does not occur naturally and occurs as two allomorphs, cellulose III_I and cellulose III_{II}, that are prepared from cellulose I or cellulose II, respectively. When cellulose I and II are treated with ammonia or any suitable amine solution, cellulose III can be obtained once the swelling agent (i.e. ammonia) is removed. Depending on the

type of starting allomorph I or II, cellulose III can be obtained in two forms; cellulose III_I and III_{II} respectively. Cellulose III has enhanced reactivity due to a higher accessibility to reagents and enzymes owing to its more open crystal structure. These characteristics are beneficial for applications in biofuel, textile and materials technologies (Wada et al. 2004). For example, the cellulose III structure enhances the softness and the plasticity of textile products (Wada et al. 2004).

The diffraction patterns of both cellulose III_I and III_{II} are similar but have different meridional intensities. The crystal structure of cellulose III_I has a monoclinic $P2_1$ (a = 4.450 Å, b= 7.850 Å, c = 10.31 Å, α= β = 90°, and γ = 105.10°) unit cell (Figure 1. 7) with a single chain in the unit cell giving a similar pattern to the parallel alignment of cellulose I. However, the C6-hydroxyl groups are oriented in gauche–trans (*gt*) conformation, and therefore have a similar hydrogen bond network to cellulose II. While fine detail of the crystal structure of cellulose III_{II} remains to be elucidated the symmetry of the unit cell is also monoclinic $P2_1$. Detailed resolution of the H-bonding network in cellulose III_{II} has been hampered by a high degree of disorder. Interestingly, both cellulose III_I and cellulose III_{II} can revert back to cellulose I and cellulose II precursors, respectively, when exposed to high temperature and humid conditions (Wada et al. 2004).

1.3.1.5 Cellulose IV

Cellulose IV had been found in higher plant primary cell walls (e.g. rice straw, beech etc) and in smaller amounts in some seaweeds (Habibi et al. 2010; Kulshreshtha 1979). Heating cellulose III_I and III_{II} in glycerol at 260 C, forms cellulose IV_I and IV_{II}, respectively. Similarly, cellulose III_I and III_{II}, polymorphs IV_I and IV_{II} can also be reverted to the initial forms (I and II). Both cellulose IV_I (a = 8.03 Å, b= 8.13 Å, c = 10.34 Å, α= β = γ= 90°) and IV_{II} (a = 7.99 Å, b= 8.10 Å, c = 10.34 Å, α= ß = γ 90°) exist in triclinic P_1 form (Ciolacu and Popa 2010). Despite the interest, studies on any kind of applications of cellulose IV appear absent from the literature.

1.3.2 Major sources of cellulose

1.3.2.1 Plants

Vascular plants are the major industrial sources of cellulose due to their abundance and targeted cultivation (George and Sabapathi 2015; Lavanya et al. 2011). Pulp and paper-making industries make use of wood feedstock (e.g. *Pinus radiata*, *Picea abies*, *Populus tremuloides*) and have a well-established infrastructure for cultivation and manufacturing. However, a wide range of plant materials are also targeted for cellulose products including cotton, ramie, hemp, jute, flax, sisal, agricultural waste materials like wheat, rice straw, sugarcane and beet pulp (George and Sabapathi 2015; Moon et al. 2011). Different parts (leaves, stem, fruits) of both aquatic and terrestrial plants are utilized in the cellulose industry (George and Sabapathi 2015).

1.3.2.2 Tunicates

Tunicates are marine invertebrate animals (formerly known as Urochordates) and are the only animal capable of synthesizing cellulose microfibrils (Moon et al. 2011). The cellulose is a major component of the tunicates test (tunic) (Moon et al. 2011) providing structural support for tunic cells which covers the whole outer layer of tunicates. The unique feature of cellulose synthase enzymes in tunicates originates from horizontal gene transfer from bacteria. However, microfibrils produced by different species of tunicates are easy to distinguish, with unique properties and structural features for cellulose derived from different species of tunicates (George and Sabapathi 2015).

1.3.2.3 Bacteria

Similar to algae, the cellulose from bacteria possesses unique properties over plant-derived cellulose, in part due to the absence of lignin and hemicellulose. In this regard, bacterial cellulose has high purity and cellulose extraction is simple compared to those from lignocellulosic materials. The cellobiose units are arranged differently within the cellulose unit cells which results in high crystallinity in bacterial cellulose. This gives rise to a more open porous structure of bacterial cellulose which has higher water retention (1000% of cellulose sample weight) compared to plant cellulose (60%) (Brigham 2018).

1.3.2.4 Algae

Cellulose is found in algae (Mihranyan 2011). Examples of macroalgal species from which cellulose has been characterised are *Cladophora* (Mihranyan 2011), *Chaetomorpha* (Prakash Menon et al. 2017), *Rhizochlonium* (Atalla et al. 1985; Prakash Menon et al. 2017), *Valonia* (Mihranyan 2011), *Dictyosphaeria* (George and Sabapathi 2015), *Siphonocladus* (George and Sabapathi 2015), and *Boergesenia* (George and Sabapathi 2015). Literature shows that algae-derived cellulose has a remarkably high degree of crystallinity (i.e. the degree of structural order of molecules in a polymer). For instance, cellulose derived from green macroalgal species such as *Valonia* and *Cladaphora* possess a degree of crystallinity of 95%. Algal cellulose also possesses some advantages compared to plant-derived cellulose such as ease of extraction and structural dimensions of extracted nanocellulose. Table 4 demonstrates a summary of characteristics of cellulose isolated from marine and freshwater macroalgae species reported in previous studies.

1.3.3 Biosynthesis of cellulose microfibrils

Single strands of cellulose are identical and are synthesized by cellulose synthase enzymes. However, the properties of cellulose microfibrils are variable and are highly characteristic of the arrangement of the organism's cellulose synthase units within the cellulose synthase complex (terminal complex (TC)) (Gu and Somerville 2010; Moon et al. 2011). The subunits of TCs are formed in two configurations; linear and rosette (Figure 1.9) (Saxena and Brown 2005). The TC has a diameter of 25-35 nm (Festucci-Buselli et al. 2007) and cellulose microfibrils are formed as multiple cellulose strands (n = 36) which are concurrently produced by the cellulose synthase enzymes within the cellulose synthase complex and subsequently coalesce (Gu and Somerville 2010). Importantly, different properties of cellulose microfibrils such as morphology, molecular weight, dimensions, shapes, crystallinity (relative quantity of crystalline material (ordered) present), and crystal structure (percentage content of Iα and Iβ) result from the differences in the TC's between organism groups (Figure 1.9) (Saxena and Brown 2005).

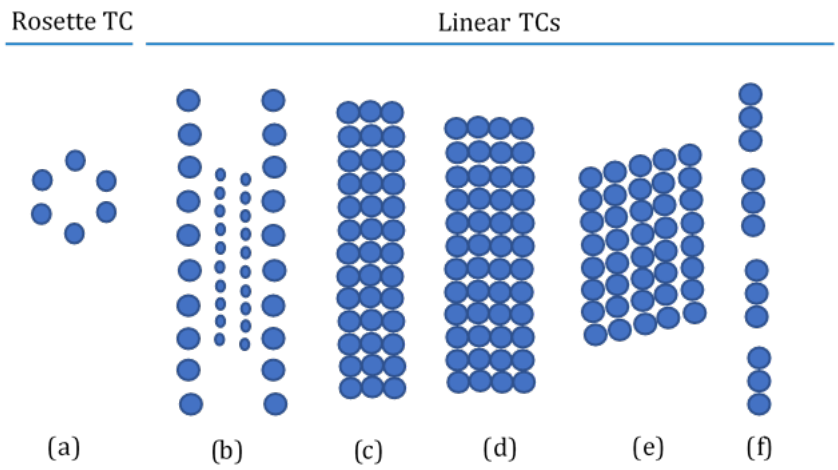

Figure 1. 9: Schematics of rosette and linear terminal complexes (a) wood, plants, green microalgae (Micrasterias), (b) tunicates, (c) green macroalgae (Valonia), (d) red algae, (e) yellow-green algae, (f) bacterial.

Table 1. 4: Characteristics of cellulose isolated from marine and freshwater macroalgae species

Environment	Class	Order	Family	Species	Cellulose characteristics			Reference
					Yield	Cr I %	Degradation temperature /C°	
Marine	Florideophyceae	Fucales	Fucaceae	*Fucus vesiculosus*	20.5	19	-	(Bogolitsyn et al.)
	Florideophyceae	Laminariales	Laminariaceae	*Laminaria digitata*	30.5	40	-	(Bogolitsyn et al.)
	Florideophyceae	Cladophorales	Cladophoraceae	*Chaetomorpha gracilis*	35	93.5	255	(Freile-Pelegrín et al.)
	Florideophyceae	Bryopsidales	Caulerpaceae	*Caulerpa taxifolia*	11	67	-	(Siddhanta et al.)
	Florideophyceae	Dictyotales	Dictyotaceae	*Padina tetrastromatica*	9.5	66	-	(Siddhanta et al.)
	Florideophyceae	Gelidiales	Gelidiaceae	*Gelidium pusillum*	9.3	64		(Siddhanta et al.)
	Ulvophyceae	Ulvales	Ulvaceae	*Ulva lactuca*		65	260	(Wahlström et al.)
	Magnoliopsida	Alismatales	Posidoniaceae	*Posidonia oceanica*	32.5	60.5	287.23	(Tarchoun et al.)
	Ulvophyceae	Cladophorales	Pithophoraceae	*Aegagropila linnaei*	18.5	-	289	(Sebeia et al.)
	Ulvophyceae	Cladophorales	Valoniaceae	*Valoniopsis pachynema*	29	71.94	250	(Sunesh et al.)
Fresh	Ulvophyceae	Cladophorales		*Aegagropila linnaei*	-	95	-	(Sebeia et al.)

Terrestrial plants have a rosette TCs with six subunits and each subunit produces six cellulose chains (six active sites) that coalesce to make a fibril with 36 cellulose chains (Figure 10). However, while much research has investigated the biosynthesis of cellulose by rosette TCs, there is less information on the biosynthesis of cellulose by linear TC configuration. Studies show that algae, tunicates and bacteria that contain linear TC configurations have highly crystalline, Iβ-rich, ribbon-like cellulose microfibrils with cross sections of approximately 20 nm by 8 nm (Moon et al. 2011; Sturcová et al. 2004). In the green alga Valonia, the TC is composed of three rows of subunits with 10-20 cellulose chains produced by each subunit (10-20 active sites) producing cellulose microfibrils with approximately 1000 chains with a square cross section of 20 nm by 20 nm. Bacteria have a single row of subunits making up the TC and produce 16 cellulose chains per subunit (16 active sites). For example, Acetobacter produces microfibrils with larger widths in rectangular cross sections of 6-10 nm by 30-50 nm (Moon et al. 2011).

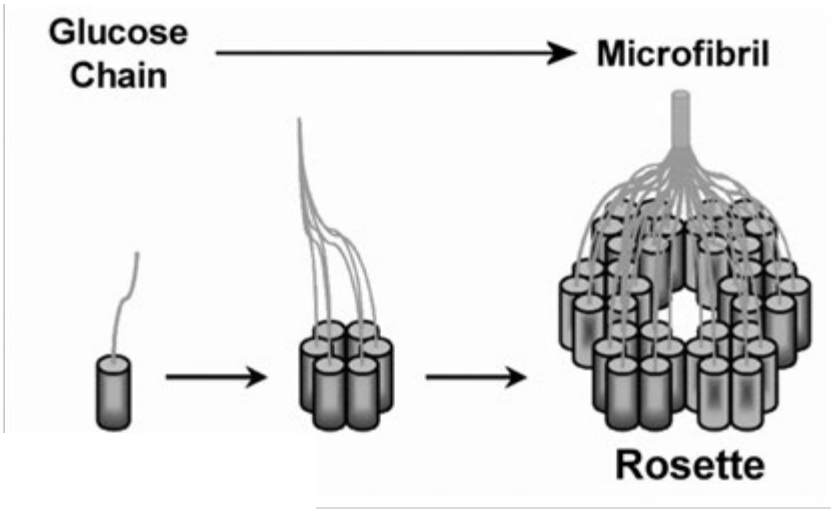

Figure 1. 10: Formation of a rosette structure. Image from Saxena and Brown (2005)

1.3.4 Cellulose extraction methods and pre-treatment effects

Most commercially produced cellulose is derived from vascular plants with only minor production from other sources (Lavanya et al. 2011). Statistical data shows that approximately 70 million trees worldwide are harvested per year to produce wood-based cellulose fibres. Wood-based cellulose fibres are attached together by a hard and brittle organic polymer called lignin (Netramai et al. 2016) which makes up to 15%-25% of wood while the cell wall is strengthened by a significant amount of hemicellulose (up to 20%-30%) (Viikari et al. 2009). Hence, pulping methods are required to detach cellulose

fibres from other components present in wood to increase the efficiency of subsequent bleaching treatments (Viikari et al. 2009). However, depending on the biomass source, cellulose isolation methods vary widely. In this regard, the choice of isolation methods directly affects the properties of nanocellulose (e.g. crystallinity, polymorphism (chemical compound showing more than one crystal structure) and aspect ratio (proportion between the longest and shortest dimension of a particle) (Festucci-Buselli et al. 2007; Quiroz-Castañeda and Folch-Mallol 2013).

1.3.4.1 Different pulping methods to extract cellulose from wood

Traditionally, the harvested wood is first cleaned and chipped prior to the pulping process (Cheremisinoff and Rosenfeld 2010). Pulping can be carried out using two main approaches: mechanical or chemical (Table 1. 5) (Prepas and Charette 2003; Warwick et al. 2013). However, hybrid-pulping methods have been developed to harness the advantages of both mechanical and chemical treatments (Table 1. 6) (Bajpai 2016; Henriksson et al. 2007; Keshri 2018). In traditional mechanical pulping, the wood chips are ground against a rotating drum to obtain cellulose fibres. During this process, the lignin is softened by the heat produced. More energy-efficient mechanical methods have now been introduced. For example, the cellulose fibres are then steamed under pressure resulting in a significant reduction in energy consumption as steaming allows better absorption of the cooking chemical into the cellulose fibres (compared with traditional cooking in chemical liquid under atmospheric pressure) (Habibi et al. 2010). Figure 1. 11 shows the cellulose extraction procedure from lignocellulosic materials.

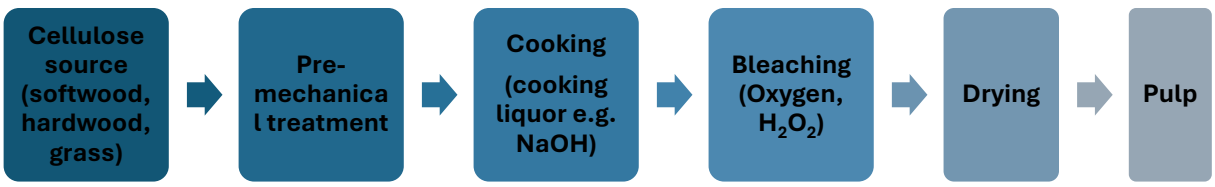

Figure 1. 11: Cellulose extraction steps from lignocellulosic materials.

Table 1. 5 : Comparison between mechanical and chemical pulping (Bajpai 2016) .

	Mechanical pulping	**Chemical pulping**
Energy consumption (kW)	1000 kW ton per 1ton pulp	Self-sufficient
Yield (%)	92-95	40-55
Fibre strength	Short and broken	Long and strong
Cost of production	Low	High

For nanocellulose products where retention of a high degree of polymerisation and crystallinity are optimal, mechanical pulping or grinding method are not recommended procedures (Kargarzadeh et al. 2017). To retain these important structural features in nanocellulose products chemical pulping techniques are often used instead. Soda pulping, the oldest chemical pulping method, cooks wood chips in hot (160-170 °C) concentrated NaOH (6-10%) (Netramai et al. 2016). While this process is suitable for extracting cellulose from agricultural residues (Windeisen and Wegener 2012) it is rarely used due to difficulty in recovery of the cooking chemical and high alkalinity (Cheremisinoff and Rosenfeld 2010). The Kraft method is the most common process since it is effective for most wood sources (Netramai et al. 2016). In this method wood chips are converted into pulp by treatment with a hot (165 – 175 °C) mixture of NaOH and sulphide (Kargarzadeh et al. 2017; Young et al. 2003). Modifications of the Kraft method include treatment with sodium chlorite ($NaClO_2$) to selectively remove lignin (Kargarzadeh et al. 2017). The sulphite pulping process is quite similar to the Kraft method, but uses strong acids (e.g. H_2SO_4, 5–25%) to dissolve the lignin with digestion carried out under high pressure (4 bar at the start and maintained at 10 bar for 2 hours) and at elevated temperatures at 100 °C (Lacerda et al. 2013). Chemical pulping methods produce longer and stronger fibres than mechanical methods, however the yield produced is low (40%-50%) as a higher proportion of cellulose linked with lignin and hemicellulose is dissolved with chemicals during the process (Bajpai 2016; Keshri 2018).

Table 1. 6 : Different processing methods used for production of nanocellulose from lignocellulosic materials.

Sources	Pre-treatment	Mechanical	Post-treatment	References
Softwood (Norway spruce)	Kraft pulping	Refining, cryocrushing	Filtration	Janardhnan and Sain (2006)
Softwood pulp	Sulphite process	Refining, homogenization	No	Henriksson et al. (2007)
Hardwood pulp (Sisal)	NaOH, chlorite treatments	Homogenization	Acid hydrolysis	Siqueira et al. (2010)
Grass	Sodium chlorite, acetic acid, NaOH treatment	Blending, homogenization	No	Chaker et al. (2013)

1.3.4.2 Bleaching/ Delignification

Depending on the intended application the pulp is then bleached to extract chromophores (i.e. whiten the pulp) which are responsible for colours (Cheremisinoff and Rosenfeld 2010). During the bleaching process, any residual lignin from the pulp is also removed (Bajpai 2016). However, bleaching is dependent on the nature of the pulp. As an example, mechanical pulps and chemical pulps are bleached differently as mechanical pulps contain a large amount of lignin (Cheremisinoff and Rosenfeld 2010). Moreover, the bleaching process also depends on the expected end product. For instance, the pulp used for high quality printing paper needs more whitening hence requires additional bleaching steps (Bajpai 2016).

There are a number of bleaching options including chlorine, hypochlorite, hydrogen peroxide, enzymes, chlorine dioxide and ozone (or oxygen) (Netramai et al. 2016). While, chlorine and hypochlorite were widely used in the past, these bleaches lead to the production of toxic by-products (e.g. dioxin, polychlorinated biphenyls (PCB), dichloro-diphenyl-trichloroethane) and have now been replaced by less toxic, elemental chlorine free alternatives (e.g. hydrogen peroxide, enzymes, and ozone) (Viikari et al. 2009). The

major reactions of the bleaching process are designed to remove non-cellulosic materials such as pectin, lignin and hemicellulose.
Note that even though chemical pulps (i.e. Kraft pulping) contain significantly less residual lignin than mechanical pulps, they still require several bleaching stages to remove all remaining lignin (Cheremisinoff and Rosenfeld 2010).

1.3.4.3 Cellulose Drying

The choice of drying method is an important consideration as it will influence the nanoscale properties and dimensions of cellulose (Peng et al. 2012). Depending on the intended application, there are a range of drying options for drying cellulose products including, evaporation at high temperatures, freeze-drying, supercritical fluid drying, and spray drying (Table 6). Conventional thermal drying methods result in an irreversible loss of water within the fibres known as hornification (Fernandes Diniz et al. 2004). At the molecular level, hornification of cellulose fibre occurs due to the attraction between the hydroxyl groups present within the fibre (Zimmermann et al. 2016). Hornification results in a loss of elastic and tensile modulus of the fibres influencing the properties of the targeted material applications.

Freeze-drying (lyophilisation), supercritical fluid drying, and spray drying limit hornification of cellulose fibres. Freeze-drying (lyophilisation) is a three-stage process that can be highly controlled. Primarily the sample is frozen, then free water is sublimed under vacuum from the frozen sample, and finally, bound water is removed under vacuum while heating. However, despite the freeze-drying conditions (-20 °C to -50 °C), the morphology of the cellulose depends on various factors such as particle size, the concentration of cellulose suspension, and surface charge (Zimmermann et al. 2016). Supercritical fluid drying (SFD) techniques in which a continuous flow of CO_2 (pressure 0-14 MPa and temperature between 40-60 ˚C with the fluid flow rate of 80–220 kg/h) is provided, is another mild approach that offers consistency in particle size and morphology (Obaidat et al. 2015; Tomic et al. 2020). In SFD the solvent is decompressed to atmospheric pressure and then kept in the gas phase without condensing. The theory behind this method is that solvent is removed without forming a liquid-vapour interface by reducing the capillary forces. This avoids the shrinkage of the cellulose material and surface tension (Zimmermann et al. 2016). Obaidat et al reported that microcrystals obtained by SFD are of a smaller and more uniform size compared to freeze-dried

microcrystals (Obaidat et al. 2015). However, both freeze-drying and SFD result in broad particle size ranges that require further mechanical treatment such as milling (Zimmermann et al. 2016). Spray drying is employed in industry as a standard drying method to dehydrate aqueous suspensions and obtain the final products as a powder (Peng et al. 2012; Zimmermann et al. 2016). It involves rapid transfer of heat and mass in the form of droplets (e.g. cellulose and water) continuously through a spray injector into a drying chamber containing hot air (Zimmermann et al. 2016). This method enables optimizing the particle size and morphologies by varying the operating conditions. One advantage of spray drying is that it is suitable for thermosensitive materials as the duration of exposure to the heat source is very short (Zimmermann et al. 2016). Moreover, the spray drying process reduces the number of subsequent stages such as grinding for separating fibres (Zimmermann et al. 2016).

Table 1. 7 : Comparison between different drying techniques for cellulose nanofibrils (CNFs). Images from (Zimmermann et al., 2016)

Drying technique	Morphology	Advantages	Disadvantages
Evaporation at high temperatures	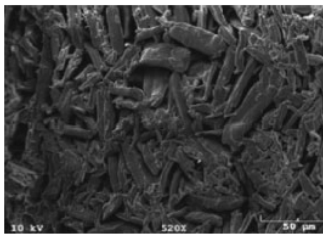	· Cost-effective · Fast process	· Hornification/ irreversible agglomeration · Loss of nanometric dimensions
Lyophilization/ Freeze drying	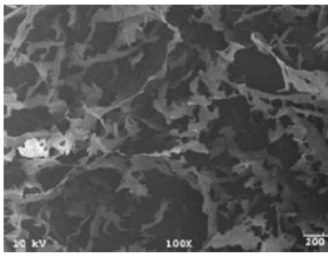	· Stable process · Applications in CNC and CNFs · Some parts of fibre are in nanometre ·Limits hornification	· Time consuming · Stability of final product is affected due to desorption of unfrozen water
Supercritical extraction	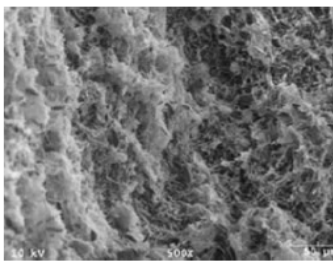	· Efficient drying · Preserves nanoscale dimensions · Used mainly for CNFs ·Limits hornification	· Expensive · Complex process · Needs large amounts of solvents and exchange of solvents · Not applicable for CNCs

Spray drying	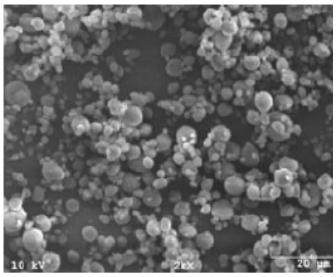	· Continuous process · Low operational expenses · Used for drying nanocrystal pulp ·Limits hornification	· Can form suspended clusters · Particle size may range from nm to mm · Can clog the system with the use of larger particles

1.3.4.4 Extraction of algal cellulose

Isolation of cellulose from macroalgae and bacteria requires milder conditions due to the lack of lignin in their respective cell walls. The extraction conditions most commonly used involve three basic steps: a bleaching step, followed by an alkali extraction of proteins, and finally a dilute acid treatment to disperse the cellulose, prior to drying (Figure 1. 12) (Mihranyan et al. 2004a). Typical bleaching systems includes buffered solutions of $NaClO_2$ (Siqueira et al. 2010) or hydrogen peroxide as a milder bleach, and results in a pigment free pulp. The bleached pulp is then subjected to alkaline treatment which helps in removing hemicellulose and other non-cellulosic compounds that are not completely eliminated during the bleaching process (Ilyas and Atikah 2021). Following several washes of water, the neutralized pulp is freeze-dried and then mechanically homogenized. To obtain cellulose crystals with high crystallinity the cellulose fraction is treated with HCl (Wahlström et al. 2020).

Figure 1. 12 : Cellulose extraction steps for macroalgae.

Cellulose pulp from algal biomass sources has been isolated from freshwater macroalgae (e.g. species of *Cladophora* (Mihhels et al. 2023; Xiang et al. 2016) and *Aegagropila linnaei* (Sebeia et al. 2019) and seaweeds (e.g. *Ulva lactuca* (Jmel et al. 2019; Wahlström et al. 2020), *Gelidiella acerosa* (Siddhanta et al. 2009), and species of Chaetomorpha (Freile-Pelegrín et al. 2020) using various pre-treatments. Of particular interest to the

current research, cellulose pulp has also been isolated from the waste biomass of commercial production of primary products (e.g. hydrocolloids) from seaweed (Barbot et al. 2016).

1.4 Nanocellulose

Isolated cellulose materials in the nanometric range (1- 100 nm) are referred to as nanocelluloses (Moon et al. 2011). The abbreviations for the nanocellulose classes used here are, cellulose nanocrystals (CNC; syn: nanowhiskers), cellulose nanofibrils (CNF; syn: micro fibrillated cellulose (MFC)), and bacterial nanocellulose (BNC**).** Figure 1. 13 shows the SEM images of CNC, CNF, and BNC, respectively (Thomas et al. 2018). Interest in nanocellulose products for nanomaterials has grown owing to their unique properties (e.g. biodegradability, high mechanical strength, lightweight, thermal stability, and transparency). These unique properties have been employed in a vast number of applications to produce novel materials (Table 1. 8).

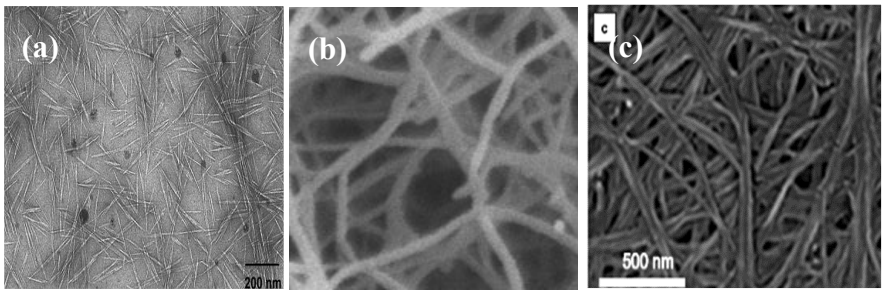

Figure 1. 13 : : Images of (a) cellulose nanocrystals (CNC), (b) cellulose nanofibers (CNF) and (c) bacterial nanocellulose BNC) Images adapted from (Thomas et al., 2018)

Table 1. 8 : Examples of recent applications of nanocellulose

Type of nanocellulose		Application	Reference
Cellulose nanocrystals	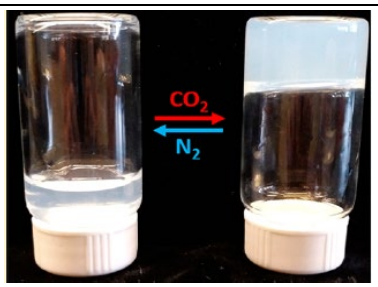	CO_2-switchable cellulose nanocrystal hydrogel	(Oechsle et al. 2018)
Cellulose nanocrystals	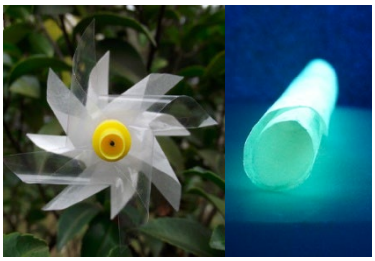	Transparent and photoluminescent foldable quantum dot paper	(Xue et al. 2015)
Cellulose nanofibers	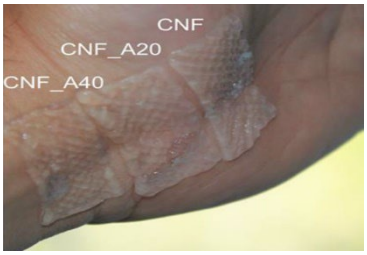	Nanocellulose-based inks for 3D printing/ wound dressing	(Espinosa et al. 2019)
Cellulose nanofibers		Transparent CNF paper electronics	(Koga et al. 2014)
Cellulose nanofibers		High thermal stability/ optical transparent CNF paper	(Nogi et al. 2013)

1.4.1 Bacterial nanocellulose (BNC)

Bacterial cellulose is synthesized by specific bacterial species such as *Acetobacter*, *Agrobacterium*, *Pseudomonas*, *Rhizobium,* and Sarcina (de Amorim et al. 2020). The synthesis of BNC is quite different to other types of nanocellulose as it is a bottom-up process. Studies show that BNC possesses unique physicochemical properties such as high purity, ultrafine fibre networks, high water retention capacity, high degree of crystallinity (≈80%), high Young's modulus (≈ 78-114 GPa), high DOP (≈2000-8000), and high-water holding capacity (de Amorim et al. 2020; Samiee et al. 2019) . BNC is used as a sustainable biomaterial in food, cosmetics, and biomedical industries as a thickening, stabilizing, and gelling agent. When compared to other forms of nanocellulose, bacterial cellulose does not require high-energy processes for purification. The purification process is less cumbersome as it only involves the removal of microorganisms and the cell wall material from the culture medium (de Amorim et al. 2020). However, low yield and relatively expensive production processes limit the scale of production.

1.4.2 Cellulose Nanocrystals (CNC)

CNCs (nanowhiskers) are rigid rod-like particles and have a range of applications including in antimicrobial films, biosensors, drug delivery, capacitors, biocomposites, batteries, separation membranes, and green catalysts (Sunasee et al. 2016). The ratio of length and diameter that determines the aspect ratio is an important structural measure informing the properties and potential application of CNCs. The aspect ratio varies according to extraction protocol and the cellulose source biomass (Table 1. 9). CNCs can be prepared by subjecting them to chemical, mechanical or enzymatic treatments that selectively remove amorphous regions (Nechyporchuk et al. 2016). A key measure of the efficiency of this process is an increase in the degree of crystallinity relative to the cellulose feedstock.

Table 1. 9 : Dimensions of CNCs extracted from different sources.

Sources	Preparation method	Length (nm)	Width (nm)	Aspect ratio	References
Wood	H_2SO_4 hydrolysis	100-300	3-5	20-100	(Koga et al. 2014; Nogi et al. 2013)
Cotton	HCl hydrolysis	100-150	5-10	10-30	(de Amorim et al. 2020)
Ramie	H_2SO_4 hydrolysis	70-200	5-15	Approx. 12	(Samiee et al. 2019)
Algae (*Valonia*)	H_2SO_4 hydrolysis	1000-2000	10-20	Approx. 100	(Sunasee et al. 2016)
Bacteria	HCl hydrolysis	160-420	15-25	7-23	(Sucaldito and Camacho 2017)

The principle of the CNC production process relies on the differential reactivity of the amorphous and crystalline regions of the cellulose structure (George and Sabapathi 2015). Their reactivity differs due to accessibility in the crystalline regions. Indeed, acid hydrolysis using concentrated solutions (45 – 65 %) of strong acids are the most common methods of extraction of CNCs as they preferentially access and hydrolyse amorphous regions relative to crystalline regions (George and Sabapathi 2015). Note that given the concentration of the strong acids used, temperature and time are important parameters to consider to avoid over-hydrolysis and reduction in yield. Additionally, depending on the choice of acid (e.g. H_2SO_4, HBr, or H_3PO_4) hydroxyls on the surface of the CNC production can be functionalized with different ester groups (e.g. SO_3^- and PO_3^-) for better dispersion (Sucaldito and Camacho 2017).

CNCs themselves possess a range of desirable properties for inclusion in materials, including high tensile strength (theoretical value= 7.5-7.7 GPa) (George and Sabapathi 2015), high thermal stability (decomposition temperature= 247.9 C°) (Yildirim and Shaler 2017), high aspect ratio (~10-100) (George and Sabapathi 2015), high surface area, anisotropy (differences in physical properties along different molecular axes), elasticity, optical transparency, low density (1.5-1.6 g/cm^3), and low coefficient of thermal

expansion (~0.1 ppm/K) (Sunasee et al. 2016). Solutions of CNCs can have shear-thinning rheology and liquid crystalline-like behaviour (Figure 1. 14). However, the properties of extracted CNCs vary according to the source biomass and the reaction conditions employed to extract them.

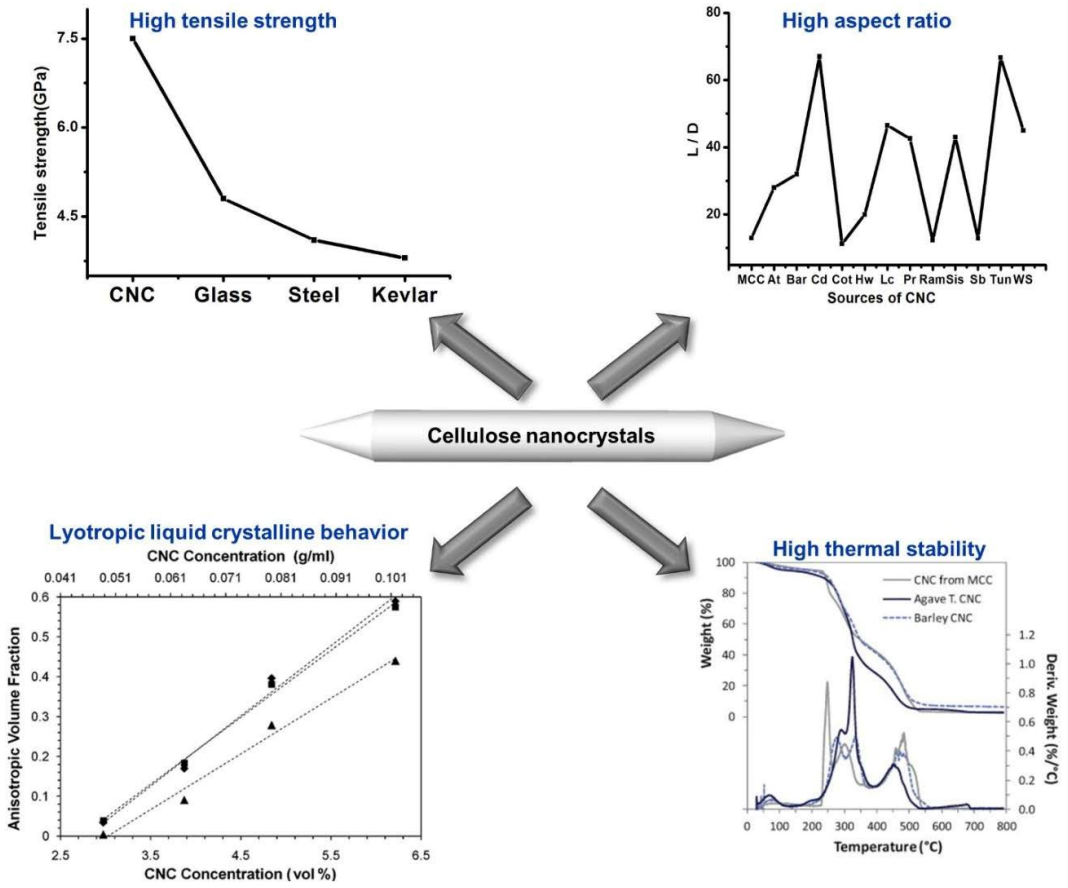

Figure 1. 14 : High tensile strength, high aspect ratio, lyotropic liquid crystalline behaviour and high thermal stability of CNCs. Image adapted from (Thomas et al., 2018)

1.4.3 Cellulose nanofibrils (CNF)

CNFs have spaghetti-like structures that are suitable for applications such as reinforcing components in biocomposites and the production of filaments for textiles (Boskovic et al. 2002). The recognition that CNFs produced from different biomass sources influences their properties has contributed to a rapidly developing field of research (Khalil et al. 2016). CNFs (cellulose microfibrils or nano-fibrillated cellulose) are prepared using mechanical methods, such as high-pressure homogenization, high-intensity ultrasonic treatments, or cryogenic grinding (freezer milling) that delaminate or peel away

interfibrillar links producing fibres (Nechyporchuk et al. 2016). Depending on the source biomass and the process employed this produces CNFs with a diameter on the nanoscale and lengths varying from nanometre to micrometre (Börjesson and Westman 2015). Unlike CNCs, both the non-crystalline and crystalline regions are retained. The methodology for the production of CNFs has evolved rapidly and generally requires a combination of chemical and physical/mechanical techniques to facilitate efficient production (Nechyporchuk et al. 2016). To reduce the need for chemical oxidants, enzymatic oxidization has also been employed successfully (Börjesson and Westman 2015; Nechyporchuk et al. 2016).

There are a number of mechanical treatments techniques that have been used to produce CNFs, including grinding, ultrasonication, blending, refining, extrusion, and cryocrushing (Börjesson and Westman 2015). The underlying principle behind mechanical treatments is to create shear forces to delaminate cellulose fibres. The two most common techniques are refining and cryocrushing.

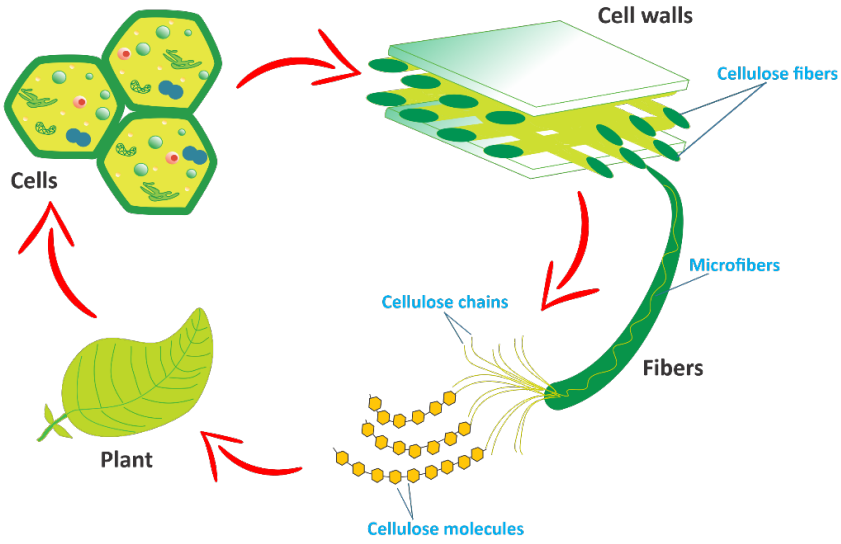

Figure 1. 15 : The different levels of cellulose structure.

When refining the pulp, a dilute solution of cellulose is subjected to shear forces in a homogeniser. This process changes the morphology and the size of the fibres. In the homogenization process, nanofibrils are separated into individual strands by shedding the external cell wall layers (Figure 1. 15). These individualized nanofibers give a stable

dispersion upon the addition of water. Moreover, refining also assists the homogenizing process by unbinding the fibre wall and causing internal fibrillation (Börjesson and Westman 2015; Nechyporchuk et al. 2016).

Cryocrushing is a process where the water-swollen cellulose pulp is frozen and mechanically crushed in a grinder. When subjected to mechanical crushing, the pressure created by the ice crystals make it easier to crack the cell wall and release fragments. The smaller fragments are later diluted in water prior to homogenization (Xie et al. 2018). The delamination of cellulose to CNFs requires high-energy mechanical disintegration, however, recent advances in methodology have reduced the energy input required (Xie et al. 2018). A major innovation is the use of the oxidizing reagent 2,2,6,6-tetramethylpiperidine-N-oxyl (TEMPO) to oxidize the cellulose prior to delamination to CNFs (Nechyporchuk et al. 2016). Oxidation of cellulose leads to conversion of surface C6 hydroxyl groups to carboxylate groups that are negatively charged at pH>~3 (Börjesson and Westman 2015). This results in repulsive forces at the interfibrillar links of the cellulose bundles aiding in delamination (Nechyporchuk et al. 2016). Given the advantages, TEMPO oxidation was used in this thesis to produce macroalgae-derived CNF.

1.4.3.1 CNF production by TEMPO-mediated oxidation

The TEMPO or (2,2,6,6-Tetramethylpiperidine-1-oxyl)-mediated reaction (Figure 1. 16**)** is carried out to implement selective oxidation of C6-primary hydroxymethyl groups at the surface of cellulose particles while protecting the secondary hydroxyl groups in polysaccharides in the presence of NaBrO and NaClO (Habibi et al. 2010). TEMPO-oxidation stands out among other traditional chemical reactions used in polysaccharide chemistry due to its high selectivity, ease of performance, and efficiency (Sadeghifar et al. 2011).

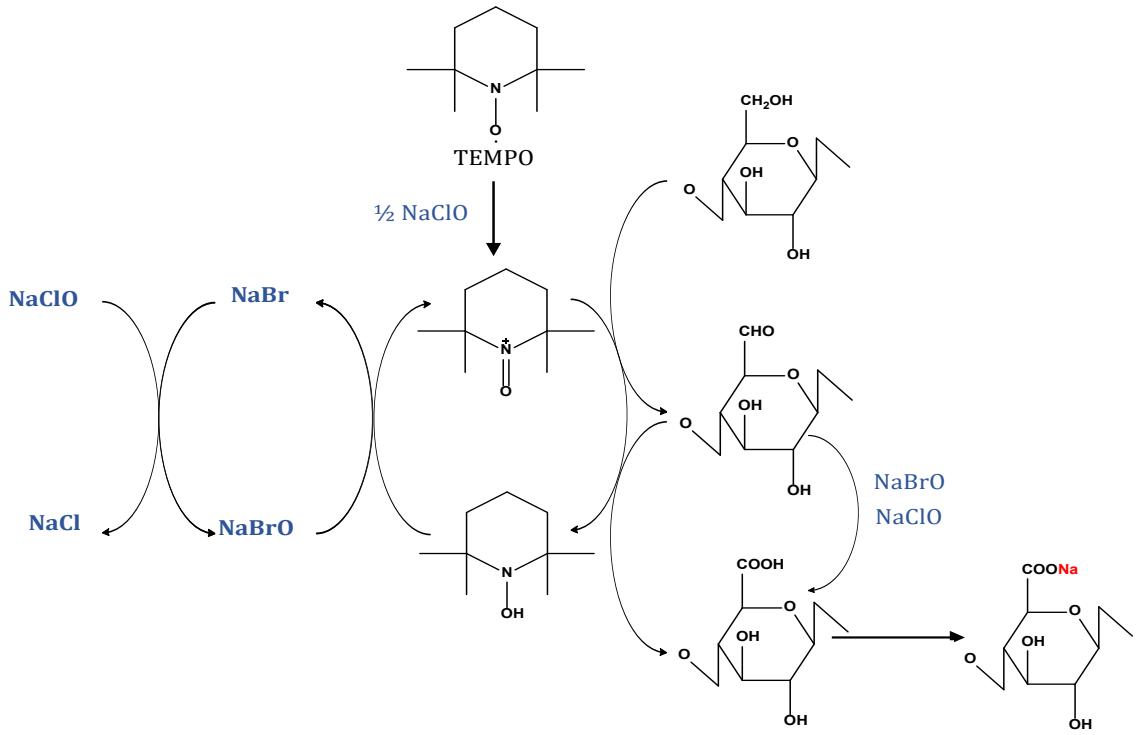

Figure 1. 16 : TEMPO oxidation reaction.

TEMPO radical which is a commercially available compound is water-soluble and stable. The resulting chemical and structural properties of TEMPO-oxidized nanocellulose vary according to the source and the oxidation conditions (Isogai et al. 2018). While the TEMPO oxidation can be carried out in alkaline conditions (pH 9-11) using NaBr and NaClO as a catalyst and primary oxidant, there can be some drawbacks to this approach. Such high pH levels can lead to side reactions such as, depolymerization of cellulose fibres (Saito and Isogai 2004) hence reducing the degree of polymerization. The degree of polymerization significantly impacts the nanofibers' mechanical properties, (Iwamoto et al. 2007); the higher the degree of polymerization of nanocellulose is the better the mechanical properties of nanocellulose (Fang et al. 2020). This reaction also could produce aldehydes as by-products, potentially compromising the thermal stability of the resulting polymers (Saito et al. 2009). These aldehyde groups are thermally unstable, and can hinder the uniform dispersion of oxidized cellulose in water due to the formation of partial hemiacetal linkages between fibrils (Saito et al. 2006). Therefore, to maintain the structural properties of cellulose fibres during oxidization it is important to conduct the reaction under neutral conditions or weak acidic conditions (Tanaka et al. 2012).

1.4.4 Nanocellulose-based Biocomposites

Recent studies demonstrate that using nanoparticles such as silicates, graphene, carbon nanotubes (CNT), and metals as reinforcement materials in polymers results in a significant improvement in physical properties (Teboho et al. 2018). However, these materials are not biodegradable. Therefore, in recent years, there has been increasing interest in cellulose fibres and bio polymers as they easily break down into harmless components. For example, bio-polymers such as polylactic acid (Trifol et al.), and the group of polyhydroxyalkanoates (PHAs) can be reinforced with cellulose nanomaterials to develop entirely bio-based composite materials, known as "green nanocomposites" (Pracella et al. 2014).

1.4.4.1 Cellulose Biocomposites preparation

The preparation of CNF biocomposites can be achieved through various methods. Common techniques include solvent casting and melt compounding (Srithep et al. 2013). Solvent casting involves dispersing the polymer and cellulose nanofibers (CNFs) in a suitable solvent, followed by casting the mixture into a mould and allowing the solvent to evaporate, resulting in a homogeneous film. Compounding, however, needs mixing the polymer and CNFs in an extruder at high temperatures, producing a uniform composite material. Given its simplicity and effectiveness in achieving a well-dispersed biocomposite using a minimum of products, solvent casting was chosen for this research, to produce PHBV/CNF films.

1.4.4.1.1 Solvent Casting method/ wet processing method

Solvent casting is one of the easiest and widely used methods of preparing nanocellulose composites due to low cost (no need for special instrumentation), fast preparation, and especially easy modification of reaction conditions (Wahid et al. 2018). In solvent casting, the solvent plays a major role as it affects the polymer surface structure. Generally water or organic solvents (e.g. alcohols, chloroform, tetrahydrofuran, acetonitrile, dimethylformamide) are used (Kong et al. 2015). Moreover, to enhance the properties of the film/composite the solution is often subjected to heat, or the pH is adjusted.

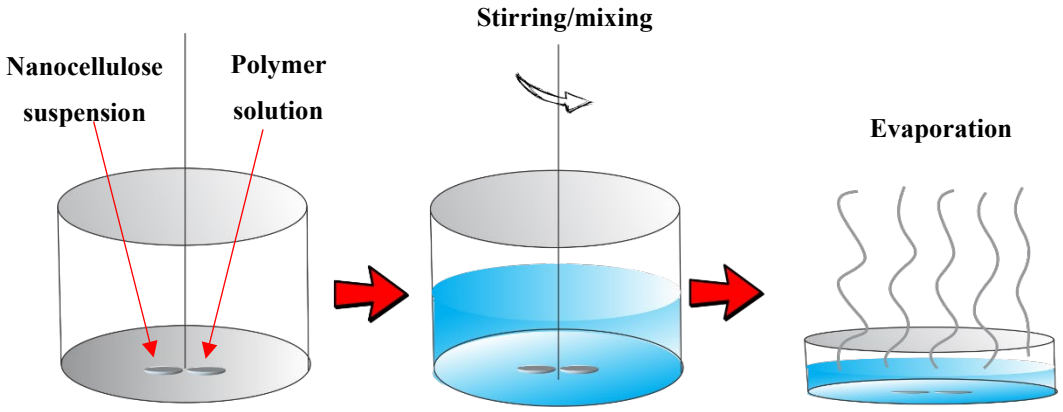

Figure 1. 17 : A schematic drawing showing the preparation of nanocellulose based nanocomposites by the solvent casting method.

The theory behind this process is to completely disperse the polymer and the filler (nanocellulose in this case) in a suitable solvent system through continuous agitation by mechanical stirring, and to transfer the solution on to a 3D mould (Figure 1. 17) (Kong et al. 2015; Wahid et al. 2018). The solvent is then evaporated leaving a matrix of uniformly dispersed particles (Wahid et al. 2018). Slow evaporation facilitates the formation of a firm nanocellulose complex linked via hydrogen bonds (Mondragon et al. 2014).

The composites formed through this method possess high thermomechanical stability and mechanical reinforcement. Hence, a vast number of nanocellulose composites have been developed using this process. For an example, Pal et al used the solvent casting method to fabricate an anti-bacterial nanocellulose (CNC) composite with PLA and reduced graphene oxide using chloroform as the solvent (Pal et al. 2017). A functional hybrid nanofiller of CNC and graphene oxide was developed by Miri et al to enhance the tensile

properties of poly vinyl (PVA) composites using water as the dispersion solvent (Miri et al. 2016). Another nanofiller was developed with PVA with mechanical and thermal improvements by Aloui et al and team using water as the solvent (Aloui et al. 2016). Moreover, a gelatine-based biocomposite was developed by Mondragon and team to improve the O_2 gas barrier properties using sulphuric acid as the solvent (Mondragon et al. 2014). Therefore, it is evident that the solvent casting method can be successfully employed with a variety of polymer matrices and a control of pore size.

1.5 Thesis Structure and Objective

The overall aim of this thesis was to investigate the potential of fully utilising the freshwater macroalgae grown in wastewater to produce bioproducts. In addition to a literature review (above) this thesis is comprised of three research chapters, each sequentially building upon the findings of the previous chapter.

1.5.1 Thesis Objectives:

1. Safe Handling of Biomass and Dual Product Extraction: Develop an inexpensive disinfection method for macroalgae biomass sourced from wastewater, ensuring safe handling and extraction of biostimulants and high-quality cellulose.

2. Freshwater Macroalgae-Derived Cellulose: Bridging the Knowledge Gap: Characterize the cellulose extracted from four different macroalgae species commonly used in bioremediation, bridging the knowledge gap in freshwater macroalgae cellulose properties compared to more commonly studied seaweeds.

3. Macroalgae-derived Cellulose Nanofiber (CNF) Production: Based on the findings of previous chapters and previous literature, identify the most suitable macroalgae species for cellulose extraction. Employ the TEMPO oxidation method to produce CNF, followed by a detailed characterization of these fibres. Compare the properties of the algae-derived cellulose and CNF with commercially available plant-derived CNF to assess quality.

4. Biocomposite Development: Utilize both algae-based and commercially available plant-derived CNF along with unmodified algae cellulose to produce PHBV

biocomposite materials. Conduct characterisation studies to assess the mechanical and thermal properties of the resulting biocomposites to determine improvements and potential applications.

Chapter 1:

Bioremediation is the removal of contaminants using living organisms such as bacteria, algae, and aquatic plants, and it provides an alternative option to small-scale wastewater treatment plants. The process generates residual biomass that is rich in valuable products like cellulose; however, handling this biomass safely is challenging due to the presence of pathogens. In the context of small-scale wastewater treatment, conventional disinfection methods, such as UV oxidation, are impractical due to their high costs. This chapter introduces an inexpensive disinfection method that utilizes a hot alkaline extraction process to disinfect biomass from wastewater-grown macroalgae, specifically *Oedogonium calcareum*. This method not only disinfects but also extracts a biostimulant, potentially could promote plant growth.

Furthermore, this chapter then reports the extraction and characterisation of cellulose from the disinfected biomass. A factorial experiment to assess the quality of cellulose for potential applications in biocomposites. The characterization of biostimulant includes elemental analysis, metal content, free amino acids, proteins, and a Gas chromatography-Mass spectrometry (GC-MS) non-targeted analysis to determine the chemical compounds present which could potentially promote plant growth activity. Furthermore, the chapter provides an in-depth understanding of properties of the cellulose derived from *Oedogonium*, using techniques such as HPLC sugar analysis, elemental analysis, X-ray diffraction (XRD), Fourier-transform infrared spectroscopy (FTIR), thermogravimetric analysis (TGA), and scanning electron microscopy (SEM), highlighting the potential of wastewater-grown macroalgae as a valuable source for sustainable material development.

This chapter is published in Bioresource Technology.

Chapter 2:

Building on the foundational work presented in Chapter 1, which ensured the safe handling of algae biomass, Chapter 2 explores the viability of using freshwater macroalgae for cellulose production. This chapter provided a comparative analysis of cellulose from four different macroalgae species commonly used in bioremediatoin, highlighting the diversity in cellulose properties and their potential applications. Wastewater-grown macroalgae is a sustainable yet underutilised cellulose source, which is otherwise discarded as waste. By comparing cellulose extracted from species namely *Rhizoclonium.sp*, *Zygnema.sp, Oedogonium.sp*, and *Stigeoclonium.sp* this research filled a significant gap in the literature and provides a foundational basis for selecting the most promising species for further application development. Limited research exists on the cellulose characterisation of these freshwater macroalgae species, presenting a significant gap in the literature compared to cellulose derived from seaweed. Therefore, this chapter focused on bridging this gap by providing a comprehensive characterisation of cellulose extracted from selected algae species, which are widely used in wastewater bioremediation systems.

The characterisation of cellulose involved sugar analysis by High-Performance Liquid Chromatography (HPLC), GC-TCD elemental analysis, X-ray diffraction (XRD), Thermogravimetric Analysis (TGA), Fourier-Transform Infrared Spectroscopy (FTIR), and Scanning Electron Microscopy (SEM). These methods provide a comprehensive analysis of cellulose's properties and a better understanding of its potential applications.

The findings from this chapter served as a basis for selecting the most suitable macroalgae species for the next research chapter of this thesis, which aims to develop biocomposite materials.

This chapter will be submitted to Cellulose Journal.

Chapter 3:

Based on the findings from Chapter 2, *Rhizoclonium.sp* was identified as the best algae species for biocomposite production due to its high crystallinity, high thermal stability and fibrous morphology. It was also observed that there are similarities with *Cladophora* cellulose, as shown in the literature. Given that *Rhizoclonium* and *Cladophora* naturally coexist, this chapter used a mixed algae culture predominantly comprising these two species.

This chapter is structured into two main sections. The first part details the production and characterisation of crude cellulose and cellulose nanofibers (CNF) from the *Rhizoclonium* and *Cladophora* mixture, employing the TEMPO oxidation method. This study assessed the physicochemical properties of algae-derived cellulose and TEMPO-oxidized algae CNF, comparing them with commercially available plant-derived CNF. The results confirmed the high quality and suitability of these materials to serve as reinforcement fillers.

The second part of this study focused on integrating commercial CNF, cellulose and CNF derived from mixed *Rhizoclonium.sp* and *Cladophora.sp* algae into PHBV composites. For the first time, to the best of our knowledge, these freshwater macroalgae-based cellulose were utilized as reinforcement fillers in PHBV biocomposite matrices. This integration enabled a direct comparison of mechanical and thermal properties between PHBV biocomposites reinforced with algae-derived cellulose materials and those using commercially available plant-based CNF. This comparison highlighted the potential of freshwater macroalgae-derived cellulose in biocomposite applications.

This chapter will be submitted to International Journal of Biological Macromolecules.

Chapter 2

Quality of cellulose and biostimulant extracts from *Oedogonium calcareum* cultivated during primary wastewater treatment.

2.1 Abstract

A practical two-product cascading biorefinery was developed to extract a biostimulant and cellulose from the freshwater filamentous macroalga *Oedogonium calcareum* grown while treating primary wastewater. Biostimulant production provides a valuable extract with production of disinfected residual biomass for further product development. Both *Escherichia coli* and F-specific RNA bacteriophage, indicators of human pathogens contamination, were absent from the residual biomass. The chemical composition of the biostimulant was complex, consisting of growth-promoting substances, free amino acids, and minerals. The *O. calcareum* cellulose fractions yielded between 9.5% to 10.1% (w/w) with purities from 84% to 90% and closely resembled microcrystalline cellulose. Biostimulant extraction improved cellulose quality by increasing crystallinity from 59% to 62%. Biomass condition, drying process, and biostimulant production influenced the crystallinity index. This study demonstrates a two-step process of biostimulant and cellulose extraction from wastewater-grown *Oedogonium*, simultaneously disinfecting biomass and isolating high-quality cellulose as a sustainable alternative to conventional extraction methods (Figure 2. 1).

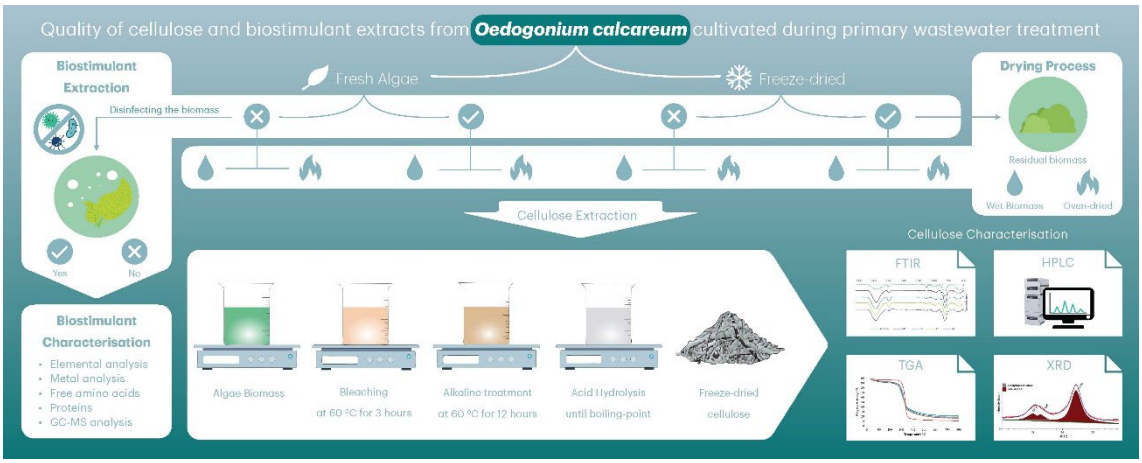

Figure 2. 1 : Graphical abstract.

2.2 Research Background

Globally, 60% of nitrogen and phosphorus-rich primary treated municipal wastewater is released untreated into streams, rivers, lakes, and coastal waters increasing eutrophication in adjacent aquatic ecosystems (Neveux et al. 2018). However, the cost of the implementation and operation of advanced wastewater treatment technologies to reduce this impact is a significant impediment to upgrading many primary wastewater treatment plants (WWTPs) (Lyu et al. 2020). Microalgal pond systems are widely known to offer a low-cost alternative to treat point source nitrogen and phosphorus-rich wastewaters with the additional benefit of nutrients being assimilated into algal biomass (Sutherland et al. 2020). Recently, there has been increasing interest in cultivating freshwater filamentous macroalgae in nutrient rich wastewaters (Hariz et al. 2023b) as macroalgae are typically easier to harvest than microalgae. Additionally, the algal biomass is suitable as a feedstock for product development (Neveux et al. 2020).

The filamentous macroalgal genus *Oedogonium* has been identified as a high performer for bioremediation of wastewater due to its broad ecological distribution, and high productivity (syn. with its capacity to take up nutrients) over varied environmental conditions (Lawton et al. 2021). *Oedogonium* biomass is also a valuable resource with applications in animal feeds (Vucko et al. 2017), biostimulants (Neveux et al. 2020), biochar/biosorbents (Kidgell et al. 2014), and cellulose (Piotrowski et al. 2020). However, the quality of biomass grown in primary effluent may be reduced due to contamination with pathogenic bacteria (e.g. *Campylobacter jejuni*, *Escherichia coli*, *Salmonella* spp. and *Vibrio cholera*) (Chahal et al. 2016), parasitic protozoa (*G. intestinalis* and *Cryptosporidium* spp.) (Berglund et al. 2017) and viruses (Hepatitis A, Hepatitis E, Echovirus and Human calicivirus) (Chahal et al. 2016) limiting the range of socially acceptable products. In this regard, a preliminary disinfection step would be beneficial in a biorefinery process targeting products from the biomass.

In advanced WWTPs microbial pathogens are inactivated during tertiary treatment with chemical oxidation processes and/or UV disinfection. In the context of a cascading biorefinery using primary wastewater-grown biomass it is important to determine if the biomass is adequately disinfected during the processing conditions, in this case, the high temperature and alkali conditions of biostimulant extraction. Biostimulants extracted in this way from *Oedogonium intermedium* were demonstrated to contain proteins, minerals,

and phytohormones, and enhanced adventitious root development in tomatoes and mung beans (Neveux et al. 2020). The decontaminated residual algal biomass could be further exploited to produce other products such as bioethanol and cellulose. Cellulose is used widely in textiles and high-tech materials (e.g., wound dressings, aerogels, and scaffolds for tissue engineering) and is predominantly sourced from wood. Cellulose can also be sourced from grasses, bacteria, and macroalgae, and its phytochemical properties vary depending on the organism's biosynthetic machinery and environmental conditions (Zanchetta et al. 2021). Cellulose from freshwater filamentous macroalgae has unique properties compared to cellulose extracted from terrestrial plants, such as ease of extraction due to lack of lignin (Roesijadi et al. 2010), high crystallinity (Zanchetta et al. 2021), and high specific surface area (Jmel et al. 2019), providing the opportunity to engineer new materials with unique properties and applications. However, the properties of cellulose isolated from *Oedogonium* species grown in primary wastewater, and the influence of biostimulant extraction and drying processes on disinfection and product quality remains unclear.

Therefore, the objectives of this study were to develop a feasible two-product cascading biorefinery suitable for *Oedogonium* grown in primary wastewater. A biostimulant was targeted as the first product in the cascade and to determine if this process would also disinfect the biomass, while a high-quality cellulose was targeted as a second product. The chemical characteristics of the biostimulant are reported, including contents of total dissolved solids, polysaccharides, phytohormones, proteins, ash, and minerals. The effect of drying and biostimulant production on the yield and quality of cellulose isolated from *Oedogonium calcareum* was determined using a range of physicochemical measures.

2.3 Materials and Methods

2.3.1 Materials

Microcrystalline cellulose (MCC) (Product No: 435236), hydrochloric acid (Product No: 258148), sodium chlorite (Product No: 244155), sodium acetate (Product No: S2889), sodium hydroxide (Product No: S5881), sulfuric acid (Product No: 258105), 2-deoxy- d-glucose (Product No: G8270), D-(+)-glucose Product No: D6134), D-(+)-mannose (Product No: M2069), D-(+) galacturonic acid monohydrate (Product No: PHR9231), L-(+) rhamnose (Product No: R3875), fucose (Product No: F2252), D-(+)- xylose (Product

No: X3877), 1-phenyl-3-methyl-5-pyrazolone (PMP) (Product No: M70800), formic acid (Product No: 27001), ammonium solution (Product No: A/3295/pb05), ninhydrin (Product No: N4876), bovine serum albumin (BSA) (Product No: B3883), arginine (Product No: A8094), were purchased from Sigma Aldrich, chloroform (Product No: 200-663-8) was from MERCK and used as received.

2.3.2 Experimental design

This study aimed to assess the effect of biostimulant extraction and drying process of primary wastewater-grown *O. calcareum* biomass on disinfection, yield and quality of cellulose produced. A three-factor experimental design to quantify the effect of three treatments; treatment 1: biomass was either fresh or freeze-dried; treatment 2: biostimulant production, the biomass was extracted with 0.1 M potassium hydroxide; treatment 3: the biomass was either used wet or oven-dried at 40 ºC for 48 hours for cellulose extraction (Figure 2. 2). Note that treatments for T5 and T6 were the same, giving a total of seven discrete treatments per batch of biomass.

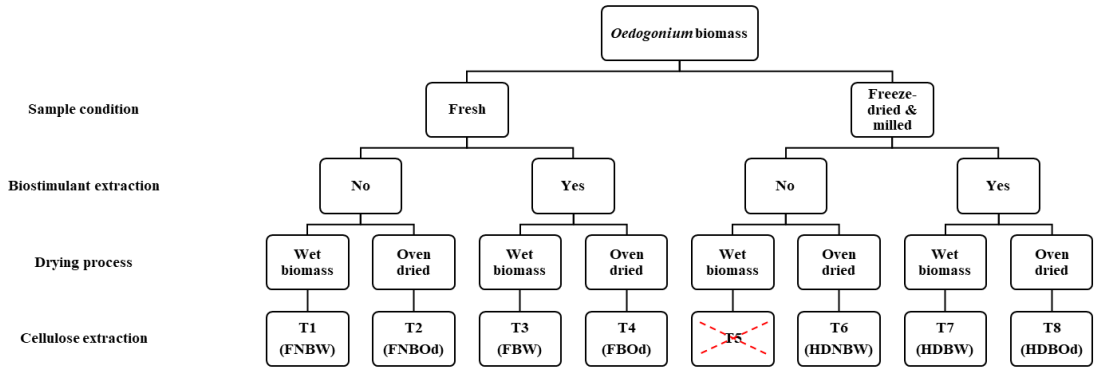

Figure 2. 2 : Experimental Design

To assess the potential use of *Oedogonium* cellulose in materials, characterisation was conducted using Fourier Transform Infrared, X-ray Diffraction and Scanning electron microscopy, and Thermogravimetric Analysis to determine bonding, morphology and thermal stability, respectively.

2.3.3 Cultivation of biomass

In this study, *Oedogonium cf. calcareum* Cleve ex Wittrock 1870 (Lawton et al. 2021) cultures were grown in an outdoor tank under high nutrient loads (14 mg/L of N and 1.2 mg/L of P), at the Facility for Aquaculture Research of Macroalgae at the University of Waikato (UoW), Tauranga, New Zealand. *Oedogonium* samples grown on primary effluent were supplied by National Institute of Water and Atmospheric Research (NIWA), Hamilton, New Zealand to assess the efficacy of biostimulant extraction (alkaline treatment) on disinfection of faecal indicator bacteria and viruses. The ammonia and phosphate concentrations of primary effluent at the NIWA facility were measured fortnightly, and the average concentrations were 40 mg/L and 10 mg/L, respectively. Three batches of *O. calcareum* biomass were cultivated over three consecutive production cycles (2 weeks per cycle). Harvested biomass was subdivided (7 x 100 g fresh weight) and stored in polyethylene resealable bags at -20 ºC prior to processing. Three samples (approximately 100.0 (±) 0.01 grams) from each batch were freeze-dried (Buchi Lyovapor L-200) and milled using a domestic blender (<0.5 mm particle size), and the rest were stored frozen at -20 ºC until further use. The freeze-dried samples were used to determine fresh weight to dry weight ratios (FW: DW) for each harvest of biomass. FW to DW ratios were used to standardise the total solids of biomass in treatments that used fresh biomass to those that used dried biomass.

2.3.4 Biostimulant production

Biostimulant was prepared using a published method (Neveux et al. 2020) with some modifications. Briefly, fresh (100 g) or equivalent mass of milled freeze-dried biomass (~20.0 g) (i.e., always corresponding to a dry weight loading of 2% w: v) was extracted with 1 L of KOH (0.1 M, pH=13) at 70 °C for 3 hours with stirring using a mechanical stirrer at a speed of 400 rpm. The residual biomass was separated from the extract by filtration using a 20-micron mesh and the alkaline liquid extract was stored at -20 °C until further use. The residual biomass was subjected to further processing according to the experimental design (Figure 19) and cellulose production as per section 2.4.

2.3.5 Extraction of cellulose

Cellulose from (20.0 (±) 0.01 g freeze-dried) *O. calcareum* biomass or residual biomass was extracted following the three-step method reported in (Mihranyan et al. 2004b). To achieve satisfactory homogeneity, a mechanical stirrer was used at a speed of 400 rpm. Step 1: biomass was treated with 36.17 g of $NaClO_2$ in 1L of acetate buffer (0.1 M, pH=4) at 60 ^oC for 3 hours. Step 2: Biomass was treated with 1L of NaOH (0.5 M, pH=13) at 60 ^oC for 12 hours. Step 3. Biomass was treated with 1L of HCl (5% w/w, pH=1) heated until boiling, cooled, washed until neutral pH and freeze-dried to obtain cellulose material. Between each step, successive washings of the biomass were carried out until neutral (pH=7) by first separating the solids (centrifugation at 3214 Relative Centrifugal Force (RCF) for 10 minutes) followed by resuspension in reverse osmosis (RO) water and centrifugation again (at 3214 RCF for 10 minutes) to collect the washed solids. The weight of the freeze-dried cellulose was recorded to obtain the yield. The freeze-dried cellulose fractions were stored in sealed plastic bags at room temperature to prevent moisture absorption and degradation until further use.

2.3.6 Characterisation of biostimulant and cellulose products

Elemental analysis (% C, N, and S) was carried out on freeze-dried *O. calcareum* biomass, biostimulant and cellulose samples using Gas Chromatography - Thermal Conductivity Detector and ash content was determined by microashing by OEA labs (http://www.oealabs.com, Callington, UK). Total dissolved solids in biostimulants were determined gravimetrically by weighing the residual solid (mg) from freeze-dried samples of biostimulant (10 mL). Results are reported in mg/mL. Residual biomass samples were analysed for F-specific RNA (fRNA) bacteriophage and *E. coli* at the Institute of Environmental Science and Research, Christchurch. Enumeration of fRNA bacteriophage was carried out using a Single Agar Layer (SAL) technique; Method 1602 (US Environmental Protection Agency 2001) and *Escherichia coli* was enumerated using a pour-plate method.

2.3.6.1 Free amino acids and protein composition of biostimulant extract

Free amino acids (FAA) in the biostimulant extract were analysed by a modified ninhydrin protocol using arginine (2.5- 40 µg/mL) as the standard (Zhu et al. 2009). Biostimulant extract was diluted (dilution factor (DF) of 100) with RO water, and the diluted sample (250 µL) was treated with ninhydrin reagent (250 µL, pH 5.5) prepared as per (Starcher 2001). This solution was then heated at 100 °C for 10 min in a water bath to allow derivatisation. After cooling to room temperature, the derivatised analyte solution (200 µL) was transferred to a polystyrene 96-well plate and the absorbance was measured at 575 nm (Starcher 2001) using a BMG Labtech SPECTROstar Nano. FAA concentrations are reported as µg of FAA/ mL of biostimulant extract. Protein content in the biostimulant extract was analysed using (BSA) as the standard. The diluted biostimulant extracts (DF of 100 with RO water) and the BSA samples (in the range of 15-250 µg/mL) were hydrolysed in NaOH (2.1 mL, 13.5 M) in a heating block at 120 °C for 20 minutes (Zhu et al. 2009). After cooling the samples, hydrolysate (400 µL) was neutralized by adding glacial acetic acid (500 µL). Then, the neutralized samples (250 µL) were treated with ninhydrin reagent (250 µL) and heated in a water bath for 10 minutes at 100 °C and following cooling to room temperature the absorbances of samples were measured as for the FAA described above. The total protein content of biostimulant extracts is reported as µg BSA equivalents / mL of biostimulant extract.

2.3.6.2 Metals analysis

Metal analysis of the biostimulant extracts was performed in helium mode using an Agilent 8900 Inductively Coupled Plasma-Mass Spectrometer (ICP-MS; Agilent Technologies, Santa Clara, California, USA) controlled by MassHunter Workstation (version 4.5). Freeze-dried biostimulant (100 mg) was pre-digested in a mixture of 1 mL of HNO_3 (65%) and 0.4 mL of concentrated H_2O_2 (30%) overnight at room temperature. This mixture was then heated at 80 °C for one hour. A further 0.4 mL aliquot of H_2O_2 was then added and the mixture heating at 80 °C for 30 minutes. The solution was cooled and diluted to 50 mL with RO water. The diluted solution (15 mL) was then filtered using a 0.45-micron filter and analysed using the ICP-MS. Standards of trace elements were prepared using stock standard IV71-A, and the standards of main elements (Ca, Si, P, S,

K, Fe) were prepared using single-element standards (Inorganic Ventures, Christiansburg, VA, USA).

2.3.6.3 Non-targeted Gas chromatography-mass spectrometry (GC-MS) profiling of biostimulant

The freeze-dried biostimulant extracts were analysed following (Rawlinson et al. 2015) to detect phytohormones. Briefly, freeze-dried biostimulant samples and standards (10 mg) were dissolved in NaOH (200 µL ,1% w/v) in a 1.5 mL Eppendorf tube followed by addition of deuterated cinnamic acid (20 µL of 20 µg/mL in methanol), methanol (147 µL) and pyridine (34 µL). The suspension was vortexed for 30 seconds to ensure proper mixing. Into this suspension, 20 µL of methyl chloroformate (MCF) was added and vortexed for 30 seconds. The latter process was repeated before the addition of chloroform (400 µL) and sodium bicarbonate solution (400 µL, 50 mM). This mixture was vortexed for 15 seconds prior to separation of organic and aqueous phases with centrifugation (60 sec at 16,000 g). The organic layer was transferred into a second 1.5 mL Eppendorf centrifuge tube and dried over anhydrous sodium sulfate prior to transferring 100 µL to a 2 mL Shimadzu GC-MS vial fitted with a 250 µL glass insert (CAT number: 226-50523-00). Samples were analysed on a Nexis GC-2030 - Shimadzu gas chromatograph coupled with a single quadrupole mass spectrometer (GCMS-QP2020 NX) using an SH-I-5Sil MS column (30m x 0.25mm x 0.25um). This column is a mid-range polar column, and it was used to detect a wide range of analytes such as amino acids, fatty acids, and phytohormones. The ion source used electron ionisation (EI), and the MS was run in scan mode to identify the analytes. Helium was used as the carrier at a flow rate of 0.96 mL/min. The flow control mode was set to linear velocity, and the pressure was set to 9.0 psi. The injection volume was set to 2 µL in spitless injection mode. The oven temperature for the method was set at 80 ^{o}C, held for 1 min and ramped up to 320 °C at a rate of 10 °C /minute, and held for 2 min. Amino acids, fatty acids, and other compounds, with a similarity index exceeding 85%, were identified in the biostimulant with reference to the GC-MS solution NIST 17 library.

2.3.6.4 Constituent sugar analysis

Cellulose samples (10 mg) were hydrolysed in H_2SO_4 (300 µL, 13M) at 30 °C for 30 min, prior to dilution to 0.72 M H_2SO_4 with Type 1 water and further hydrolysed at 120 °C for 40 minutes (Manns et al. 2014). Hydrolysates were derivatised with PMP as per the protocol by (Rozaklis et al. 2002) with some modifications. Briefly, hydrolysed cellulose (100 µL) was neutralised with NaOH (71.6 µL, 2M) prior to the addition of PMP-derivatising reagent (400 µL), and internal standard 2-Deoxy-glucose (40 µL of 1 mg/mL). The reaction mixture was then heated at 70 °C for 90 min with stirring. On completion the samples were neutralized with formic acid (400 µL, 0.8M), and the excess PMP extracted with $CHCl_3$ (750 µL) prior to centrifugation (5 min at 13,000 g) of the aqueous phase. The aqueous supernatant was transferred to a HPLC vial and analysed with a Shimadzu LC-20AD Prominence fitted with a Restek Raptor C18 column (5 µm particle size, 150 mm x 4.6 mm) with an oven temperature of 30 °C and flow rate of 0.8 mL/min. Samples (5 µL) were injected and fractionated using a gradient elution (25% B 0-15 min, 25-100% B at 15-40 min, 100% B 40-55 min, 25% B 55-60 min) at pH 7 using 0.1 M phosphate buffer in 10 % acetonitrile (v/v) (solvent A) and 0.1 M phosphate buffer in 17 % acetonitrile (v/v) (solvent B). Peak areas were obtained using Shimadzu LabSolutions software. Monosaccharides (fucose, arabinose, rhamnose, galactose, glucose, xylose, mannose, galacturonic acid, glucuronic acid, and iduronic acid) were quantified using response calibration curves of standards with concentrations ranging between 0.05 – 3 mg/mL. The results were reported as w/w% of the anhydrous sugar content.

2.3.6.5 Attenuated total reflectance-Fourier transform infrared spectroscopy (ATR-FTIR)

FTIR spectra (4000 – 400 cm^{-1}) of dried *O. calcareum* and extracted cellulose fractions were recorded at room temperature using a Shimadzu IRSpirit fitted with a QATR-S accessory with an average number of 45 scans per sample. Microcrystalline cellulose (MCC) was used as the reference. The data were ATR and baseline corrected and normalized relative to 1022 cm^{-1} peak using Shimadzu LabSolutions IR software.

2.3.6.6 Scanning electron microscopy (SEM)

The morphology of extracted cellulose was visualised by scanning electron microscopy with a Hitachi Regulus SU8230 FE-SEM. To prepare the freeze-dried cellulose samples for SEM, they were attached to the sample disks using double-sided carbon tape and sputter-coated with fine platinum particles with a Q150V Plus sputter coater.

2.3.6.7 Thermogravimetric analysis (TGA)

The thermal stability of extracted cellulose and MCC was determined using a Netzsch Jupiter STA449 F5 instrument. Samples (10 mg) were analysed in alumina crucibles using a temperature program ranging between 30 - 800 °C with a constant heating rate of 10 °C/min and an argon flow rate of 50mL/min. The ash content was calculated as the weight remaining at the end of the heating program.

2.3.6.8 X-ray diffraction

The crystallinity of extracts of cellulose from *O. calcareum* biomass and MCC was determined using a Panalytical Empyrean XRD using CuKα (λ = 1.54 nm) radiation equipped with a PixCel linear detector. Data was collected over a scan range of 10° - 40° at a step of 0.01° and an equivalent exposure time of 40 s with a voltage and current of 45 kV and 40 mA, respectively. The crystallinity index (CI) of cellulose was calculated according to Equation 1 (Segal et al. 1959) where I_{110} (crystalline peak of cellulose Iα) refers to the intensity of the peak at 2θ ~ 22°, and I_{am} (amorphous region of cellulose) refers to the intensity at 2θ = 18.5°.

Equation 1 :

$$Crystalinity\ index\ (\%) = \frac{I_{110} - I_{am}}{I_{110}} \times 100$$

The algal cellulose data was fitted to a simulated pattern of cellulose Iα (the dominant cellulose polymorph in most macroalgae (Moon et al. 2011; Onyianta et al. 2020)) using HighScore® Plus software. The crystal information file for cellulose Iα was obtained from (Nishiyama et al. 2003). Commercially sourced MCC was analysed under the same conditions as a reference.

2.3.6.9 Statistical analysis

In this study, all experiments were carried out in triplicate using biomass cultivated in three different production cycles (each harvest was 2 weeks apart). Data was analysed using non-parametric permutational multivariate analysis of variance (PERMANOVA) in PRIMER7 software using Euclidian distance resemblance matrices, TYPE III (partial) sum of squares and based on 9,999 unrestricted permutations of raw data (Clarke and Gorley 2015). One-way PERMANOVA was used to test the effect of the biomass condition (fresh or freeze-dried) on the C, N, ash, FAA and protein contents in the biostimulant. To compare the overall effect on the quality of cellulose in terms of purity, yield, chemical composition, and crystallinity index, three-way PERMANOVAs were run with "biomass condition" (fresh or freeze-dried), "biostimulants extraction" (yes/no), and "drying process" (oven dried or wet) as fixed factors. Permutation t-tests were conducted to examine pairwise differences between factors. The measure of effect size (η^2) between factors was calculated using the following equation (Eq. 2), where: SS_{factor} refers to the sum of squares of a particular factor and SS_{total} refers to the total sum of squares.

Equation 2 :

$$\eta 2\ (\%) = \frac{SS_{factor}}{SS_{total}} \times 100$$

2.4 Results and discussion

This study demonstrated the suitability of a cascading biorefinery process to sequentially extract a biostimulant and a high-quality cellulose product from *O. calcareum* biomass cultivated in primary wastewater. The biostimulant was rich in amino acids, fatty acids and minerals, and the extraction process disinfected the residual biomass improving the quality of cellulose obtained.

2.4.1 Biostimulant Characterisation

One of the primary goals of this study was to determine if biostimulant extraction effectively disinfected the remaining wastewater-grown algal biomass. Microbiological

assessment of the remaining algal biomass showed that biostimulant extraction was an effective disinfection step, resulting in levels of fRNA (0 Plaque forming units (PFU)/100 mL) bacteriophage and *E.Coli* (no *E.coli* present) that were below levels of detection. The use of high pH conditions, specifically above pH 12, combined with heat treatments (above 65 °C), has been proven to denature the intact RNA of microbial pathogens below the limit of detection (Lemire et al. 2016). Therefore, this confirms the biostimulant extraction process carried out in 0.1 M KOH (pH=13), is an effective method for disinfecting the biomass, ensuring its safety for further applications.

Full compositional analysis of the biostimulant samples extracted from fresh or freeze-dried biomass are detailed in. Briefly, freeze drying the biomass had no effect on the C, N, ash, and protein content, but did increase the free amino acid content ($p= 0.0496$) (30% lower in the biostimulant produced from fresh than from freeze-dried biomass). The significantly higher free amino acid content observed in the freeze-dried sample is likely due to a result from cellular disruption during the drying process. Freeze-drying mechanically breaks cell walls and membranes, potentially releasing intracellular amino acids that were previously sequestered within protein structures. While the Ninhydrin assay provides a colorimetric approach to amino acid quantification, this method has some limitations. Specifically, Ninhydrin does not exclusively react with α and ε amino groups but also responds to ammonia nitrogen and various free amines (Kerr 1995). Therefore, future research should focus on utilizing analytical techniques such as high-performance liquid chromatography (HPLC) with fluorescence detection. While the recovery of N from the biomass into biostimulant was 16.5%, the nitrogen content (13,800 ppm) of the biostimulants was 9-fold higher than the biostimulant reported by Neveux et al (1,500 ppm) (Neveux et al. 2020), reflecting the exceptionally high nitrogen content of the biomass used here (8.2 – 9.4 % of dw biomass). Potassium made up approximately 93% of the elements detected through ICP-MS, and along with P, S, Ca, Na, Ca, Mg, and Fe made up over 99% of the metals, and this was similar to (Neveux et al. 2020). The high content of ash is a result of the production process (63 % of the total ash resulted from the KOH solution), and while active organic compounds contribute most of the plant growth promoting effects in an algal biostimulant, this inorganic potassium helps regulate the water status of plants, controls photosynthesis through the opening and closing of stomata, and influences meristematic growth (Hernández-Herrera et al. 2014).

Compound identification was conducted using the NIST 17 mass spectral library, with matches requiring a minimum similarity index of 85%. An example of representative mass spectra for both hit and no-hit compounds is presented to illustrate the identification process in Figure A.1 in the appendix. *With the method used here, only* phenyl acetic acid, a known auxin with growth-promoting activity (Cook 2019), *was detected.* Neveux *et al.* reported an auxin-like activity equivalent to 5×10^{-5} M indole-3-butyric acid and the presence of all five major classes of phytohormones (abscisic acid and metabolites, cytokinins, auxins, gibberellins, and ethylene) in their alkali extract of *O. intermedium.* Differences in composition between the biostimulants produced here and in Neveux et al. (2020), are expected, with the current study using a lower biomass loading (2% w/v vs. 5% w/v) and harsher extraction conditions (0.1 M KOH vs. 0.01 M KOH), which were chosen specifically to ensure disinfection of the biomass feedstock. Nevertheless*,* a range of amino acids and fatty acids (Table A 2 in the appendix) demonstrated to be important for plant health and nutrition (Yang et al. 2020) were identified in this study.

In addition to *Oedogonium*, freshwater macroalgae species such as *Cladophora* and *Rhizoclonium* have been identified for their potential in wastewater bioremediation (Hariz et al. 2023b; Zrimec et al. 2022). However, future research should incorporate pure chemical standards for each detected compound. Cross-referencing with pure standards will provide definitive confirmation of the molecular structures present in the *Oedogonium* biostimulant extract, addressing potential misidentification from library matching alone.

Previous research indicates that *Cladophora* species contain high levels of proteins (16% to 21.5% of dry weight), fatty acids comprising 11.71% of dry weight, micro and macro-elements, vitamins and phytohormones, all of which stimulate plant growth (Lewandowska et al. 2022; Nutautaitė et al. 2021). Specifically, *Cladophora glomerata* biostimulant extracts, obtained through ultrasound extraction in distilled water, have demonstrated significant effects on the gowth parameters of soybean and red radish, such as increased yield, root length, and plant height, compared to control conditions (Dziergowska et al. 2021; Lewandowska et al. 2022). Mungmai et al. (2014) reported presence of proteins (0.3 - 0.4 ng/g of crude weight) and a series of amino acids in *Rhizoclonium hieroglyphicum* such as phenylalanine, alanine, proline and serine (Mungmai et al. 2014). *Nevertheless,* a range of amino acids and fatty acids (see supplementary material) demonstrated to be important for plant health and nutrition (Yang et al. 2020) were identified in this study. Furthermore, Stirk et al. have mentioned

that storing the biomass at -20 °C in the dark can preserve the biostimulant properties such as proteins, lipid and fatty acid content the up to fifteen months without a significant decrease (Stirk et al. 2021). This suggests that similar long-term storage conditions could be applicable for the biostimulant produced in this study. Additionally, in line with the regulatory framework, this biostimulant extract would need to comply with the European Union Fertilising Products Regulation (EU) 2019/1009, which recognises products that enhance plant nutrition processes, to fit the macroalgae-derived biostimulant into the established parameters for agricultural application (Kapoore et al. 2021).

2.4.2 Cellulose Characterisation

Cellulose was extracted from the residual (following biostimulant production) biomass or untreated *O. calcareum* biomass using a mild extraction technique that has previously been shown to yield a high purity product (Mihranyan et al. 2004b). The average percentage yield of cellulose was 9.8 ± 0.3 % of the dry weight biomass, ranging from 9.5 -10.1% between treatments which were not statistically different. This is lower than the cellulose contents in an *Oedogonium* sp. (24-58%) grown in municipal wastewater effluent with carbon dioxide supplementation in Minnesota, USA (Piotrowski et al. 2020). However, no quantification of purity and composition (e.g., FTIR, sugar analysis, nitrogen, or ash content), or functional analyses, were performed in that study except for the morphological analysis by SEM, and SEM micrographs of extracted cellulose in that study closely resembles the raw biomass in this study. Higher yields of cellulose have also been reported for other freshwater macroalgae species, e.g., *Chladophora glomerata* (21.6 %) (Xiang et al. 2016). While the contents of cellulose clearly vary between species, growing conditions (seasonal changes/temperature, and CO_2 availability) (Piotrowski et al. 2020) and the maturity of algae (Wahlström et al. 2020) are also important drivers of cellulose content. There were significant differences in the content of C, H and N in the cellulose between treatments due to the starting condition of the biomass (i.e., fresh *vs.* freeze-dried), where the starting condition of the biomass accounted for 25.6%, 26.9%, and 31.4% of the variation of C, H, and N contents of the cellulose fractions, respectively. Cellulose products had a low content of nitrogen (<1%) and ash (<1%) (Table 2. 1), indicating that the pulping and purification processes effectively removed proteins and other biomolecules from the biomass, as well as the salts generated during the pulping process. Consistent with these indicators of purity, the cellulose samples had a high

glucose content (85-90%) and a low mannose content (<0.5%), while other sugars characteristic of hemicellulose, such as xylose, rhamnose, fucose and galactose (Ren and Sun 2010), were not detected. There was no significant difference in the glucose content of the celluloses between the treatments (Table A 6 in the appendix).

Table 2. 1: Yield and quality of cellulose products from each treatment (T) expressed O. calcareum biomass. Yield is expressed as % dry weight biomass (% dw) and quality measures (C, H, N, ash, glucose (Glu) and mannose (Man) as % w/w of cellulose product. Entries are expressed as averages ± standard deviations (n=3). (Treatment abbreviations are as follows F=Fresh, HD= freeze-dried biomass, NB=no biostimulant extraction, B=biostimulant extraction W= wet biomass, Od= oven-dried biomass after biostimulant extraction)

Treatment	Yield	C	H	N	Ash	Glu	Man
	(% dw)	(% w/w)					
T1 (FNBW)	10.0 ± 0.1	45.5 ± 1.2	7.0 ± 0.2	0.40 ± 0.2	0.1 ± 0.1	89.6 ± 0.1	0.4 ± 0.1
T2 (FNBOd)	10.0 ± 0.2	45.0 ± 0.7	6.9 ± 0.1	0.2 ± 0.1	0.1 ± 0.1	85.0 ± 5.2	0.3 ± 0.1
T3 (FBW)	9.5 ± 0.2	44.0 ± 1.2	6.7 ± 0.2	0.2 ± 0.2	<0.1 ± 0.1	87.6 ± 4.5	0.4 ± 0.1
T4 (FBOd)	9.7 ± 0.1	44.8 ± 0.4	6.8 ± 0.1	0.3 ± 0.2	0.1 ± 0.1	87.7 ± 3.6	0.5 ± 0.1
T6 (HDNBW)	9.6 ± 0.1	44.0 ± 1.4	6.7 ± 0.2	0.2 ± 0.1	<0.1 ± 0.1	90.1 ± 1.1	0.4 ± 0.1
T7 (HDBW)	9.5 ± 0.3	43.8 ± 1.3	6.6 ± 0.2	0.2 ± 0.2	0.2 ± 0.1	89.1 ± 3.1	0.4 ± 0.1
T8 (HDBOd)	9.9 ± 0.1	43.2 ± 0.3	6.6 ± 0.1	0.1 ±0.1	0.1 ± 0.1	89.5 ±1.1	0.4 ± 0.1

2.4.2.1 Fourier Transform Infrared (FTIR) analysis.

Cellulose has a unique FTIR fingerprint region in the range of 1800-600 cm^{-1}. To assess the quality of cellulose produced in the current study the FTIR of isolated cellulose fractions were compared with a commercial sample of MCC (Figure 2. 3). All cellulose fractions from *O. calcareum* had absorbances characteristic of cellulose and were highly analogous with the spectrum obtained for MCC (Figure A 1 in the appendix A). All spectra exhibited absorbance peaks in the 3000 to 3500 cm^{-1} region, indicating stretching and bending vibrations due to hydroxyl groups, while the peak at 2896 cm^{-1} was identified as the C-H stretching of methylene groups (Paniz et al. 2020). The O-H bending at 1654 cm^{-1} indicated the presence of absorbed water (Oh et al. 2005). Other peaks characteristic of cellulose included C-H scissoring at 1424 cm^{-1}1, C-H bending at 1363 cm^{-1}, O-H in-plane bending at 1333 cm^{-1}, CH_2 wagging at 1310 cm^{-1}, and C-O-C antisymmetric ring stretching at 1158 cm^{-1}. Furthermore, 1054 cm^{-1} and 1029 cm^{-1} peaks were associated with C-O stretching and C-O deformation at C6, respectively (Paniz et al. 2020). The peak at 898 cm^{-1} is attributed to the C-O-C asymmetric stretch of β-glycosidic linkages (Wahlström et al. 2020).

In addition, the broad band emerging at 2850 cm^{-1} in the untreated algae biomass is attributed to aliphatic chains (e.g., lipids) in algae biomass (Paniz et al. 2020). The absence of the peak at 2850 cm^{-1} in T6-T8 samples indicate successful removal of lipids in algae. Although this peak is not as distinct as in the raw biomass, this peak is still evident in other cellulose samples (T1-T4), indicating incomplete lipid removal during the pre-treatment process.

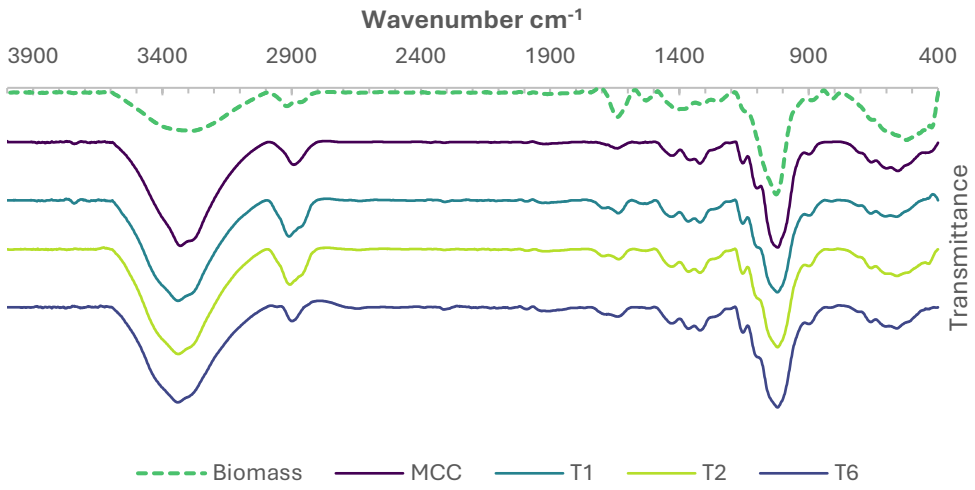

Figure 2. 3 : FTIR spectra of untreated O. calcareum biomass, MCC, and cellulose fractions T1 (FNBW), T2 (FNBOd) and T6 (HDNBW)

2.4.2.2 X-ray diffraction

The crystal structure and crystallinity index of cellulose samples were determined by XRD and compared to MCC. Figure 2. 4 (a) shows diffractograms of cellulose from different treatments of *O. calcareum* overlaid with the diffractogram of MCC. Cellulose is classified as crystalline when its crystallinity index (CI) falls within the range of 40-95%; while cellulose with CI values below this range are classified as amorphous (Quiroz-Castañeda and Folch-Mallol 2013). The crystallinity index of *O. calcareum* (58-65%) was indicative of a moderately high crystallinity index (CI of MCC = 76.2%). These results were higher than the extracted cellulose from Ulva *lactuca* (Wahlström et al. 2020) with a crystallinity index of 48%, but lower than cellulose extracted from *Cladophora rupestris following the method by Siddhanta et al. (Siddhanta et al. 2009) with a crystallinity index of 93.3%.* The proportion of amorphous regions within the *Oedogonium* cellulose may offer an advantage by increasing susceptibility to enzymatic degradation (Ioelovich 2021), potentially enhancing biodegradability and bioconversion processes.

In the current study there was a significant main effect of biostimulant extraction ($p=0.0052$) and a significant interaction effect between biomass condition (i.e., fresh or freeze-dried and milled) and drying process (i.e., oven dried or wet) ($p = 0.0151$) affecting the crystallinity index with biostimulant extraction explaining 18.2 % of the variance and

the interaction 12.5 %. Note that T1 (FNBW) and T2 (FNBOd) cellulose samples without the disinfection step show a split in the peak at 2θ = 21.6° (Figure 2. 4 (b)), possibly due to the presence of silica from diatoms present during cultivation (Flores-Rojas et al. 2021). This shows that the additional step to extract the biostimulant improved the quality of the cellulose produced.

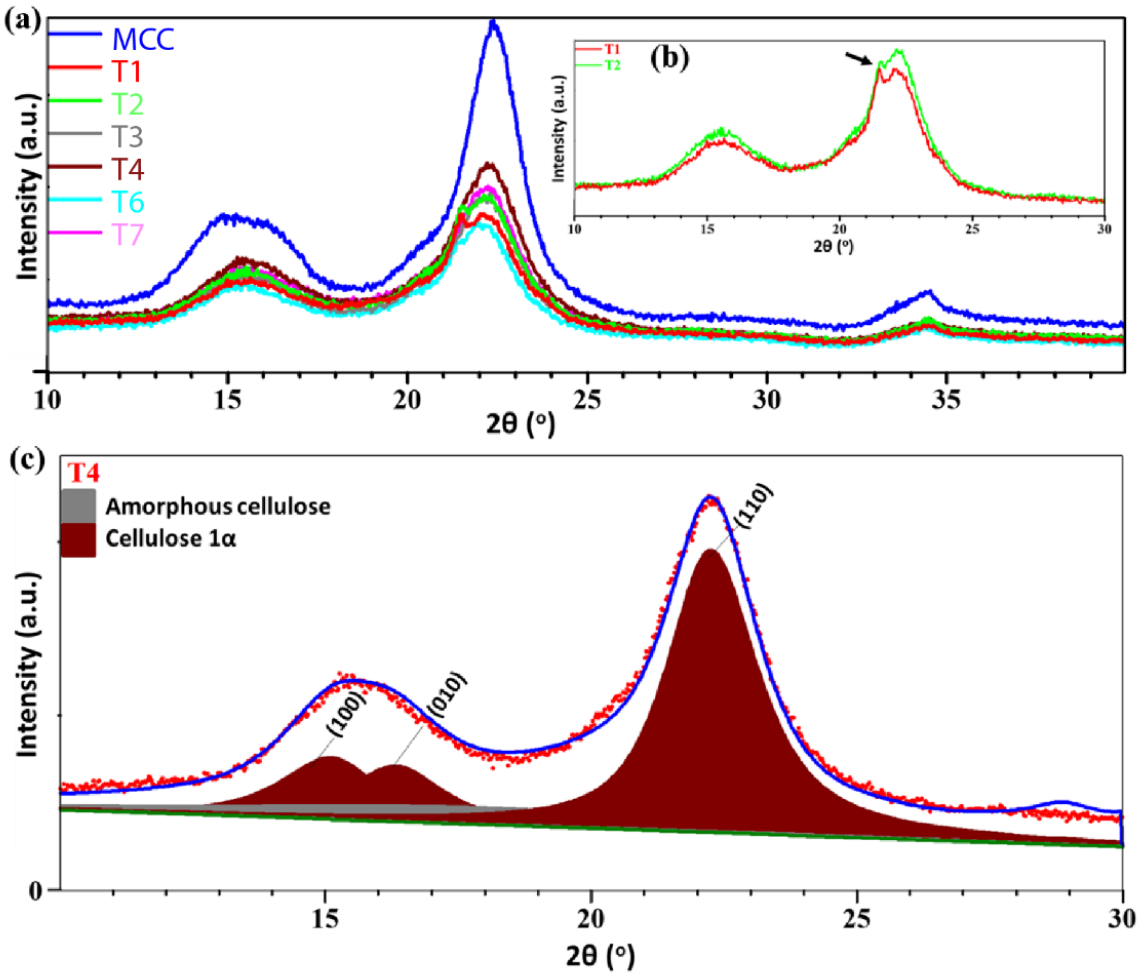

Figure 2. 4 : X-ray diffraction pattern of (a) cellulose samples and MCC. The insert in (b) shows the shoulder peaks of T1 (FNBW) and T2 (FNBOd). (c) Experimental diffraction pattern (red dots) of T4 (FBOd) sample fitted with simulated cellulose 1α structure (blue)

Similar to most other cellulose sources, cellulose from macroalgae consists of cellulose I, containing the polymorphs I_α, with a triclinic crystal structure, and $I_ß$, with a monoclinic crystal structure, typically with a higher proportion of cellulose I_α (Moon et al. 2011; Siddhanta et al. 2009; Siddhanta et al. 2013).Crystallographic data from a previous study was used to model these results with cellulose I_α structure demonstrating the characteristic peaks at 2θ = 16° and 22° and 34°, corresponding to crystal planes of cellulose I_α, (100)/(010) and (110), respectively (French 2014; Nishiyama et al. 2003) (Figure 2. 4 c).

While it is possible to observe a good fit between the experimental pattern (red dots, Figure 2. 4 c) and the modelled profile (blue line, Figure 2. 4 c), cellulose I_{β} may also be present in cellulose samples extracted from *O. calcareum.*

2.4.2.3 Thermal analysis

The raw biomass, extracted cellulose fractions, and MCC were analysed by TGA (Figure 2. 5). The TGA analysis indicated three distinct thermal processes. Primarily, between 50-150 °C there is a weight loss of 5-7 % due to vaporisation of bound water in the *Oedogonium* cellulose samples. In a previous study, the weight loss due to bound and non-freezing water was shown to be negatively correlated with the crystallinity index (Nakamura et al. 1981). The results agree with this, as MCC with a high crystallinity index has a lower content of absorbed water (3 %), and *O. calcareum* cellulose fractions with a lower crystallinity index have higher contents of water. Secondly, a weight loss of 46-55 % w/w was recorded between 250-340 °C due to the thermal degradation of cellulose. Finally, a gradual decline in weight 14-19 % is recorded between 350-600 °C. The most significant mass loss was initiated around 260 °C, showing that *Oedogonium* cellulose is thermally stable up to 260 °C.

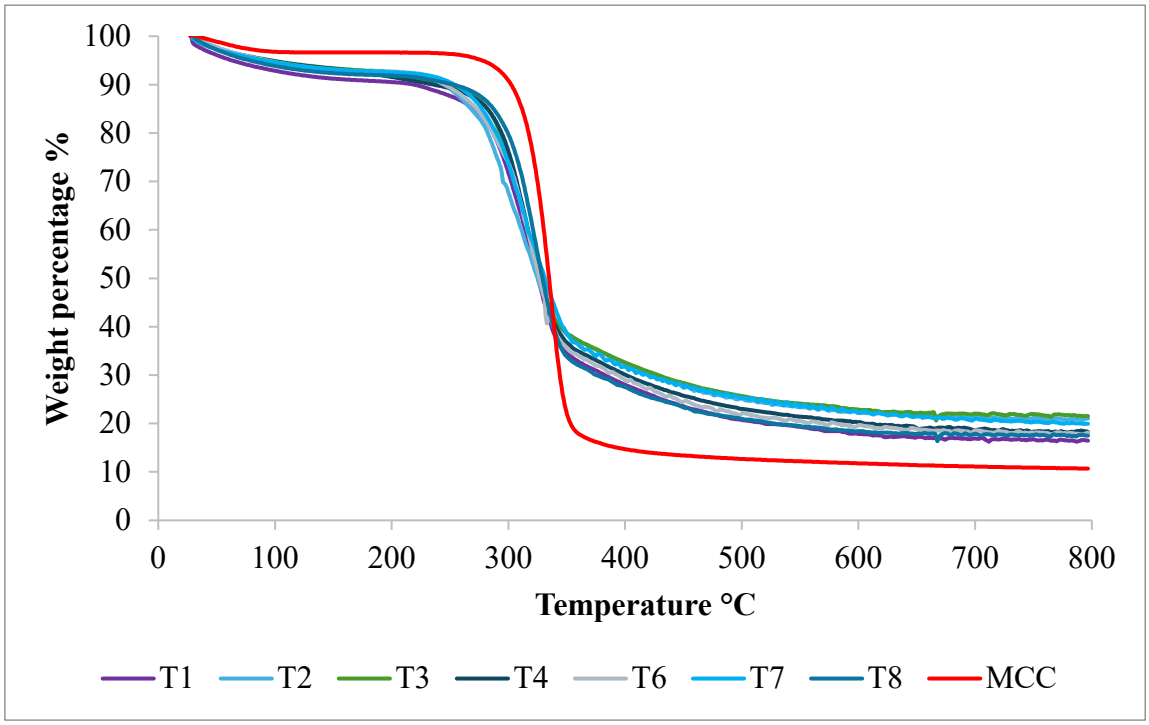

Figure 2. 5 : Thermogravimetric analysis curves of MCC and the representative average of each harvest.

This thermal stability falls towards the lower end found for freshwater macroalgae and seaweeds (260 - 365.7 °C) (Sucaldito and Camacho 2017; Wahlström et al. 2020; Zanchetta et al. 2021). Cellulose extracted from the seaweed *Ulva lactuca* collected along the Swedish west coast showed a thermal stability up to 260 °C (CI= 63%) (Wahlström et al. 2020). However, macroalgal cellulose extracted from the freshwater alga *Cladophora rupestris* grown in a volcanic lake in Philippines had a very high thermal stability of 365.7 ±2.2 °C (CI= 93 %) (Sucaldito and Camacho 2017). The thermal stability has been demonstrated to be proportional to the crystallinity index of cellulose (Wahlström et al. 2020). Therefore, the low thermal stability of the cellulose from *O. calcareum* is in accordance with the measured crystallinity index (65 %).

2.4.2.4 Morphologic characterisation

The morphology of untreated *O. calcecarum* biomass and cellulose extracts was assessed using SEM (Figure 2. 6). Filaments and cell structures of untreated freeze-dried *O. calcecarum* are visible, while in the extracted cellulose fractions, the cell structures are not visible demonstrating that the pulping process is effective in degrading these cell structures. Nanofibril formation requires close packing of molecules which is indicative of purified linear polysaccharides like cellulose (Wahlström et al. 2020). These intertwining fibres form sponge-like aggregate structures with pores on the surface that are likely due to water evaporation during the freeze-drying process.

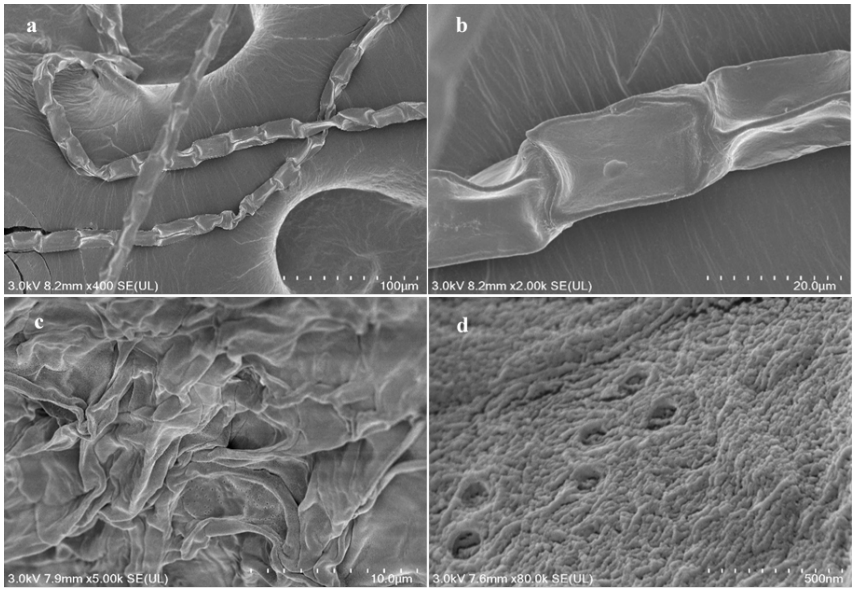

Figure 2. 6 : SEM images of untreated *O. calcareum* biomass at two magnifications (a) x 400 and (b) x 2000, and cellulose extract T8 (HDBOd) at two magnifications (c) x 5000 and (d) x 80,000.

Based on the findings, this two-step process can be seamlessly integrated into the existing small-scale WWTPs; implementing biomass disinfecting methods such as UV oxidation can be impractical due to high implementation and operational costs (Lyu et al. 2020). Therefore, hot alkaline extraction method used in this study may offer a practical approach, disinfecting the biomass directly at the wastewater treatment facility and ensuring safe handling for further use. Furthermore, the biostimulant drying step after biostimulant extraction did not affect the quality of cellulose, which could facilitate dry biomass transport and enhance logistical efficiency. This integration could enhance the value chain of macroalgal wastewater treatment plants and contribute to the circular economy by enabling the recovery of valuable bioproducts from wastewater-grown macroalgae feedstocks. Considering the moderately high crystallinity index, high purity and low ash content, and thermal stability up to 260°C, *O. calcareum* cellulose has promising characteristics for potential use as a biodegradable filler in thermoplastic-based composite materials. In addition, derivatives obtained from *O. calcareum* cellulose, such as microcrystalline cellulose, cellulose nanocrystals and cellulose nanofibres, could also be used for the production of cellulose-based foams and packaging with good barrier properties (Zanchetta et al. 2021). Moreover, future work should focus on pilot-scale studies to evaluate the operational feasibility and scalability of incorporating this biorefinery process into established small-scale WWTPs.

2.4.3 Conclusion

This two-step cascading biorefinery model provides a proof-of-concept to produce disinfected and high-quality bioproducts from wastewater-grown algal biomass. Primarily, this work demonstrated that the extraction of a biostimulant also provides an effective disinfection step for macroalgae grown on primary wastewater. For the first time, the composition and structural characteristics of cellulose from *Oedogonium* were analysed. The cellulose produced had a moderately high crystallinity index and was predominantly cellulose I_{α}. Producing biostimulant and semi-crystalline *Oedogonium* cellulose improves the safe handling of biomass, and provides an alternative source of cellulose, which may be less intensive to extract compared with conventional source.

Chapter 3

Extraction and characterization of cellulose from four selected freshwater macroalgae species grown in a phycoremediation process.

3.1 Abstract:

The four freshwater algae genera, *Rhizoclonium*, *Zygnema*, *Oedogonium* and *Stigeoclonium* are often used in filamentous algae phycoremediation systems. This study explores the potential to use the algal biomass that is produced by the phycoremediation system as a valuable feedstock for cellulose production. Cellulose extraction involved bleaching, alkali treatment and acid hydrolysis, followed by freeze-drying. The characteristics of macroalgae cellulose were assessed in terms of yield, thermal properties, crystallinity index and microstructure. *Oedogonium* had the highest cellulose yield (8.4%), while *Zygnema* had the lowest (2.2%), with *Stigeoclonium* and *Rhizoclonium* yielding 4.8% and 6.9% respectively. *Rhizoclonium* cellulose had a 92% crystallinity index and was thermally stable up to 345°C. X-ray diffraction analysis revealed a unique crystalline structure for *Rhizoclonium* cellulose differing from typical cellulose I patterns but resembling *Cladophora* cellulose. Morphologically, *Rhizoclonium* cellulose exhibited a web-like structure, characteristic of nanofibril formation. Consequently, *Rhizoclonium* grown in phycoremediation systems stands out as a promising sustainable source of cellulose, with high crystallinity, thermal stability and unique nanofibril morphology making it particularly suitable for application as a structural reinforcement in biodegradable composites.

3.2 Introduction

Cellulose is the most abundant macromolecular polysaccharide on earth. It is the main component in parenchyma cells in terrestrial plants (Le Gars et al. 2020) and can also be derived from bacteria (Blaker et al., 2014; Le Bras et al., 2015), tunicates, (Nechyporchuk et al. 2016) and algae (Moon et al. 2011; Nechyporchuk et al. 2016; Trache et al. 2020).

Cellulose is made of glucose units linked together by beta-1,4 glycosidic bonds (Moon et al., 2011) and it is renewable and non-toxic leading to its diverse applications across multiple industries (Bhaladhare and Das 2022).

In the biomedical field, cellulose has been used as a drug carrier and thickening agent in compounded medicines leading to the development of drug-loaded cellulose-based bandages and dressing materials to cover burns (Du et al. 2019; Seddiqi et al. 2021). Flexible and biodegradable cellulose films have been used to protect agricultural crops through improved thermal management (Chen et al. 2023). In the packaging industry, cellulose is being developed into biodegradable food packaging materials with good barrier properties, addressing environmental concerns related to waste and sustainable packaging (Liu et al. 2021b).

Many industries are working to replace petrochemical based plastic with biodegradable and/or bioderived alternatives. As a result, bioplastics have gained increasing attention over the recent decades, along with the use of natural fibres to replace conventional reinforcing materials such as glass and carbon fibres (Prasad et al. 2024). Through further processing, cellulose can also be converted to nano-cellulose, where at least one dimension is shorter than 100 nm (Huang et al., 2018). Nanocellulose stands out as a favourable reinforcing filler material (Börjesson & Westman, 2015) due to its high tensile strength, high aspect ratio, high stiffness, light weight, and renewability (Amara et al. 2021; Gan et al. 2020). These properties are advantageous for applications requiring lightweight and strong materials, such as packaging and bio composites. Nano-cellulose can also be used as a reinforcement for bioplastics, and recent studies have examined its performance in materials such as polylactic acid (Trifol et al.) (Wahib et al. 2022), polyhydroxyalkanoates (PHA) (Mármol et al. 2020) and polyhydroxy butyrate (PHB) (Panaitescu et al. 2020). There has been recent interest in using cellulose in additive manufacturing for 3D printing applications due to its potential for enhancing the mechanical and thermal properties of biocomposites when combined with materials like polylactic acid (Gauss and Pickering 2023). . Moreover, the application of cellulose nanofibers extends to the cement industry, where it has been used as a reinforcement filler for more durable cement composites. A 5% of addition by cement weight significantly improved compressive strength by 43%, flexural modulus by 71% and toughness by 192% (Das et al., 2021).

With the recent advances in cellulose applications, it is important to explore novel sources of cellulose and their properties. The physicochemical properties of cellulose, such as crystallinity, crystal structure, morphology, and aspect ratio, depend on the cellulose source and the extraction process (Wahib et al. 2022). Therefore, it is important to explore alternative sources of cellulose to understand how different sources could influence these properties.

Macroalgal-derived cellulose offers several advantages over plant-derived cellulose, including typically having high crystallinity, thermal stability, and ease of extraction due to the absence of lignin, requiring only mild extraction conditions (Wahlström et al. 2020). Additionally, cellulose materials obtained from various macroalgal genera exhibit distinct structural and physicochemical properties and are more diverse than terrestrial plant cellulose (Koyama et al. 1997; Piotrowski et al. 2020; Zanchetta et al. 2021). For instance, crystallinity index of plant-derived native cellulose usually varies from 40-70% (Trache et al. 2020). Cellulose extracted from the Antarctic algae species *Cystosphaera jacquinottii* exhibited a crystallinity of 70% (Paniz et al. 2020) whereas that of the marine algal species *Cladophora* and *Valonia* is exceptionally high at 95% (Mihranyan 2011),

Freshwater filamentous macroalgae biomass cultivated during phycoremediation may provide a sustainable source of cellulose. The cellulose content in freshwater algae typically ranges from 1-15% of dry weight (Ramachandra and Hebbale 2020), depending on growth conditions and species. Freshwater macroalgae have other advantages such as rapid growth rate (Ge et al. 2018), ability to grow in a variety of wastewaters (Hariz et al. 2023b) and are easier to harvest compared to terrestrial plants due to their accessibility and the ability to be continuously harvested without disturbing their growth cycle (Alam et al. 2021). The full utilisation of macroalgae cultivated in wastewater for valuable products, such as cellulose, remains largely untapped however (Jayasooriya et al. 2024).

While there is some research on the extraction and properties of cellulose from marine algae, there is a noticeable lack of research on cellulose from freshwater filamentous algae, particularly those suitable for phycoremediation purposes. Jayasooriya et al. (2024) proposed a low-cost biostimulant extraction technique (using hot alkali) that disinfected the macroalgae biomass before processing into cellulose. This method effectively removes the risk of the macroalgal biomass being contaminated with harmful bacteria and viruses, while also preserving the physicochemical properties of the cellulose and

facilitating its extraction (Jayasooriya et al. 2024). The objective of the present study was to extract and fully characterize cellulose from the four genera of wastewater grown filamentous algae: *Rhizoclonium*, *Zygnema*, *Oedogonium* and *Stigeoclonium* and highlight the potential use in biocomposites.

3.3 Methods

3.3.1 Materials

Microcrystalline cellulose (MCC) (Product No: 435236), hydrochloric acid (Product No: 258148), sodium chlorite (Product No: 244155), sodium acetate (Product No: S2889), sodium hydroxide (Product No: S5881), sulfuric acid (Product No: 258105), 2-Deoxy-d-glucose (Product No: G8270), D-(+)-glucose Product No: D6134), D-(+)-mannose (Product No: M2069), D-(+) galacturonic acid monohydrate (Product No: PHR9231), L-(+) rhamnose (Product No: R3875), Fucose (Product No: F2252), D-(+)- xylose (Product No: X3877), 1-phenyl-3-methyl-5-pyrazolone (PMP) (Product No: M70800), formic acid (Product No: 27001), ammonium solution (Product No: A/3295/pb05), arginine (Product No: A8094), were purchased from Sigma Aldrich, and chloroform (Product No: 200-663-8) was purchased from MERCK. All the chemicals were used as received.

3.3.2 Algae species selection, description, and cultivation

Four filamentous macroalgae species native to New Zealand, that are commonly found in phycoremediation systems were chosen for this study. The algae strains used in this study were sourced from National Institute of Water and Atmospheric Research (NIWA) in Hamilton, New Zealand. The algae cultures were grown in indoor tanks under controlled conditions (light intensity above the water level 350 umol) on a growth media with nutrient concentrations representative of a wastewater treatment pond (14 mg/L of nitrate N and 1.2 mg/L of P, added weekly), at the Facility for Aquaculture Research of Macroalgae (Chen et al.) at the University of Waikato (UoW), Tauranga, New Zealand. For each species, three batches of algae biomass were cultivated over three consecutive production cycles (2 weeks per cycle). After harvesting, 100 grams of fresh weight from each species were freeze-dried (Buchi Lyovapor L-200) and then powdered using a domestic blender.

3.3.3 Extraction of cellulose

Cellulose was extracted from the macroalgae biomass according to the 3-step protocol reported in (Mihranyan et al. 2004b). Between each step, the biomass was strained and thoroughly washed with water until reaching neutral pH (7) to remove any residual chemicals. Step 1: the powdered freeze-dried biomass (10 g) was treated with 18.08 g of $NaClO_2$ in 500 mL of acetate buffer (0.1 M, pH=4) at 60 ºC for 3 hours using a magnetic stirrer with a hotplate. Step 2: the biomass was treated with 500 mL of NaOH (0.5 M, pH=13) at 60 ºC for 16 hours. Step 3 the biomass was treated with 500 mL of HCl (5% w/w, pH=1), heated until boiling point, cooled, and again washed to obtain cellulose material at neutral pH. The insoluble fraction was equally distributed in 450 mL centrifuge buckets and mixed thoroughly with water until the solid was re-suspended. Then the solution was centrifuged using a 5810 R - Benchtop Centrifuge at 3214 relative centrifugal force for 15 minutes, and the supernatant was decanted. The cellulose material was then freeze-dried, and the total yield of cellulose was determined gravimetrically by calculating the ratio of the weight of freeze-dried cellulose to the original weight of the freeze-dried algal biomass.

3.3.4 Elemental analysis of cellulose fractions

Elemental analysis (% C, H, N) was carried out on fractions of freeze-dried cellulose using gas chromatography with thermal conductivity detector (GC-TCD) and ash content was determined by microashing. Both analyses were conducted at OEA labs (http://www.oealabs.com, Callington, UK).

3.3.5 Constituent sugar analysis by HPLC

The constituent sugars of cellulose fractions were determined according to a modified method described (Rozaklis et al. 2002). Cellulose fractions (~10 mg) were hydrolysed in H_2SO_4 (13M, 300 µL) at 30 ºC for 30 min, then diluted to 0.72 M H_2SO_4 with Type 1 water and heated at 100 ºC for 3 hours (Manns et al. 2014). Samples (100 µL) of the sugar hydrolysates were then neutralised with 2M NaOH (71.6 µL), and then mixed with the internal standard 2-Deoxy-glucose (40 µL of 1 mg/mL) and then the derivatization agent 1-phenyl-3-methyl-5-pyrazolone (PMP) (400 µL). The reaction mixture was then heated at 70 ºC for 90 min with constant stirring. Upon completion, formic acid (400 µL, 0.8 M)

was added to neutralize and the excess PMP was extracted with $CHCl_3$ (750 µL). The samples were then centrifuged for 5 minutes at 13,000 rcf. Following that, samples were transferred to HPLC vials and analysed with a Shimadzu LC-20AD Prominence fitted with a Restek Raptor C18 column (5 µm particle size, 150 mm x 4.6 mm) with an oven temperature of 30 ºC and flow rate of 0.8 mL/min. Samples (5 µL) were injected and fractionated using a gradient elution (25% B 0-15 min, 25-100% B at 15-40 min, 100% B 40-55 min, 25% B 55-60 min) at pH 7 using 0.1 M phosphate buffer in 10% acetonitrile (solvent A) and 0.1 M phosphate buffer in 17% acetonitrile (solvent B). Peak areas were obtained using Shimadzu lab solutions software. Monosaccharides (fucose, rhamnose, galactose, glucose, xylose, mannose, galacturonic acid, glucuronic acid) were quantified using response calibration curves of standards with concentrations ranging 0.05 – 3 mg/mL.

3.3.6 Fourier transform-infrared (FTIR) analysis

The freeze-dried algae biomass, and cellulose fractions were characterized by FTIR spectra in the range 4000-400 cm^{-1} at room temperature using a Shimadzu IRSpirit fitted with a QATR-S accessory with an average number of 45 scans per sample. MCC was used as the reference. The data were ATR and baseline corrected and normalized using Shimadzu LabSolutions IR software.

3.3.7 X-ray diffraction (XRD)

The X-ray diffraction (XRD) measurements were performed on cellulose extracts from algae biomass using a Panalytical Empyrean XRD using CuKα (λ = 1.54 nm) radiation equipped with a PixCel linear detector. The diffraction patterns were measured over a 2θ scan range of 10-40° at a step of 0.01° and an equivalent exposure time of 40 s. The voltage and current were set to 45 kV and 40 mA, respectively. The crystallinity index of the cellulose fractions was calculated according to the following equation (Segal et al. 1959):

$$Crystalinity\ index\ (\%) = \frac{I_{110} - I_{am}}{I_{110}} \times 100$$

where I_{110} (crystalline peak of cellulose Iα) refers to the intensity of the peak at 2θ ~ 22°, and I_{am} (amorphous region of cellulose) refers to the intensity at 2θ = 18.5°. Commercially sourced MCC was analysed under the same conditions as a reference.

The full width at half maximum (FWHM) of each cellulose peak was determined using Origin software (OriginPro 2023, OriginLab Corporation). Peak analysis was conducted by fitting the diffraction peaks with a Gaussian function to measure the FWHM.

The crystallite sizes (τ) of algae cellulose samples were calculated using the Scherrer equation (Nam et al. 2016):

Equation 3 :

$$\tau = \frac{K \ \lambda}{\beta \cos \theta}$$

where K is the correction factor (0.9), λ is the wavelength of the X-ray radiation (0.15406 nm), β is the full width at half maximum (FWHM) of the diffraction peak in radians, and θ is the diffraction angle of the peak (~ 22°).

The d-spacings of Rhizoclonium cellulose were calculated using Bragg's Law: d = λ/(2 * sin(θ)) where λ = 0.15406 nm (Cu-Kα). The dominant cellulose I type was determined using the methodology reported by (Wada and Okano 2001).

3.3.8 Thermogravimetric analysis (TGA)

The thermal stability of extracted cellulose fractions was determined using a PerkinElmer STA 8000 instrument in terms of thermogravimetric analysis (TGA) and derivative thermogravimetric analysis. Samples (10 mg) were analysed in alumina crucibles using a temperature program ranging 30 - 600ºC with a constant heating rate of 10ºC/min under argon atmosphere at a flow rate of 50 mL/min. The ash content was calculated as the weight remaining at the end of the heating program.

3.3.9 Surface morphology analysis

Surface morphology analysis was carried out using scanning electron microscopy images of cellulose fractions and raw milled algae were obtained using a Hitachi Regulus SU8230 FE-SEM. The freeze-dried samples were sputter coated with fine platinum particles with a Q150V plus sputter coater to prevent charging. The images were obtained at 5kV.

3.4 Results and Discussion

The filamentous macroalgae species used in this study were easily identified by their morphology under microscopic observation (Figure B.1 in the appendix B) and comparison with taxanomic keys: *Rhizoclonium* (sparcely branched filaments, of large cells) *Zygnema* (unbranched filaments of smaller cells), *Oedogonium* (unbranched filaments of smaller cells often with several ringlike caps in the cross walls), and *Stigeoclonium* (branched filaments with pointed apical cells) (National Institute of Water and Atmospheric Research 2019).

Freeze-dried algae biomass of each species was subjected to a mild sequential extraction process involving bleaching, alkali treatment and acid hydrolysis to isolate cellulose following a published protocol for green macroalgae (Mihranyan et al. 2004b). Over the three harvests *Oedogonium.sp* had the highest cellulose yield (8.5 ± 0.2 %), followed by *Rhizoclonium.sp* (6.9 ± 0.2) and *Stigeoclonium.sp* (4.8 ± 0.5), and then *Zygnema.sp* (2.2 ± 0.5%) (Table 3.2). These dry-weight percentage yields of cellulose fall within the range (1-32%) found in previous studies for marine and freshwater macroalgae (Piotrowski et al. 2020; Siddhanta et al. 2009; Wahlström et al. 2020). The cellulose yields of the species used in this study were towards the lower end, but are likely not representative of the highest yield attainable since cellulose yields can vary depending on several factors such as growth conditions (seasonal changes in light and temperature, and CO_2 availability), the maturity of cell wall as well as the genetic variation between species (Piotrowski et al. 2020; Wahlström et al. 2020). Therefore, these yields do not provide an indication of the quality of the cellulose extracts.

3.4.1 Fourier transform-infrared (FTIR) analysis

The FT-IR spectra of the algae species, the extracted cellulose, and reference sample microcrystalline cellulose (MCC) are shown in Figure 3.1. The broad bands emerging at 2927 $cm^{-1}$and 2850 cm^{-1} for the algae biomass samples are associated with the presence of aliphatic chains, particularly lipids (Paniz et al. 2020). A noticeable difference between the algae samples and the cellulose fractions can be observed in the range of 1800-600 cm^{-1}. In the algae samples, the two distinct peaks at 1637 cm^{-1} and 1530 cm^{-1} are attributed to C=O stretching, N-H bending and C-N stretching in amide complexes indicative of proteins respectively (Bartošová et al. 2015; Wahlström et al. 2020). Additionally, the

dried algae biomass did not present any of the characteristic cellulose bands as the cellulose was still enclosed within the hemicellulose cell.

All the extracted cellulose fractions demonstrated peaks characteristic of polysaccharides (Table 3.1). The broad bands at 3500-3000 cm^{-1} and 1640 cm^{-1} refer to OH stretching and bending vibrations of absorbed water molecules (Oh et al. 2005). The *Rhizoclonium* cellulose had a much narrower band in the range (3500-3000 cm^{-1}) compared with the other cellulose fractions. Additionally, the absence of a distinct peak at 1640 cm^{-1} suggests that *Rhizoclonium* cellulose absorbed less water compared to other cellulose materials (Oh et al. 2005). The band between 3000-2800 cm^{-1} is distinctive to the asymmetric stretches of CH, CH2, and CH3 groups and found in all cellulose fractions.

The two bands at 1424 cm^{-1} and 1310 cm^{-1} are present in all cellulose fractions due to CH_2 symmetric stretching and wagging, respectively. In addition, the peaks observed exclusively in cellulose samples at 1363 cm^{-1} and 1333 cm^{-1} can be attributed to the bending of CH bonds and OH bonds at positions C(2) or C(3), respectively.

The characteristic region for FTIR analysis of carbohydrates lies between 1200-800 cm-1 (Paniz et al. 2020; Wiercigroch et al. 2017). Intense peaks can be observed within this wavelength range in the cellulose spectra, whereas the algae biomass spectra had weak peaks and shifted wavenumbers indicating differences in the structural composition of the freeze-dried algae compared to the extracted cellulose. The *Oedogonium*, *Rhizoclonium* and *Zygnema* cellulose fractions all had the characteristic bands of cellulose I occurring at 1430, 1160, 1106 and 890 cm-1 (Paniz et al. 2020), suggesting that the cellulose extracted from these three macroalgae closely resembles MCC obtained from plants Jayasooriya et al. (2024). The *Stigeoclonium* cellulose, however, did not show a peak at 1106 cm^{-1} corresponding to C-O stretch/ C-C stretch which may indicate variations in the cellulose crystalline structure specific to *Stigeoclonium.sp*.

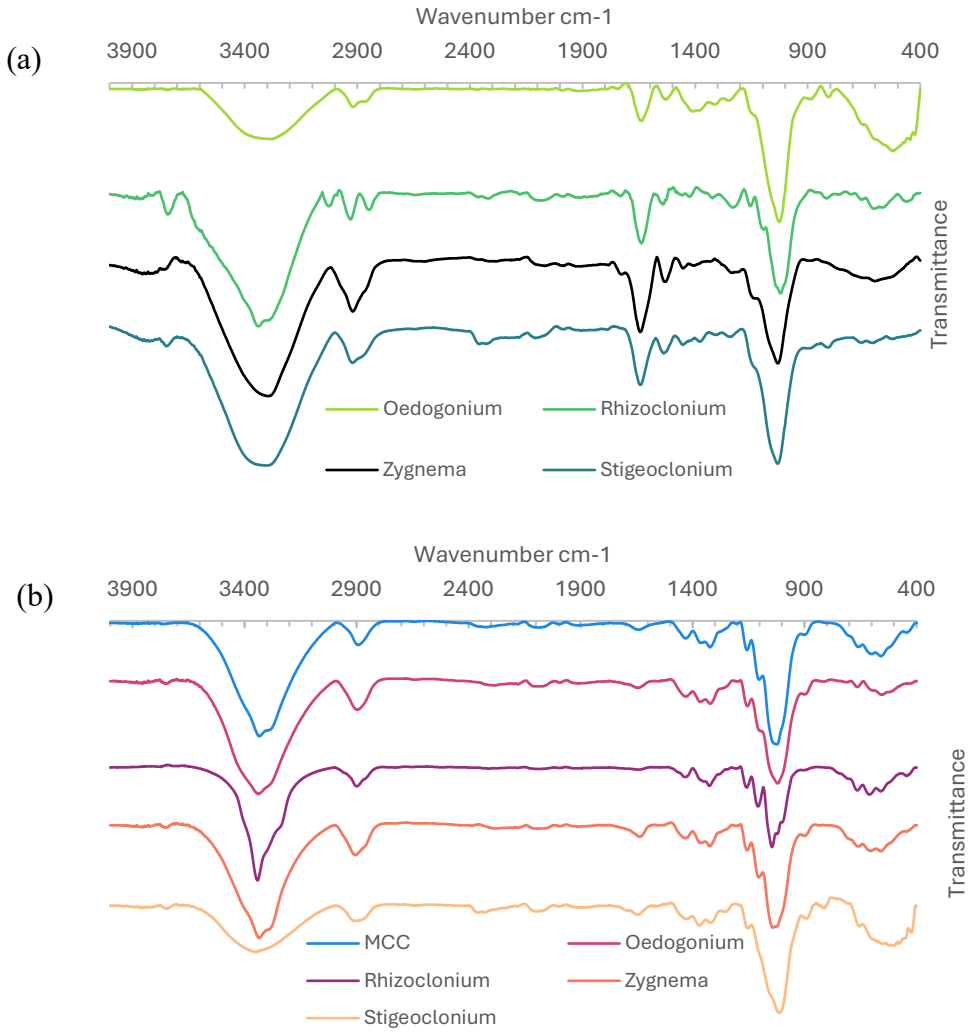

Figure 3. 1 : (a) FTIR spectra of freeze-dried algae biomasses (b) FTIR spectra of MCC, and cellulose fractions of *Rhizoclonium*, *Zygnema, Oedogonium*, and *Stigeoclonium*

Based on the FTIR peak assignments discussed previously, the following can be concluded regarding the efficacy of the cellulose extraction process. The peak at 2850 cm^{-1} was absent in *Oedogonium* and *Rhizoclonium* cellulose fractions indicating lipids were removed during the extraction process. However, this peak was present in *Zygnema* and *Stigeoclonium* cellulose fractions indicating incomplete lipid removal during the extraction process. The absence of a peak at 1530 cm^{-1} in the cellulose fractions indicates the successful removal of proteins. The peak at 1637 cm^{-1} is caused by amide complexes was distinct in the raw biomass, but was only slightly visible in the cellulose fractions. This residual presence of amide complexes might explain the minute amounts of nitrogen detected in the elemental analysis (Table 3.2).

Table 3. 1 : FTIR absorbance peaks in cellulose, their bond assignment, and functional group attributed to each specific peak. (*The abbreviations for cellulose fractions are as follows: Oed= Oedogonium, Rhiz= Rhizoclonium, Zyg= Zygnema, Stig=Stigeoclonium*)

Assignment	**Functional group / sugar**	**Macroalgae cellulose absorbance (cm^{-1})**				**References**
		Oed	*Rhiz*	*Zyg*	*Stig*	
OH	Hydroxyl groups/ monosaccharides	3336	3340	3333	3349	(Halib et al. 2012; Paniz et al. 2020; Wahlström et al. 2020)
–OH stretching	Hydroxyl groups	-	-	3289	-	(Somord et al. 2018)
C-H stretching	Methylene groups	2890	2897	2905	2902	(Halib et al. 2012)
C=O	COOH or Acetate esters /Xylan	-	-	-	-	(Higgins et al. 1961)
O-H bending	Adsorbed water	1640	-	1633	1640	(Oh et al. 2005)
C-H scissoring	Cellulose	1427	1428	1427	1424	(Higgins et al. 1961)
C-H bending	Cellulose	1364	1363	1364	1364	(Paniz et al. 2020)
O-H in plane bending	Cellulose	1337	1337	1337	1339	(Paniz et al. 2020)
CH2 wagging	Cellulose	1316	1319	1320	1316	(Higgins et al. 1961)
C-O-C antisymmetric ring stretch	Cellulose	1153	1156	1154	1152	(Paniz et al. 2020)
Antisymmetric ring stretch	C-O stretch/ C-C stretch	1102	1106	1103	-	(Higgins et al. 1961)
C-O stretch at C6	Cellulose	1017	1043	1040	1014	(Paniz et al. 2020)
C-O deformation at C6	Cellulose					(Oh et al. 2005; Paniz et al. 2020)
C-O-C asymmetric stretch	β-glycosidic linkage	899	893	890	896	(Paniz et al. 2020)

3.4.2 Elemental and Sugar Analysis

The nitrogen content of all cellulose fractions was low (<0.5 %), indicating the successful removal of the majority of proteins during cellulose extraction (Table 3). The carbon content of all cellulose samples varied between 41 and 44%, and these results are consistent with the range (40-44%) reported for cellulose from other plant-derived sources (Gupta et al., 2016), indicating successful extraction and high purity. The elemental analysis results and low ash percentages indicate that all cellulose fractions have high purity. Another measure of cellulose purity is the glucose content, as cellulose is made up of anhydro glucose units (Moon et al. 2011) The cellulose glucose percentage was highest for *Rhizoclonium* (83% w/w) *followed by Oedogonium* (74%), and *Zygnema* (70%) and then *Stigeoclonium* (66.5%).

Table 3. 2 : Average percentage yield of cellulose, C, H, N, ash, glucose, and mannose composition of cellulose samples extracted from the four freshwater macroalgae species.

Macroalgae *sp.*	**Yield %**	**N%**	**C%**	**H%**	**Ash%**	**Glucose %**	**Mannose %**
Rhizoclonium.sp	6.9 ± 0.2	0.09± 0.1	41.3 ± 3.9	5.9 ± 0.6	0.5 ± 0.6	83.8 ± 0.3	12.0 ± 0.2
Zygnema.sp	2.2 ± 0.5	0.38 ± 0.1	43.6± 0.5	6.7± 0.1	0.5± 0.5	69.8 ±0.6	0.3 ± 0.1
Oedogonium.sp	8.5 ± 0.2	0.08 ± 0.1	42.5 ± 0.2	6.5 ± 0.1	0.3 ± 0.1	74.1 ± 0.6	1.2 ± 0.2
Stigeoclonium.sp	4.8 ± 0.5	0.07± 0.1	41.2± 0.1	6.4 ± 0.1	0.1± 0.1	66.5 ± 5.8	10.4 ± 6.1

3.4.3 Morphologic characterisation

The SEM images of cellulose from *Rhizoclonium.sp*, *Zygnema.sp*, *Oedogonium.sp*, and *Stigeoclonium.sp* are demonstrated in Figure 3.2. *Rhizoclonium* cellulose, when viewed at low magnification, has bundles of cellulose fibres. At higher magnification, the SEM image (Figure 3.2a) shows numerous nanofibrils forming web-like networks, similar to the fibrous network structure observed in previous studies on *Cladophora* cellulose (Mihranyan 2011; Sucaldito and Camacho 2017). The presence of this nanofibril formation implies the close packing of molecules, characteristic of purified linear polysaccharides (Wahlström et al. 2020). *Zygnema* cellulose had a sponge-like structure but on closer examination at 20,000x magnification, fine fibres were observed (Fig. 3b). Neither *Stigeoclonium* nor *Oedogonium* cellulose had any noticeable fibre-like structures.

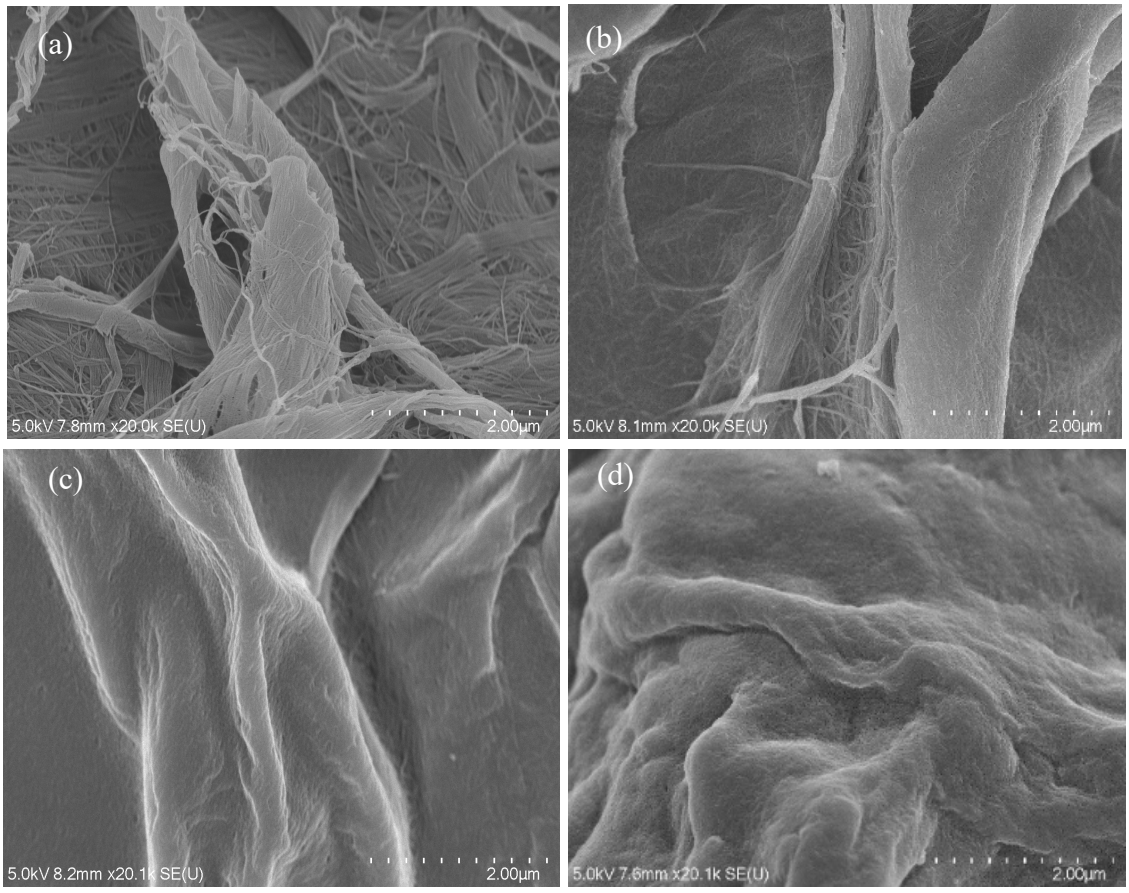

Figure 3.2: SEM images (2 µm scale bar) of cellulose from (a) *Rhizoclonium* (b) *Zygnema* (c) *Oedogonium* (d) *Stigeoclonium*.

3.4.4 X-ray diffraction

Figure 3.3 shows the diffractograms of cellulose from the four species determined by XRD. The results demonstrate distinct differences in XRD patterns and crystallinity indices among the four macroalgae cellulose fractions. All cellulose fractions show a major peak at 2θ=22.2° which corresponds to the crystalline structure of cellulose I.

Rhizoclonium cellulose (Figure 3.3 a) demonstrated a unique XRD pattern similar to Cladophora cellulose and bacterial cellulose which are not typically found in cellulose from higher plants (Mihranyan 2011; Zhou et al. 2019). Specifically, the XRD pattern of Cladophora cellulose has well-defined and narrow peaks at 2θ values of 14° and 16° (Sucaldito and Camacho 2017). Typically, in cellulose I structures, the peaks at 2θ = 14° and 2θ = 16°, corresponding to the crystallographic planes (100) and (010) for cellulose Iα and (1-10) and (110) for cellulose Iβ, respectively, are often observed as a single, convoluted peak due to the proximity of these planes (Huang et al. 2019). The distinct separation of these peaks in Rhizoclonium cellulose indicates a higher degree of crystallinity and a more precise alignment of cellulose chains along these crystallographic planes.

Algal cellulose are typically composed of both cellulose Iα and cellulose Iβ polymorphs with Iα as the predominant form, while plant cellulose is predominantly composed of cellulose Iβ (Koyama et al. 1997). To further characterise the unique crystalline structure of Rhizoclonium cellulose, the method developed by Wada et al. was used to distinguish cellulose allomorphs (Wada et al. 2001). This approach utilises d-spacing values from X-ray diffraction peaks to classify cellulose types into algal-bacterial (Iα-rich) or cotton-ramie (Iβ-dominant) types. For Rhizoclonium cellulose, the calculated d-spacing values for the distinctive peaks at 14°, 16° and 22° (d_1 = 0.611 nm, d_2 = 0.531 nm, and d_3 = 0.391 nm) were similar to those observed for Valonia algae cellulose (Wada et al. 2001). Using the function defined by Wada et al., $Z = 1693d_1 - 902d_2 - 549$, the resulting Z value of Z = 6.3 (Z>0) suggests that Rhizoclonium cellulose has an Iα-rich cellulose allomorph composition. This method provides a quantitative basis for previous structural observations, offering deeper insights into the unique crystalline arrangement of Rhizoclonium cellulose.

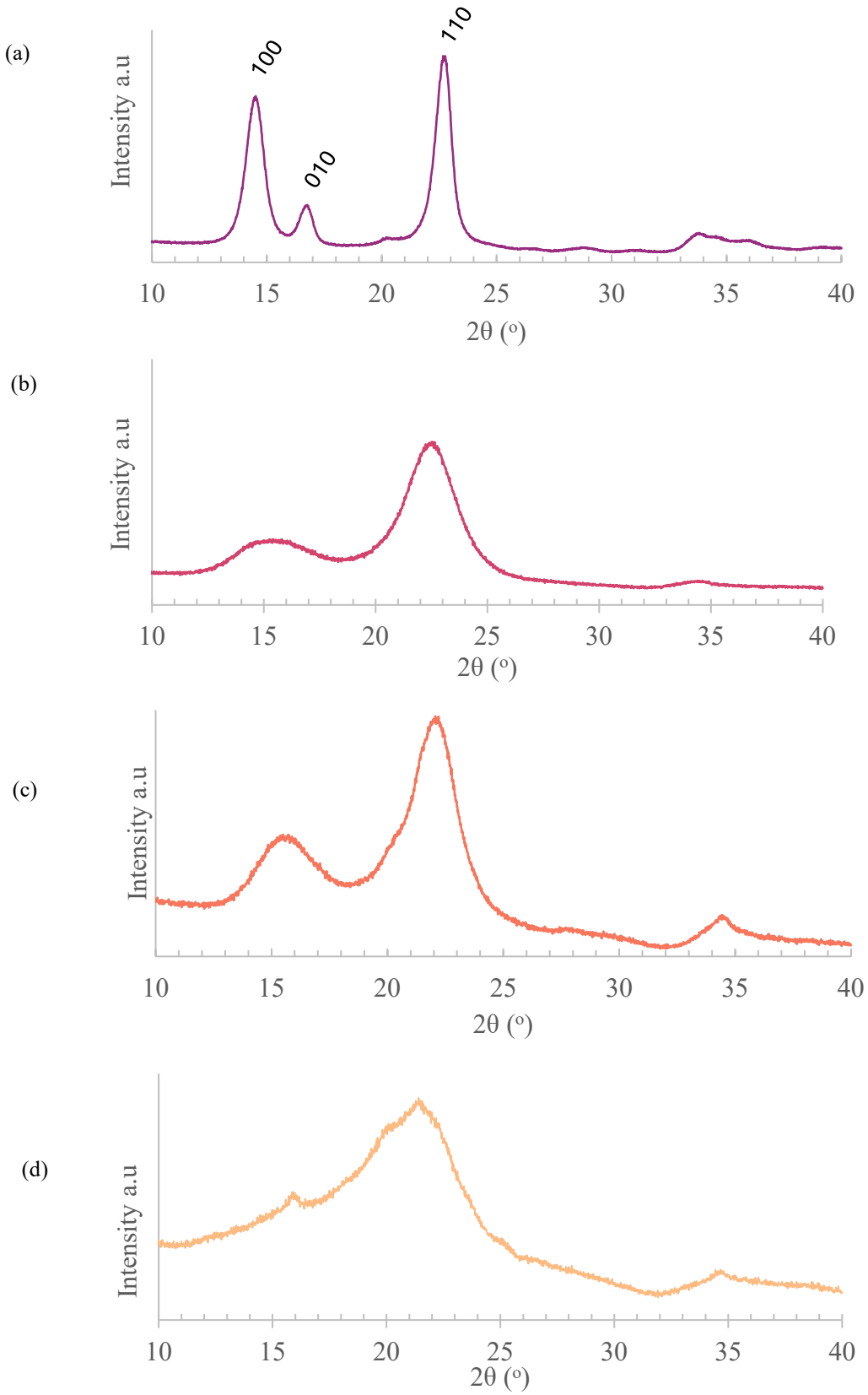

Figure 3.3 : XRD spectra of cellulose from (a) Rhizoclonium, (b) Zygnema, (c) Oedogonium, (d) Stigeoclonium

To better understand the XRD pattern of Rhizoclonium, Mercury 3.0 software (free version 3.1) was used as described by French (2014). For this, previously published crystallographic data files (.cif) of cellulose Iα by Nishiyama et al were used (Nishiyama et al. 2002; Nishiyama et al. 2003). The Rhizoclonium cellulose XRD spectrum was simulated using the Iα diffraction pattern with the calculated FWHM of 0.9° (Figure 3.4 a). However, the simulated pattern did not exactly match the experimental pattern. A closer match was obtained by adjusting the β parameter, which represents the angle between the a and c crystallographic axes in the monoclinic unit cell, to 125.8° to better simulate the actual experimental XRD pattern, as shown in Figure 3.4b.

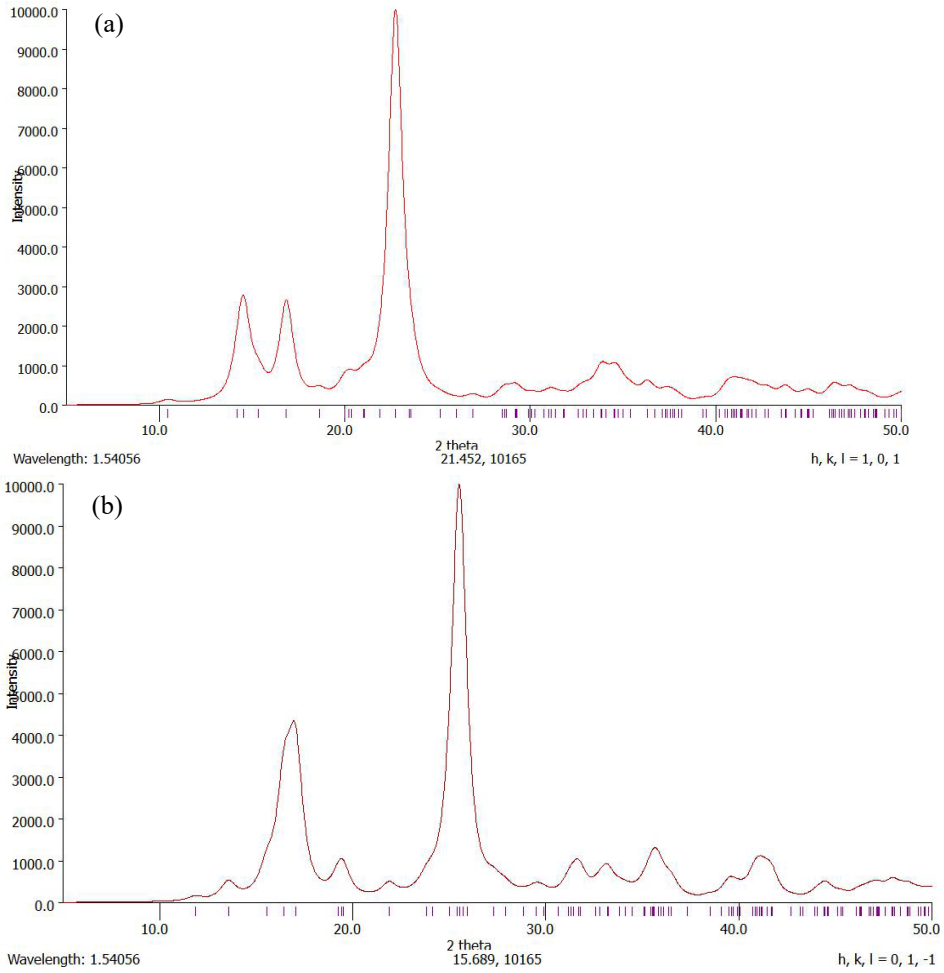

Figure 3. 4 Simulated XRD pattern of (a) I α with calculated FWHM for Rhizoclonium = 0.9 and (b) I α with FWHM=0.9 and β = 125.8

The diffraction patterns of Oedogonium cellulose and Zygnema cellulose closely resembled each other and both had the characteristic peaks at 2θ = 16°, 22° and 34°, corresponding to crystal planes of cellulose I, (100)/ (010), (110) and (11-4) respectively (French 2014; Nishiyama et al. 2003).

Cellulose is classified as crystalline when its crystallinity index (CI) falls within the range of 40-95%; while cellulose with CI values below this range are classified as amorphous (Quiroz-Castañeda 2013). One of the earliest highly crystalline celluloses was reported in the marine algae *Valonia ventricosa* (Honjo and Watanabe 1958). The crystallinity indices calculated as per the Segal method and crystallite sizes calculated as per Scherrer method are shown in table 3.3. The crystallinity index of Rhizoclonium (~91%) was significantly higher than that of other macroalgae species used in this study and similar to reported values in literature for cellulose from Cladophora (CrI=95%) (Mihranyan 2011), *Cladophora rupestris (CrI=93%) (Sucaldito and Camacho 2017), and* Valonia *(95%) (*Zhou *et al.*, 2019). Moreover, the crystallinity index of Rhizoclonium surpasses those of commercial microcrystalline cellulose (MCC), which typically ranges from 70% to 85% (Kian et al. 2017; Moon et al. 2011; Sainorudin et al. 2018). Their high crystallinity index of cellulose indicates superior mechanical properties and thermal stability (Amara et al. 2021; Gan et al. 2020), which are important attributes if cellulose is used as reinforcement in the preparation of strong and durable biocomposites (Al-Haik et al. 2022). Additionally, higher crystallinity reduces the material's water absorption due to the dense packing of cellulose chains, which decreases the availability of hydrophilic sites (Wahib et al. 2022). This property enhances the water barrier characteristics of the composite, making it more suitable for applications requiring moisture resistance (Wang et al. 2018). In this study, Oedogonium and Zygnema demonstrated moderately high crystallinity (60% and 73%, respectively), while Stigeoclonium exhibited low crystallinity (40%).

Table 3.3 : Crystallinity indices, full width at half-maximum (FWHM) and crystallite sizes (110 peak) of cellulose from macroalgae species used in this study.

Cellulose source	Crystallinity index %	FWHM (degree)	Crystallite Size (nm)
Rhizoclonium	91	0.90	9.5
Zygnema	73	2.87	3.00
Oedogonium	60	2.56	3.37
Stigeoclonium	40	8.58	1.00

While calculating the crystallinity index using the Segal method, peak heights cannot reliably estimate cellulose crystallinity as it neglects variations in peak width, which can be influenced by crystallite size (Park et al. 2010). Moreover, the peak area provides a more representative measure of the crystalline portion of the cellulose material (French and Santiago Cintrón 2013).

Therefore, incorporating FWHM values and calculating crystallite size using the Scherrer equation provides a more comprehensive understanding of cellulose crystallinity (Park et al. 2010).

The crystallite sizes calculated for 110 peaks using the FWHM values varied across the studied species (Table 3.3). Rhizoclonium showed a significantly narrow FWHM of 0.90°, indicating highly ordered and well-defined crystalline domains. On the other hand, Stigeoclonium showed a broad FWHM of 8.58°, with a crystallinity index of 40%. Rhizoclonium's smaller FWHM correlates with its high CrI of 91%, and its crystallite size was calculated to be 9.5 nm, consistent with Cladophora algae belonging to the same family, Cladophoraceae (Mihranyan 2011).

3.4.5 Thermal analysis

The thermal stability of cellulose is influenced by various factors, including the cellulose source, the cellulose extraction methods used, and the crystallinity of cellulose (Gan et al. 2020). Figure 3.5 shows the TGA and DTG curves of cellulose fractions from the four macroalgae species. TGA analysis includes three prominent thermal events. Initially, a weight loss occurs between 50-150 °C (Jonjaroen et al. 2020) and is associated with the evaporation of both free and bound water (Xiang et al. 2016). All cellulose fractions tested exhibited a weight loss below 105 °C, and *Rhizoclonium* cellulose, characterized by a high crystallinity index (92%), had a significantly lower weight loss (0.3%), indicating the reduced affinity for water in highly crystalline material (Nakamura et al. 1981). Secondly, the most substantial weight loss is observed between 250-400 °C, due to the thermal degradation of cellulose and the depolymerization of glycoside units (Jonjaroen et al. 2020). Finally, from 450-600 °C, a breakdown of carbonaceous residues occurs (Jonjaroen et al. 2020). *Rhizoclonium* cellulose had the lowest residual mass (8.5%) among the cellulose materials in this study, indicating higher purity in comparison to *Zygnema* cellulose (13%), and cellulose from *Oedogonium* and *Stigeoclonium*, both yielding residual masses of 19%.

The results for the macroalgae cellulose fractions analysed in this study are summarized in Table 3.4. The DTG curves for *Rhizoclonium* cellulose show that it had the highest degradation which peaked at 391 °C, which is consistent with the findings for the peak degradation temperature (390 °C) of cellulose extracted from *Cladophora glomerata (Xiang et al. 2016)*. Cellulose from *Zygnema* had a similar degradation temperature (352 °C) to that of cellulose obtained from obtained from *Cystosphaera jacquinottii* (350 °C) (Paniz et al. 2020). The other cellulose fractions all had distinct but lower temperature degradation peaks: *Stigeoclonium* at 317 °C, and *Oedogonium* at 329 °C.

Thermal stability is an essential parameter to be considered when processing thermoplastic-based composites reinforced with cellulose fibres. The decomposition temperature of plant-derived cellulose is approximately 200–300 °C, which limits the compounding/extrusion temperature and choice of polymer that can be used for

biocomposites (Dos Santos et al. 2013; Gan et al. 2020). Therefore, the high thermal stability of *Rhizoclonium* cellulose may be beneficial in the preparation of cellulose-reinforced bio composites.

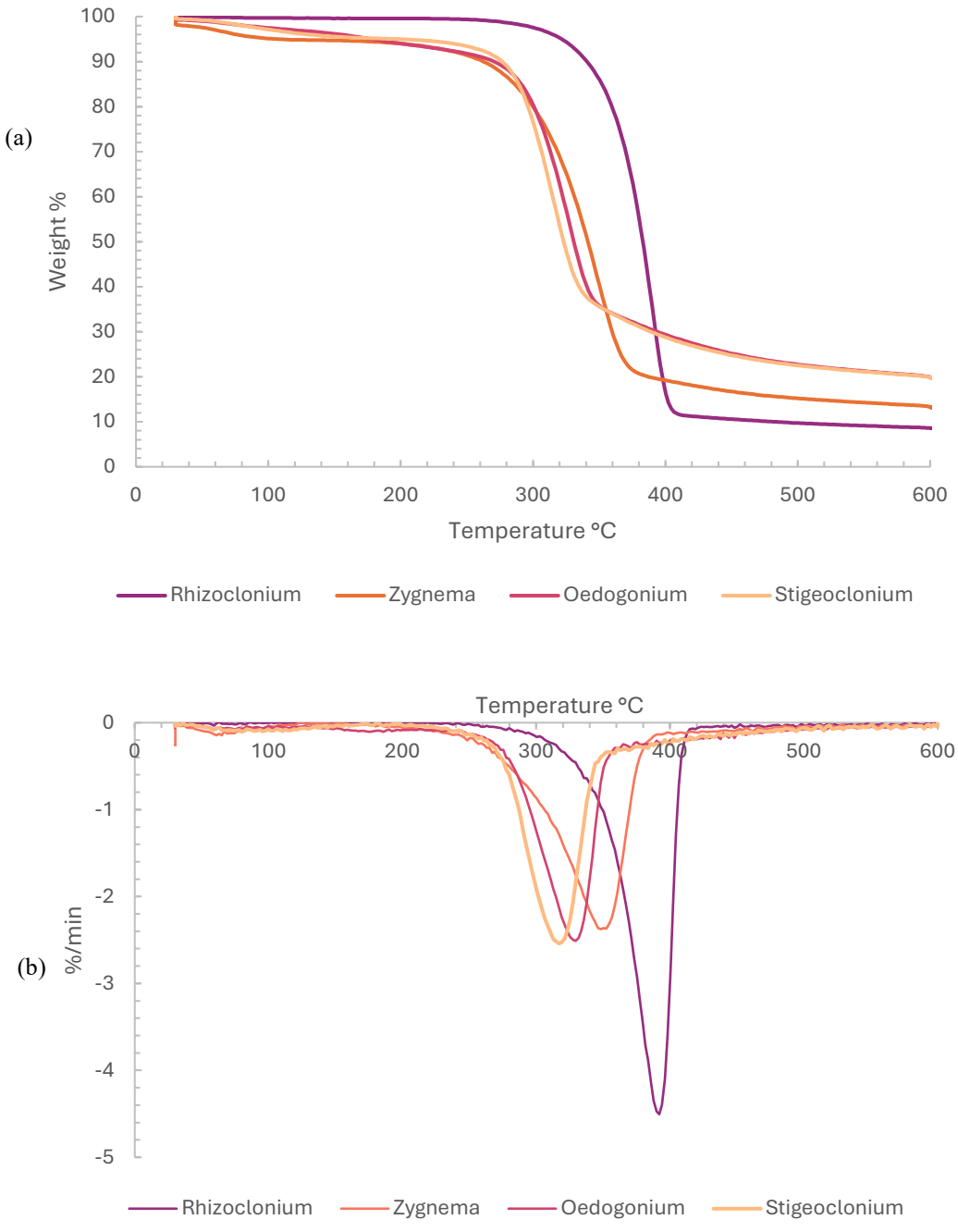

Figure 3. 5 : (a) TGA and (b) DTG curves of cellulose fractions of Oedogonium, Rhizoclonium, Stigeoclonium, and Zygnema

Table 3. 4 : Weight loss, degradation temperatures, crystallinity indices and residual mass at 600 °C of cellulose material

Cellulose source	Weight loss at 105 °C (%)	Onset degradation temperature (TGA)	Temperature of maximum degradation rate (DTG)	Crystallinity index %	Residual mass % at 600 °C
Rhizoclonium	0.3	344.7	391.6	91	8.5
Zygnema	4.99	297.4	352.4	73	13
Oedogonium	2.66	289.4	329.4	60	19
Stigeoclonium	3.1	282.7	317.0	40	19

3.5 Conclusion and Further Research

This study investigated the extraction and characterization of cellulose from four genera of freshwater filamentous algae; *Rhizoclonium*, *Zygnema*, *Oedogonium* and *Stigeoclonium* which are commonly found in filamentous algae phycoremediation systems, for the potential of sustainable cellulose production. Among the species, *Rhizoclonium* cellulose stood out with a very high crystallinity index of 92%, excellent thermal stability up to 345°C and favourable morphological properties characterised by the fibrous network structure. Additionally, it demonstrated high purity (41.3% carbon content, 5.9% hydrogen content, 0.5% ash content) and a cellulose yield of 6.9%. Comparatively, the cellulose of *Oedogonium* and *Zygnema* had only moderate crystallinity indices and thermal stability, which may be used for applications such as the production of microcrystalline cellulose, nanocellulose and cellulose-based hydrogels. Additionally, *Stigeoclonium* exhibited lower crystallinity and the least thermal stability among the studied species.

The high crystallinity, fibrous morphology, and thermal stability of *Rhizoclonium* cellulose indicate the potential for use as a reinforcement material in biocomposite preparation targeting applications such as packaging with reduced oxygen and water permeability (Wang et al. 2018). This is due to its tightly packed molecular structure

which minimizes the space between cellulose chains, thereby reducing diffusion of oxygen and water. Future research should focus on utilising *Rhizoclonium* cellulose for the production of nanocellulose, such as cellulose nanocrystals (CNC) and cellulose nanofibrils (CNF). For instance, due to high crystallinity and the fibrous morphology, *Rhizoclonium* nanocellulose could be used to reinforce thermoplastics, produce hydrogels and nanocomposites. Investigating the methods for producing CNC and CNF could expand new applications in high-strength nanocomposites and advanced materials. Assessing the compatibility of *Rhizoclonium* nanocellulose with specific polymer matrices and assessing its performance in particular bio composite applications would provide valuable insights. Such research could lead to the development of novel biodegradable materials with enhanced mechanical properties, thermal stability, and potential for use in a wide range of industrial applications such as biodegradable packaging for perishable goods, high-strength nanocomposites, and bio-derived reinforcement in construction industry.

Chapter 4

Preparation and Characterization of Poly(3-hydroxybutyrate-co-3-hydroxyvalerate) PHBV composite films with Cellulose Nanofibers from Freshwater Green Algae (*Cladophora.sp* and *Rhizoclonium.sp*) grown in primary effluent.

4.1 Abstract

This study explores the extraction of cellulose nanofibers (CNFs) from wastewater-grown mixed freshwater macroalgae biomass comprised of two species (*Rhizoclonium* sp. and *Cladaphora* sp.) and their integration into poly(3-hydroxybutyrate-co-3-hydroxyvalerate) (PHBV) composites. Through sequential bleaching, alkaline treatment, and acid hydrolysis, cellulose was extracted with a 15.55% yield, and subsequently processed into CNFs using the TEMPO oxidation method under neutral conditions. The resultant CNFs exhibited a high crystallinity of 94% and thermal stability of up to 381.6 °C, surpassing commercially purchased CNFs. Scanning Electron Microscopy (SEM) analysis showed that the TEMPO-oxidised nanocellulose had a highly porous structure, which may contribute to better dispersion and improved mechanical properties.

PHBV composites were produced by a solvent casting technique using either the TEMPO oxidised algae cellulose, unmodified algae cellulose, or a commercial CNF at 1-3 (%w/w) concentrations. The incorporation of algae-derived cellulose enhanced the mechanical properties of the PHBV composites. The composite with 3% CR exhibited the highest tensile strength which was6.6%higher than that of the neat PHBV film. The Young's modulus also increased, particularly with 3% CR cellulose, which was 12% higher than that of neat PHBV film. Differential Scanning Calorimetry (DSC) analysis revealed an increase in the PHBV crystallinity index with the addition of cellulose, with the highest

being 52.6% for composites containing 3% CNF, which also conferred an improvement in thermal properties.

Thermal analysis indicated improved thermal stability for the PHBV composites with CNF and algae cellulose, demonstrated by higher onset degradation temperatures. The composite with 3% CR cellulose increased the onset temperature by 22°C more than that of the neat PHBV film. SEM images also showed that the films with CR cellulose exhibited a more uniform surface than those with commercial CNF. This study demonstrates the potential of macroalgae-derived cellulose in improving the mechanical and thermal properties of PHBV biocomposites, suggesting its promising application in sustainable material development.

4.2 Research Background

Cellulose, the most abundant natural polymer, is a rigid polymer formed by linking anhydroglucose rings with 1–4 glycosidic bonds (Bhaladhare and Das 2022). It is found in plants, tunicates, bacteria and algae in nature (Moon et al. 2011). The native form of cellulose, known as cellulose I, is commonly utilized to fabricate composites. In recent decades, there has been extensive research on cellulose from plants, bacteria, and algae as a cost-effective, biodegradable and eco-friendly natural fibre.

When processed in the nanometre level, cellulose exhibits superior mechanical and physical properties (Mariano et al. 2014). This improvement is due to the elimination of structural defects in cellulose, such as disorganized regions along the cellulose chains, inconsistencies in hydrogen bonding, and disruptions in the crystalline structure (Ding et al. 2020). Therefore, cellulose I is often converted to nanocellulose to be fabricated in a vast number of applications in the packaging, biomedical, and textile industries. Nanocellulose are cellulose structures with at least one dimension between 1-100 nm (Nasir et al. 2017) and are categorized into two types: cellulose nanocrystals (CNC) and cellulose nanofibers (CNFs). CNCs and CNFs vary in terms of in their shape, dimensions, and crystalline characteristics (Xu et al. 2013). CNCs are shorter, measuring between 5-70 nm in length with a rigid, rod-like structure that promotes strength and stiffness, whereas CNFs are longer and more fibrous, lending flexibility and efficient stress transfer

to composite materials (Moon et al. 2011). While both CNCs and CNFs are equally utilized as reinforcement additives to enhance the structural attributes of composites, CNFs stand out due to the improved mechanical (Frank et al. 2018) and thermal properties (Gan et al. 2020) owing to their high aspect ratio (with a diameter in the range of 5-50 nm and a length of a few micrometres) and fibril entanglement which enable CNFs to form effective networks within the composite matrix.

CNFs are conventionally processed through mechanical and physical approaches such as homogenization (microfluidizer or high-pressure homogenization), electro spinning, sonication, grinding, refining, and mechanical milling (Lee and Mani 2017; Zeng et al. 2021). However, the limitations of these physical and mechanical approaches include high costs, use of toxic chemical chemicals, difficulty in collecting the fibres, and inability to control their dimensions. Therefore, prior to these mechanical treatments, pretreatment methods are required to lower the energy demands of the fibrillation process such as partial enzymatic degradation, carboxymethylation, and a recent greener approach to produce cellulose nanofibers through a chemical catalytic reaction that is known as TEMPO mediated production of cellulose nanofibers (Liu et al. 2021a). Figure 4. 1 demonstrates the TEMPO-mediated oxidation process of cellulose using the TEMPO reagent, 2,2,6,6-Tetramethylpiperidine 1-oxyl, commonly known as TEMPO.

TEMPO oxidation has several advantages over other types of CNF processing methods. It does not require harsh chemical conditions or a high temperature and has relatively low energy consumption (1 kWh/kg) (Isogai and Bergström 2018). TEMPO oxidized cellulose nanofibers (TO) have more COOH groups which provide the potential for surface modification and complete dispersion in water. Complete dispersion is important for the uniform mixing of fibres and their integration with other materials, facilitated by the abundant COOH groups in TEMPO oxidized cellulose nanofibers. Moreover, TEMPO oxidation can be carried out in smaller batches and is much gentler than other mechanical treatment processes due to the catalytic pretreatment (Saito et al. 2006). TEMPO oxidation, typically performed in alkaline conditions with NaBr and NaClO, can cause depolymerization of cellulose fibers due to high pH, reducing their mechanical properties and degree of polymerization (Saito and Isogai 2004). Additionally, this process can produce aldehydes, which compromise thermal stability and hinder water

dispersion by forming unstable hemiacetal linkages (Saito et al. 2006; Saito et al. 2009). Therefore, to preserve the structural properties of cellulose fibres, it is important to conduct the oxidation under neutral conditions or weak acidic conditions (Tanaka et al. 2012).

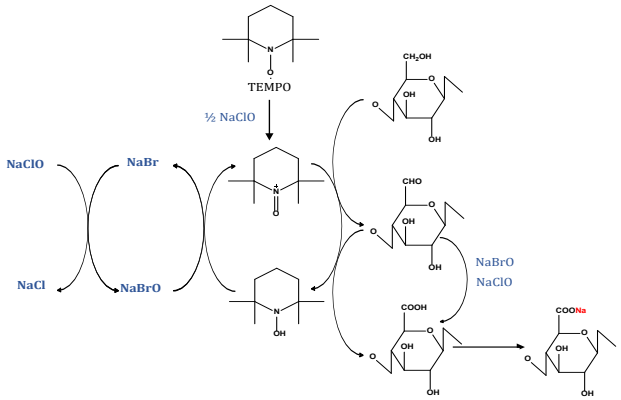

Figure 4. 1 : TEMPO mediated oxidation reaction.

Recently, there has been increased research into sustainable and alternative sources of cellulose, other than plant-based cellulose. Algae-based biomass has potential as a feedstock for diverse and high quality nanocellulose due to its unique properties, such as high crystallinity and ease of extraction due to the absence of lignin (Samyn et al. 2022). Wastewater treatment plants using high-rate filamentous algae ponds generate significant quantities of algal biomass as a byproduct. This biomass presents an opportunity to sustainably recycle wastewater nutrients into a valuable resource. In particular, two macroalgae species *Cladophora* sp. and *Rhizoclonium* sp. have been shown to provide effective bioremediation (Hariz et al. 2023a; Vadiveloo et al. 2019). These algae species, often coexist together (Grayburn et al. 2013), and have exceptional cellulose I composition, characterized by high thermal stability up to 381.6 ˚C and exceptionally high crystallinity up to 94% (Sucaldito and Camacho 2017; Xiang et al. 2016; Zhou et al. 2019). While *Cladophora* sp. cellulose has received much attention in literature, comprehensive studies on *Rhizoclonium* sp. cellulose are limited. Atalla *et al.* (1985) mention the extraction of highly crystalline cellulose from *Rhizoclonium hieroglyphicum* and the findings in the previous chapter (Chapter 3) highlight the similar high-quality characteristics of *Rhizoclonium* sp. cellulose to those of *Cladophora* sp. cellulose. This makes *Rhizoclonium* sp. an excellent candidate for nanocellulose production, suitable for

reinforcement applications. Therefore, the coexistence of these two species in the algal biomass by-product of high-rate filamentous algae wastewater treatment ponds provides an opportunity for the production of high quality nanocellulose that could be used to reinforce thermoplastic biopolymers such as PHBV.

Over the last decade, PHBV, a bio-based thermoplastic, has gained attention due to its biodegradability and physical-mechanical properties as an alternative to petroleum-based polymers (Jost and Langowski 2015). PHBV is a highly crystalline copolymer of PHA family. It is a microbial polymer produced by gram-positive and gram-negative bacteria when grown under nutrient stress (Tebaldi et al. 2019). PHBV has gained attention as a polymer owing to its properties such as, flexibility, stiffness and gas barrier properties (Keskin et al. 2017; Rivera-Briso and Serrano-Aroca 2018; Tebaldi et al. 2019). While it is a promising biopolymer for the application of packaging material owing to above mentioned properties, PHBV also has properties of low impact resistance, narrow processing window, reduced elongation at break and fragility (Rivera-Briso and Serrano-Aroca 2018). Therefore, this research aims to show that the performance of PHBV composites can be enhanced by incorporating cellulose and CNF extracted from wastewater-grown macroalgae, as a sustainable reinforcement filler. This study specifically explores how macroalgal cellulose and CNF affect the mechanical strength and thermal stability of the composites in comparison to commercially available plant-based CNF. The objective was to develop biocomposites with improved properties for applications such as environmentally friendly packaging and other biocomposites.

4.3 Methods

4.3.1 Materials

Poly(-3-hydroxybutyrate-co-3-hydroxyvalerate) (PHBV) polymer (PHI003) was purchased from NaturePlast®. According to the ASTM-D6866 standards, it is 94% biobased and, according to ASTM D6400 norm, it is industrially compostable. Sodium chlorite (Product No: 244155), sodium acetate (Product No: S2889), sodium hydroxide (Product No: S5881), and 2,2,6,6-Tetramethylpiperidine 1-oxyl,2,2,6,6-Tetramethyl-1-piperidinyloxy (TEMPO) reagent (Product No: 214000) were purchased from Sigma

Aldrich, chloroform (Product No: 200-663-8) was purchased from MERCK and used as received. Commercial Cellulose nanofibers (CNF) (CAS Number: 9004-34-6) were purchased from the University of Maine, Orono. The wastewater-grown mixed algae culture of *Rhizoclonium* sp. and *Cladophora* sp. mixed algae sample was identified and provided by National Institute of Water and Atmospheric Research (NIWA), Hamilton, New Zealand.

4.3.2 Extraction of cellulose

Cellulose from the mixed algae sample grown in wastewater, was extracted according to the protocol reported in Chapter 2 (Mihranyan et al. 2004b).

4.3.3 Production of TEMPO oxidized CNFs

After cellulose extraction from algae, CNFs were obtained through TEMPO oxidation under neutral conditions as per a published protocol (Saito et al. 2009). Briefly, freeze-dried algae cellulose fibres (1 g) were suspended in 0.05 M sodium phosphate buffer (90 mL, pH=6.8). TEMPO reagent (0.016 g) and sodium chlorite (1.13 g) were then added to an airtight flask. A 2 M sodium hypochlorite solution (0.5 mL l) was diluted to 0.1 M with 0.05 M sodium phosphate buffer as the oxidation medium and added in one step to the flask. The flask was immediately stoppered and stirred at 500 rpm and 60 º C for 36 hours. After cooling the suspension to room temperature, the TEMPO-oxidized cellulose was thoroughly rinsed thrice with reverse-osmosis (RO) water by centrifuging at 3500 rpm, to ensure complete removal of residual TEMPO catalyst and sodium chlorite. The oxidized cellulose slurry (1.0 g) was dispersed in 100 g of (RO) water and defibrillated using an Omni General Laboratory Homogenizer (GLH 850) with a 10 x 115 mm Saw Tooth (Fine) Generator Probe at 10,000 RPM for 3 minutes. The cellulose suspension was then centrifuged at 3500 rpm, removed from the supernatant and then freeze-dried (Buchi Lyovapor L-200).

4.3.4 Composite film preparation by solvent exchange

Initially, PHBV polymer (1 g) was completely dissolved in chloroform (40 mL) to form a homogenous solution. The dissolution process involved two key temperature stages: the mixture was first heated to 55 ºC for 2 hours with stirring, then the temperature was increased to 70 ºC for an additional 10 minutes (Lo Faro et al. 2021). After heating, the solution was allowed to cool to room temperature, with continuous stirring to prevent agglomeration.

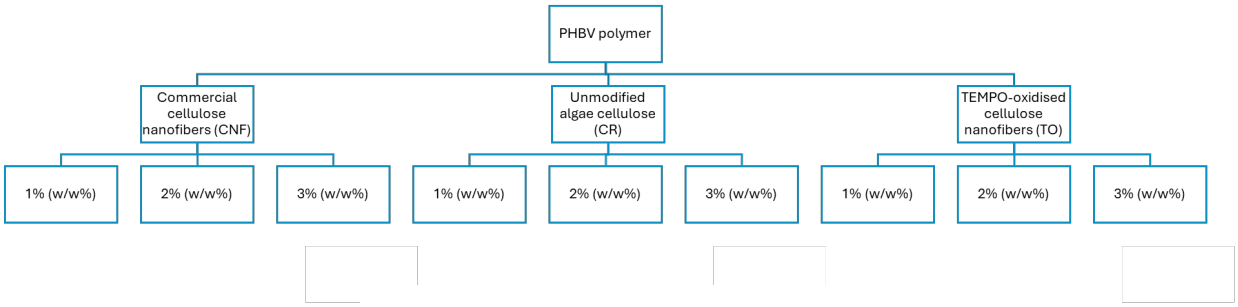

Figure 4. 2 : Experimental Design

The experimental design (Figure 4.2) included comparing three different concentrations of cellulose (1%, 2%, and 3%) that were used in the final composite utilising commercial cellulose nanofibers (CNF), unmodified algae cellulose (CR), and TEMPO-oxidized cellulose nanofibers (TO). To improve the nanocellulose dispersion within the PHBV films, each of the different cellulose concentration samples were subjected to a solvent exchange process (Suryanegara and Yano 2014). The nanocellulose was initially dispersed in RO water (20 mL) to separate individual fibres and then centrifuged at 3000 rpm for 15 minutes and the resulting supernatant (National Institute of Water and Atmospheric Research) decanted. Subsequently, acetone (20 mL) was added to the nanocellulose followed by centrifugation at 3000 rpm. This step was repeated twice, ensuring the effective elimination of any residual water. Then chloroform was introduced to the nanocellulose and removed by centrifugation. The prepared nanocellulose was then homogenized with the 40 mL of previously prepared PHBV solution using a laboratory homogenizer at 5000 rpm. The PHBV/nanocellulose solutions were poured on to borosilicate glass dishes (9 cm x 13 cm) and placed under a fume hood for solvent

evaporation at room temperature. A constant and slow airflow was maintained to facilitate the formation of uniformly dispersed nanocellulose-reinforced PHBV composite films.

4.3.5 Light Microscope and Scanning Electron Microscope (SEM)

To gain a visual understanding of cellulose and degree of disintegration of cellulose fibres after TEMPO oxidation, the cellulose samples (commercial CNF, algae cellulose and TEMPO oxidated cellulose after mechanical treatment) were analysed using an Olympus light microscope. First, 10 mg of each cellulose sample was dissolved in 10 mL of reverse osmosis (RO) water, ensuring the cellulose fibres were sufficiently dispersed. A slide was then prepared with this cellulose solution, aiming for a thin, even layer to facilitate clear visualization under the microscope. The images of the cellulose were captured at a 200-micrometre scale.

For surface morphology analysis, scanning electron microscopy (SEM) images of the cellulose samples and composite films were captured using a Hitachi Regulus SU8230 FE-SEM. Prior to imaging, samples were coated with fine platinum particles using a Q150V plus sputter coater to prevent charging. Imaging was performed at an accelerating voltage of 5 kV.

4.3.6 Fourier-transform infrared spectroscopy (FTIR)

The FTIR spectra of the cellulose, commercial CNF, TEMPO oxidized cellulose and the composite films were obtained using a Shimadzu IRSpirit fitted with a QATR-S accessory. The spectral analysis covered the range of 4000-400 cm^{-1}, with an average of 45 scans per sample. Attenuated total reflectance (ATR) and baseline corrections were applied, and the data were normalized using Shimadzu LabSolutions IR software.

4.3.7 X-ray diffraction (XRD)

The X-ray diffraction (XRD) measurements were performed on cellulose samples using the same procedure described in Section 3.3.6. The crystallinity indices (CrI) were calculated for each cellulose type using the Segal equation (Equation 4) (Segal et al. 1959):

Equation 4:

$$Crystalinity\ index\ (\%) = \frac{I_{110} - I_{am}}{I_{110}} \times 100$$

where I_{110} (crystalline peak of cellulose Iα) refers to the intensity of the peak at 2θ ~ 22°, and I_{am} (amorphous region of cellulose) refers to the intensity at 2θ = 18.5°.

The crystallite sizes (τ) of algae cellulose and TEMPO-oxidised cellulose were calculated using the Scherrer equation (Equation 5) (Nam et al. 2016):

Equation 5:

$$\tau = \frac{K\ \lambda}{\beta \cos \theta}$$

where K is the correction factor (0.9), λ is the wavelength of the X-ray radiation (1.54056 Å), β is the full width at half maximum (FWHM) of the diffraction peak in radians, and θ is the diffraction angle of the peak (~ 22°). The FWHM values were calculated using MATLAB software.

4.3.8 Thermogravimetric Analysis (TGA)

The thermal stability of the algal cellulose, commercial CNF, TEMPO oxidated cellulose, and the composite films was evaluated using a PerkinElmer STA 8000 instrument through thermogravimetric analysis (TGA). Each sample (10 mg) was placed in alumina crucibles and subjected to a heating program with temperatures ranging from 30 °C to 600 °C, with a constant heating rate of 10°C/min under an argon atmosphere at a flow rate of 50 mL/min. The ash content was determined by measuring the remaining weight at the end of the heating program.

4.3.9 Differential scanning calorimetry (DSC)

The crystallization behaviour of PHBV composites was assessed by Differential Scanning Calorimetry (DSC). Samples of approximately 5 mg weight were extracted from the composite films and examined using a Netzch DSC3500 Sirius differential scanning calorimeter equipped with aluminium crucibles. The testing protocol involved three steps: initially, the samples were cooled to -70°C, using the DSC's built-in cooling system. This was followed by gradual heating from -70°C to 200°C at a rate of 20°C/min, then a 5-minute hold was applied to eliminate any thermal history effects. The samples were then cooled from 200°C to -70°C at a rate of 10°C/min to determine the cold crystallization temperature (T_c); and reheating to 200°C at 20°C/min to determine the melting temperature (T_m). The degree of crystallinity (Debzi et al.) of PHBV composites was calculated using Equation 6 (Jun et al. 2017)

Equation 6 :

$$\mathrm{Xc}\ \% = \frac{\Delta \mathrm{Hm}}{(1\ -\ \mathrm{w(CNF)})\ \Delta \mathrm{H100}} \times 100\%$$

where, H_m refers to the heat of melting and w(CNF) refers to mass fraction of cellulose nanofibers. H_{100} refers to the heat of fusion of 100% crystalline PHBV (146.6 J/g) (Yu et al. 2011).

4.3.10 Mechanical testing

The mechanical properties of the samples were tested using an Instron® 5982 tensile tester with 500 N load cell to determine the tensile strength, young's modulus, and elongation at break (tensile strain at break), following ASTM D882-18 guidelines. Samples with dimensions of 50 mm × 15 mm X 0.06 mm underwent tensile testing at a loading rate of 5 mm/min. Tensile strain at break was measured using the crosshead displacement of the test frame recorded by the Instron machine. For each composite type, 10 samples were tested, and 5 replicates were selected for analysis after removing statistical outliers based on the lower and upper bounds. Data was analysed using non-parametric permutational multivariate analysis of variance (PERMANOVA) in PRIMER7 software using Euclidian distance resemblance matrices, TYPE III (partial) sum of squares and based on 9,999 unrestricted permutations of raw data (Clarke and Gorley 2015). Permutation t-tests were conducted to examine pairwise differences between different additions of cellulose.

4.4 Results and Discussion

4.4.1 Characterisation of TEMPO-oxidised cellulose

The cellulose was extracted using a mild three-step extraction process involving: bleaching, alkaline treatment and acid hydrolysis, following a published protocol for macroalgal cellulose extraction (Mihranyan et al. 2004a) and the yield was 15.6%. This extracted algal cellulose was then subjected to a TEMPO-catalysed reaction under neutral conditions in a pH 6.8 phosphate buffer, as described by Saito et al. (2009), with NaClO and NaClO2 serving as the oxidizing agents. This oxidation selectively transforms primary hydroxyl groups on the cellulose fibril surface into carboxylate groups. The final process of the TEMPO oxidation process is the mechanical treatment to disintegrate the oxidized-cellulose fibres. Following this chemical modification, the oxidized cellulose fibres were subjected to a mechanical treatment to disintegrate the fibres, which was sufficient to break down the cellulose into nanofibers with minimal energy input, aligning with the findings of Kalia et al. (2014) and Levanič et al. (2020).

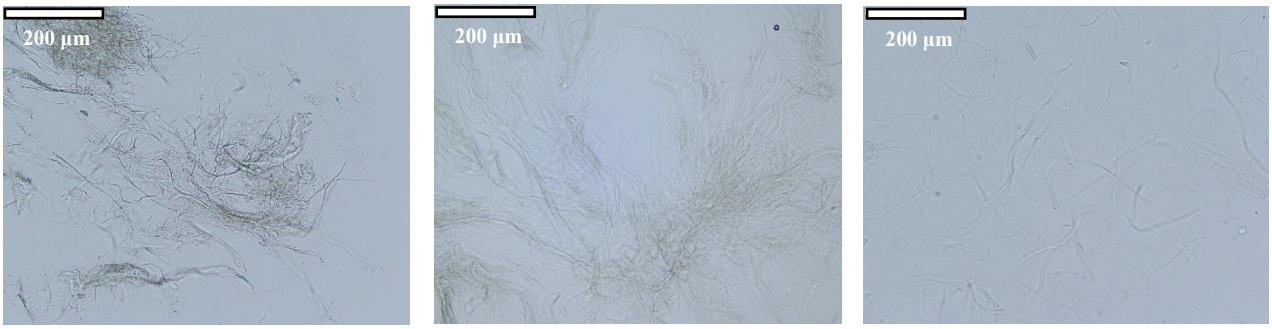

Figure 4.3 : Microscopic Images of (a) Commercial CNF, (b) Algae cellulose (C) TEMPO mediated cellulose after mechanical defibrillation for 3 minutes (10mg of each dissolved in 10 mL of water).

Figure 4.3 shows microscopic images at X20 magnification of commercial CNF, algae cellulose, and TEMPO-oxidized cellulose following mechanical homogenization, each at a concentration of 1mg/mL in water. Commercial CNF and algae cellulose both exhibit a web-like cellulose network (Figures 4.3 (a) and (b)). Following TEMPO oxidation of the algae cellulose and a three-minute homogenization at 10,000 RPM (Figure 4.3 (c)), the web-like algae cellulose nanofibers are mostly disintegrated into individual nanofibers indicative of successful defibrillation (Xie et al. 2016). After homogenization, the TEMPO mediated cellulose was freeze-dried, and the yield was 90% which is consistent with previous studies for TEMPO cellulose extracted from wood (Isogai et al. 2011).

Further morphological details were analysed by SEM (Figure 4.4). Nanofibers can be seen in algal cellulose (Figure 4.4 b), and TEMPO mediated cellulose (Figure 4.4 c). In comparison, commercial CNF (Figure 4.4 (a)) has individual and distinct fibres with visible porosity within the fibre network of intertwined cellulose. The algae cellulose shows more of a compact dense structure with tightly packed network (Sucaldito and Camacho 2017) compared to the commercial CNF. However, the fibres seem to be finer as seen in *Cladophora* cellulose reported in previous studies (Mihranyan 2010; Sucaldito and Camacho 2017). The SEM images of TEMPO mediated nanocellulose shows a high porous structure with visible presence of voids, gaps, or spaces between the cellulose fibres which could be due to the introduced COOH groups which in return helps in individualizing the fibres (Levanič et al. 2020) forming a mesh-like structure. Furthermore, another advantage of TEMPO oxidation process is its ability to preserve the

original fibrous morphology at the micron level, without significant internal swelling. (Isogai et al. 2011).

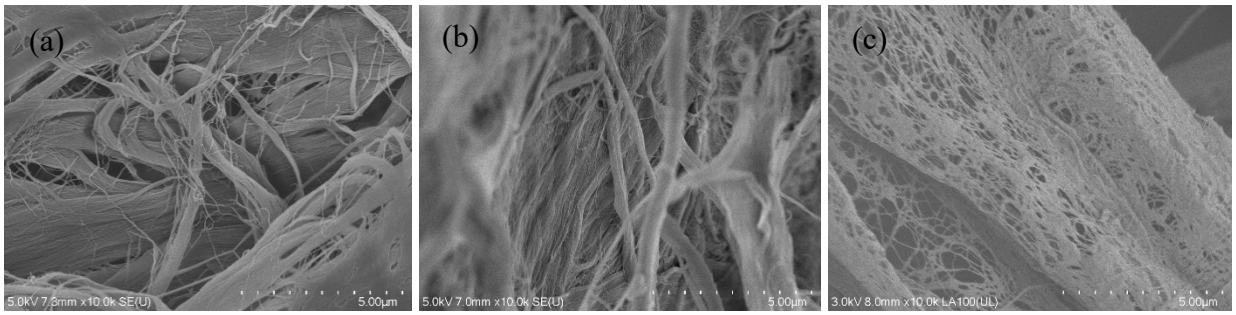

Figure 4. 4 : SEM images of (a) commercial CNF, (b) algae crude cellulose, and (c) TEMPO mediated cellulose at 10,000 magnifications.

4.4.1.1 Fourier-transform infrared (FTIR) analysis

The FTIR spectra of all cellulose materials showed the characteristic bands of cellulose, as outlined in Table 4.1. The backbone of the cellulose chain remained unchanged across all samples, each displaying the distinctive peaks associated with native cellulose.

During TEMPO oxidation, the C6-OH is oxidized into COOH as illustrated in Figure 4.1. This chemical transformation is evident in the FTIR spectrum (Figure 4.5) where an apparent shift in the absorbance peak from 1645 cm^{-1} to 1600 cm^{-1} is observed. This shift, attributed to the stretching vibrations of the carboxylate groups, confirms the introduction of COOH functionalities (Chitbanyong et al. 2018; Thi Thanh Hop et al. 2022) and successful conversion of C6 hydroxyl groups to sodium carboxylate groups, consistent with the findings of Wu et al (Wu et al. 2012).

This conversion process further increases the carboxylate content of cellulose, improving solubility and reactivity. This occurs by creating an electrical double layer around the nanofibers, which generates a high zeta potential providing colloidal stability (Isogai et al. 2011). For cellulose nanofibers that have been TEMPO-oxidized, typical zeta potential values can be approximately -75 mV as reported by Isogai et al. (2010). This strong negative surface charge (-75 mV) that significantly enhances electrostatic repulsion among nanofibers. Therefore, this stability inhibits the agglomeration of CNF and

facilitates the formation of individual fibres (Isogai et al. 2011) as the repulsive forces exerted by the carboxyl groups outdo the attractive forces of hydrogen bonding, therefore maintaining the dispersion and stability of the individual nanofibers (Faradilla et al. 2016).

Table 4. 1 : FTIR absorbance peaks in commercial CNF, unmodified algae cellulose, and TEMPO oxidised cellulose their bond assignment, and functional group attributed to each specific peak. Peaks denoted with an asterisk (*) are characteristic of native cellulose I.

Assignment	**Functional group**	**Macroalgae cellulose absorbance (cm^{-1})**			**References**
		CNF	*Algal cellulose*	*TEMPO*	
OH	Hydroxyl groups/ monosaccharides	3334	3340	3343	(Halib et al. 2012; Paniz et al. 2020; Wahlström et al. 2020)
–OH stretching	Hydroxyl groups	3283	3303	3303	(Somord et al. 2018)
C-H stretching	Methylene groups	2897	2895	2895	(Halib et al. 2012)
C-H scissoring	Cellulose*	1427	1427	1428	(Higgins et al. 1961; Paniz et al. 2020)
C-H bending	Cellulose	1364	1360	1361	(Paniz et al. 2020)
O-H in plane bending	Cellulose	1337	1337	1337	(Paniz et al. 2020)
CH2 wagging	Cellulose	1311	1317	1311	(Higgins et al. 1961)

C-O-C antisymmetric ring stretch	Cellulose*	1156	1157	1157	(Paniz et al. 2020)
Antisymmetric ring stretch	C-O stretch/ C-C stretch*	1102	1109	1117	(Higgins et al. 1961; Paniz et al. 2020)
C-O stretch at C6	Cellulose	1053	1054	1054	(Paniz et al. 2020)
C-O deformation at C6	Cellulose	1029	1030	1030	(Oh et al. 2005; Paniz et al. 2020)
C-O-C asymmetric stretch	β-glycosidic linkage*	896	896	896	(Paniz et al. 2020)

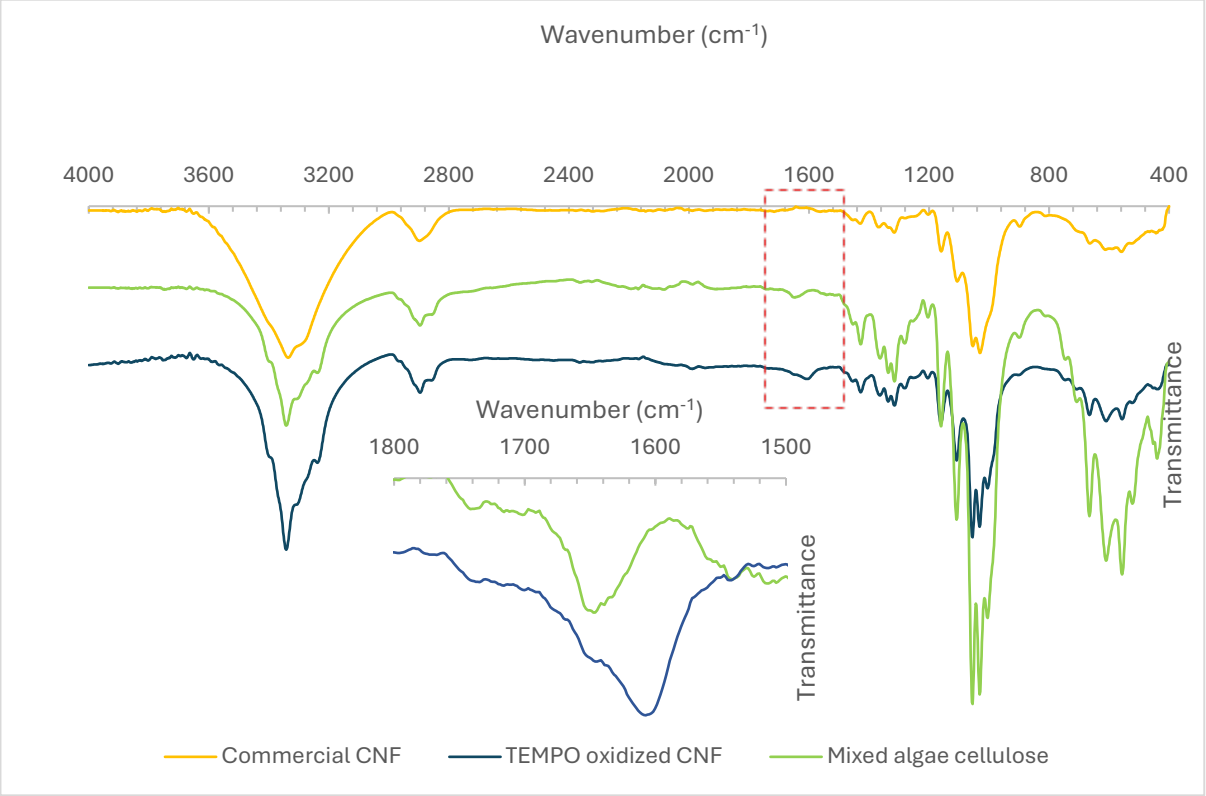

Figure 4. 8 : FTIR spectrum of commercial CNF, algal cellulose and TEMPO mediated algal cellulose.

4.4.1.2 X-ray diffraction (XRD) analysis

All cellulose materials show characteristic peaks at 2θ=22.2° and 2θ=14° which corresponds to the cellulose I structure (Figure 4.6). Typically, celluloses from higher plants like wood and cotton are mainly composed of thin microfibrils with a low crystalline form of cellulose I_β. However, cellulose from bacteria and *Cladophora* algae possess composite structures of cellulose Iα and Iβ, although they differ in crystal size and the composite ratio of Iα to Iβ (Okita et al. 2010). However, in the case of algae, the cellulose predominantly exists in the Iα polymorph (Jayasooriya et al. 2024).

In this study, the XRD patterns of the algae cellulose show a similar XRD pattern to that of *Cladophora* cellulose (Mihranyan 2011; Sucaldito and Camacho 2017; Xiang et al. 2016) exhibiting unique characteristics that are not commonly observed in cellulose derived from plants. The distinct and sharp peaks at 2θ angles of 14° and 16° suggest a single plane alignment, a feature that distinguishes it from typical plant cellulose (Sucaldito and Camacho 2017). The clear separation of the two peaks (100) and (010) suggests a higher degree of crystallinity and more defined arrangement of cellulose chains along these crystallographic planes (Huang et al. 2019). The unmodified algae cellulose had a higher crystallinity index of 92% compared to that of commercial CNF (62%), which is indicative of a highly ordered structure as has been observed in previous studies for *Cladophora* macroalgae cellulose (Mihranyan 2011; Sucaldito and Camacho 2017; Zhou et al. 2019).

Furthermore, the XRD patterns of the mixed algae cellulose and the TEMPO-oxidized cellulose show similar patterns, suggesting that the TEMPO oxidation process preserves the original crystal structure of cellulose material (Saito et al. 2009). These patterns significantly differed from the commercial CNF XRD analyses (Figure 4.6 a). A notable decrease in the crystallinity index to 87% was observed following TEMPO oxidation. This reduction in crystallinity could be primarily due to the mechanical treatment step of the TEMPO oxidation process which could convert certain crystalline regions into amorphous ones, thereby decreasing the overall crystallinity index.

While calculating the crystallinity index using the Segal method, a simple comparison of peak heights cannot reliably estimate cellulose crystallinity as it neglects variations in peak width, which can be influenced by crystallite size (Park et al. 2010). Therefore, incorporating the full width at half maximum (FWHM) values to calculate the crystallite size using the Scherrer equation provides a more comprehensive understanding of cellulose crystallinity (Nam et al. 2016). Crystallite sizes of CR and TO cellulose were determined using the Scherrer equation.

In this study, unmodified algae cellulose exhibited a narrower FWHM of 0.79 ° (Figure 4.7), resulting in a larger crystallite size of 10.89 nm (CrI of 92%). TEMPO-oxidized algae cellulose showed a higher FWHM value of 1.079 ° (Figure 4.7), corresponding to a crystallite size of 7.9 nm (CrI= 87%). Okita et al. reported average crystallite sizes for cellulose from various sources: softwood cellulose (3.8 nm), cotton (5.4 nm), bacterial cellulose (5.8 nm), and *Cladophora* algae cellulose (13.1 nm) (Okita et al. 2010). Comparing these results, it is evident that *Cladophora* algae-derived cellulose generally has larger crystallite sizes than cellulose from terrestrial plants. The unmodified algae cellulose in this study, while slightly lower in crystallite size reported for *Cladophora* cellulose, still aligns with these findings. This suggests that the TEMPO oxidation process, while effective in defibrillating cellulose and introducing functional carboxylate groups, reduces crystallite size and crystallinity due to partial disruption of the crystalline regions.

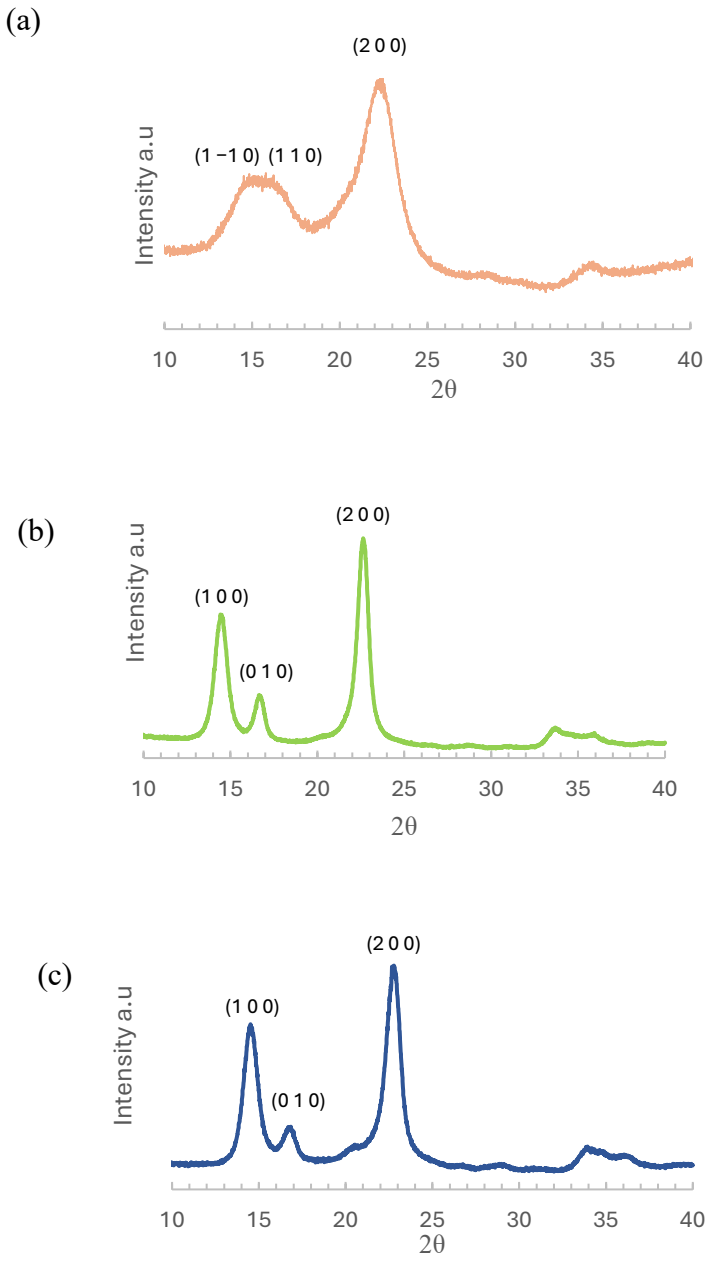

Figure 4. 9 : XRD spectra of (a) commercial CNF (b) unmodified algae cellulose (c) TEMPO oxidized algae cellulose.

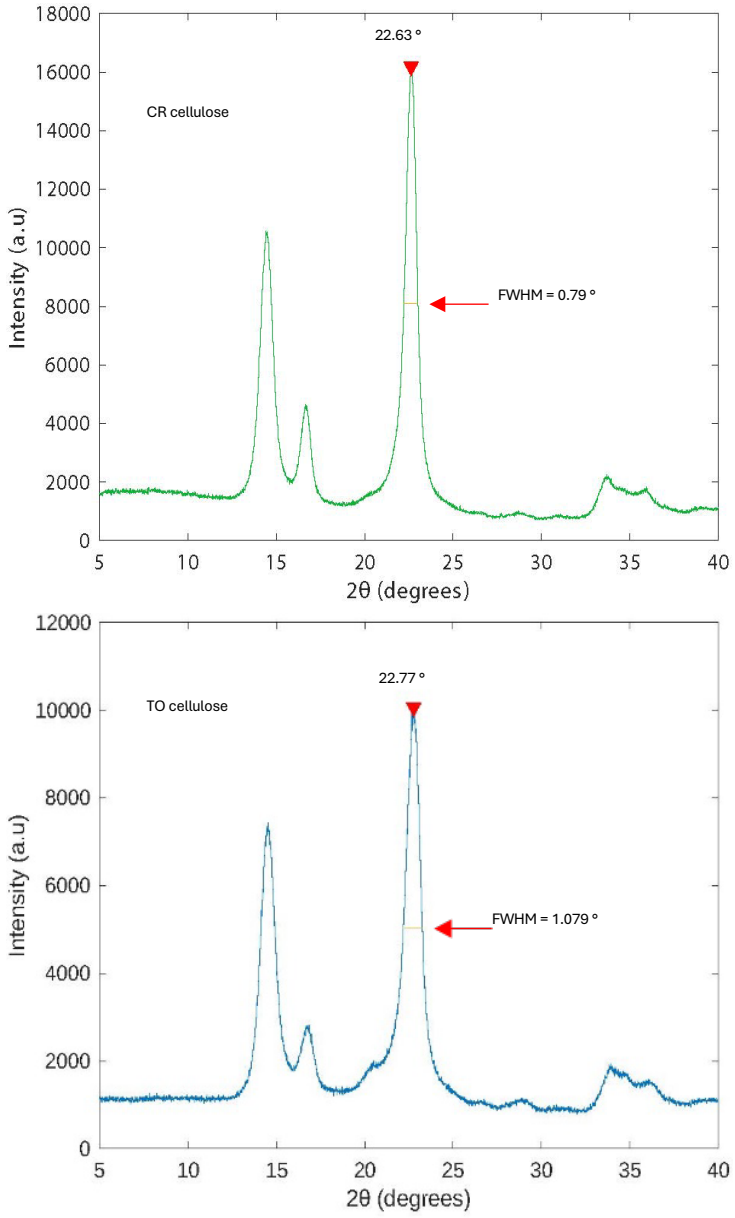

Figure 4. 10 : XRD spectra showing the FWHM measurements for CR cellulose and TP cellulose

4.4.1.3 Thermogravimetric analysis (TGA)

Figure 4.8 shows the TGA and DTA curves for commercial CNF, unmodified algae cellulose and TEMPO-oxidized cellulose. The initial weight loss for all samples below 105 °C is attributed to the evaporation of bound water (Xiang et al. 2016), with respective weight losses for commercial CNF, algae cellulose, and TEMPO-oxidized cellulose, being 6.0%, 1.0%, and 4.0%.

The primary thermal degradation of cellulose occurs between 240-400 °C (Jonjaroen et al. 2020). However, onset temperature for degradation of TEMPO-oxidized cellulose was 240 °C, which was significantly lower than that of algae cellulose at 350 °C and commercial CNF at 300 °C. This is likely the result of the sodium carboxylate groups, as evidenced by the distinct peak at 1600 cm^{-1} in the FTIR spectra, which indicates a reduced thermal stability due to the presence of sodium anhydroglucuronate units (Fukuzumi et al. 2010), a common characteristic in TEMPO-oxidized materials. The lower onset temperature of TO cellulose (240 °C), compared to algae cellulose (350 °C) and commercial CNF (300 °C), could impact the thermal stability of composite materials incorporating these fibres, potentially limiting their high-temperature applications.

For cellulose, the derivative thermogravimetric (DTG) curves demonstrate degradation peaks indicating the maximum rate of mass change typically between 290-375 °C. The initial peak at 240 °C corresponds to the decomposition of sodium anhydroglucuronate groups, while the second peak at 316 °C aligns with the degradation of the original cellulose (Fukuzumi et al. 2010). This indicates that the introduction of anhydroglucuronate units at C6 of cellulose microfibril surface leads to an earlier DTG peak and suggests a significantly reduced thermal stability of the modified cellulose compared to unmodified algae cellulose and the commercial CNF (Fukuzumi et al. 2009; Isogai et al. 2011).

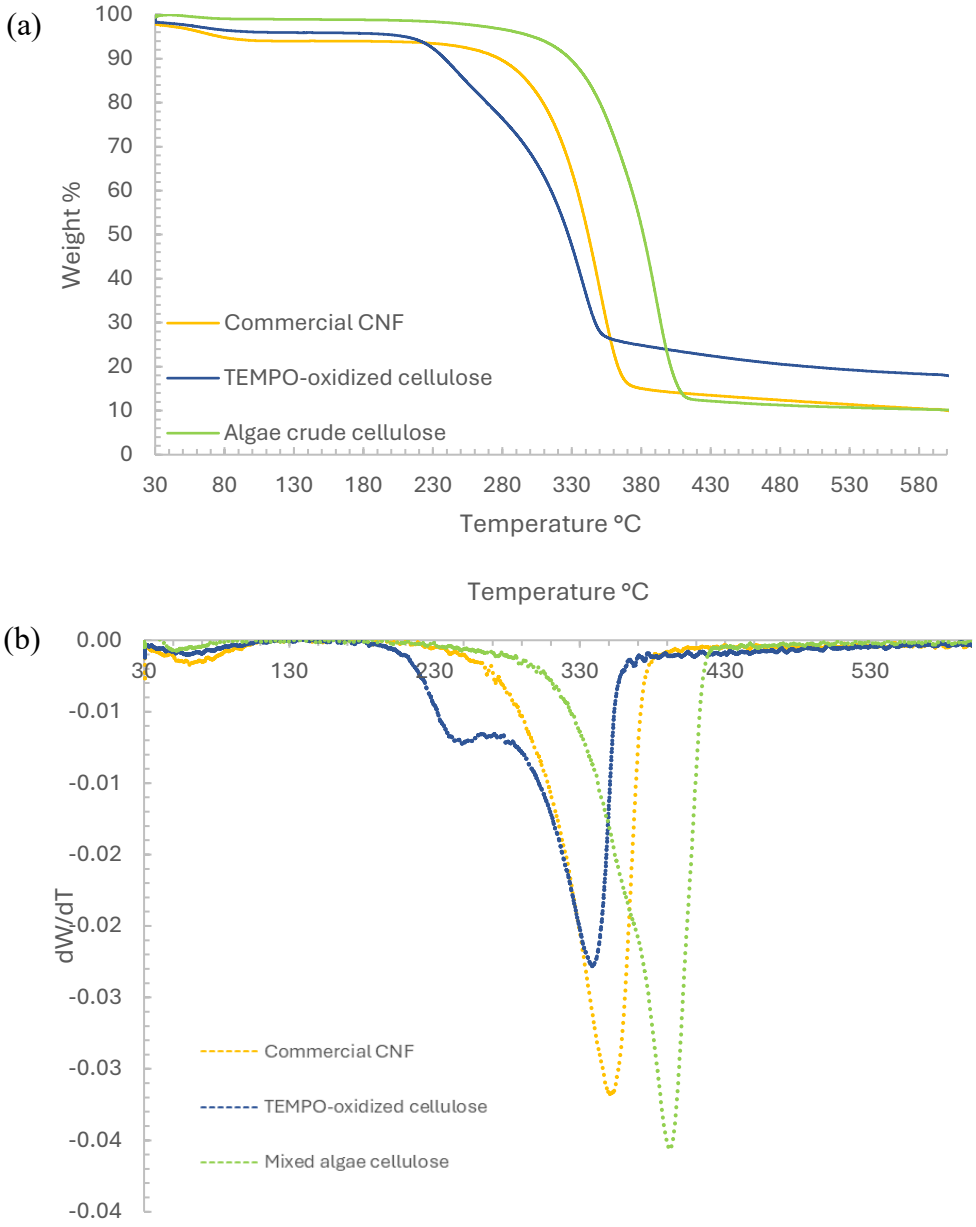

Figure 4. 11 : TGA and (b) DTG of commercial CNF, mixed algal cellulose (CR) and TEMPO mediated algal cellulose.

4.4.2 Characterization of PHBV/ nanocellulose composite films.

4.4.2.1 Preparation of PHBV composite films

The PHBV/cellulose films, with cellulose concentrations ranging from 1-3%, were prepared using a solvent exchange method (Suryanegara and Yano 2014). This method involved dispersing the cellulose in RO water, followed by acetone to remove any residual water, and finally introducing chloroform to integrate the nanocellulose with the PHBV dissolved in chloroform. The solvent exchange method significantly improved the nanocellulose dispersion within the PHBV films, when compared with films prepared through solvent casting without solvent exchange. These challenges are demonstrated in Figure C.1 in the appendix, showing the film quality with and without the use of the solvent exchange method. Without the solvent exchange method, the PHBV/nanocellulose films were prone to breakage due to cellulose agglomeration that disrupts the alignment and uniform distribution of fibres within the matrix. While surface modification techniques such as esterification, acylation and methylation are typically used to improve the compatibility between the hydrophobic polymer matrix (PHBV) and the hydrophilic filler (nanocellulose) (Stepanova and Korzhikova-Vlakh 2022), these findings highlight the role of physical dispersion of reinforcing nanocellulose fibres to improve the overall performance of the composite.

Upon visual observation, the films obtained through solvent casting were flexible and transparent indicating reduced thickness. The average thickness of obtained films was 0.06-0.07 ± 0.01 µm which was thinner compared to the PHBV reported by Benini *et al*, where a 5% of PHBV-to-solvent weight ratio was used (Benini et al. 2017). The reduced thickness of films in this current study can be mainly attributed to the lower PHBV-to-solvent ratio employed, specifically 1.8% (1 g of PHBV in 40 mL of chloroform), which resulted in thinner films. However, the thickness of the films can also be affected by other factors such as size and shape of the dish, evaporation rate, temperature, and moisture.

Visual inspection of the films showed a more uniform distribution of nanocellulose compared to the earlier attempts (Figure C.1 in the appendix), indicating successful film casting was achieved through solvent exchange. Upon visual inspection, the films

containing algae unmodified cellulose and TO cellulose showed better transparency compared to those containing commercial CNF (Figure 4.9). However, the visibility of nanofibers within the films suggests partial integration, a characteristic often observed in solvent casting processes. This partial integration may result in uneven distribution of mechanical properties across the film.

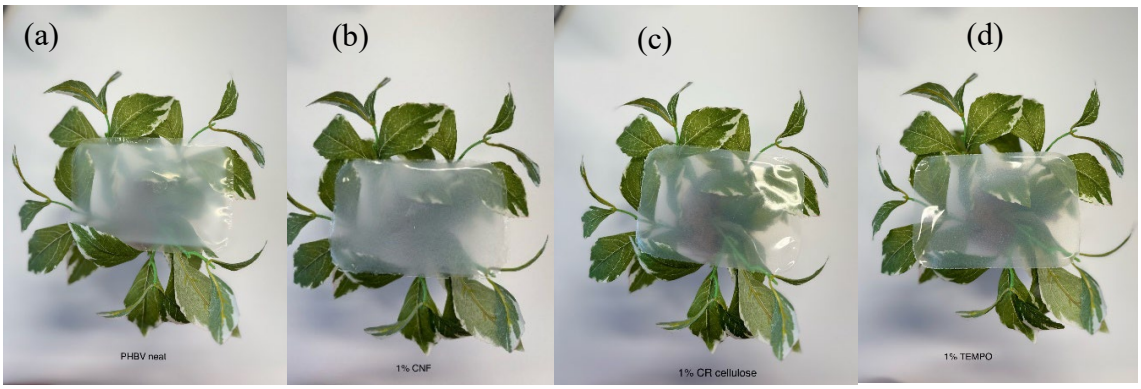

Figure 4. 12 : Visual comparison of PHBV composite films (a) neat PHBV, and with 1% cellulose reinforcement using either: (b) commercial CNF, (c) crude algal cellulose, (d) or TO cellulose.

The dispersion quality of the filler within the matrix significantly influences the overall properties of the composites. Factors such as the interaction between the filler and matrix, the sample preparation method, and the concentration of the filler play important roles (Malmir et al. 2017). To analyse the dispersion and morphology of the cellulose within PHBV matrix, SEM was carried out. The SEM analysis (Figure 4.10 (a)) showed that the neat PHBV film exhibited a smooth and consistent surface, due to absence of fillers. The PHBV film containing 1% unmodified algae cellulose displayed more prominent surface irregularities, likely due to the algae cellulose's raw and natural packed fibrous state, which suggests a potential variation in distribution. Moreover, the PHBV film with 1% TO cellulose showed some agglomeration, likely due to polarity differences between the oxidized cellulose and PHBV matrix, affecting the composite material’s uniformity. The PHBV film with 1% commercial CNF demonstrated a slightly textured surface, suggesting the presence and dispersion of CNFs within the polymer matrix without significant agglomeration, indicating effective dispersion (Figure 4.10 (b)).

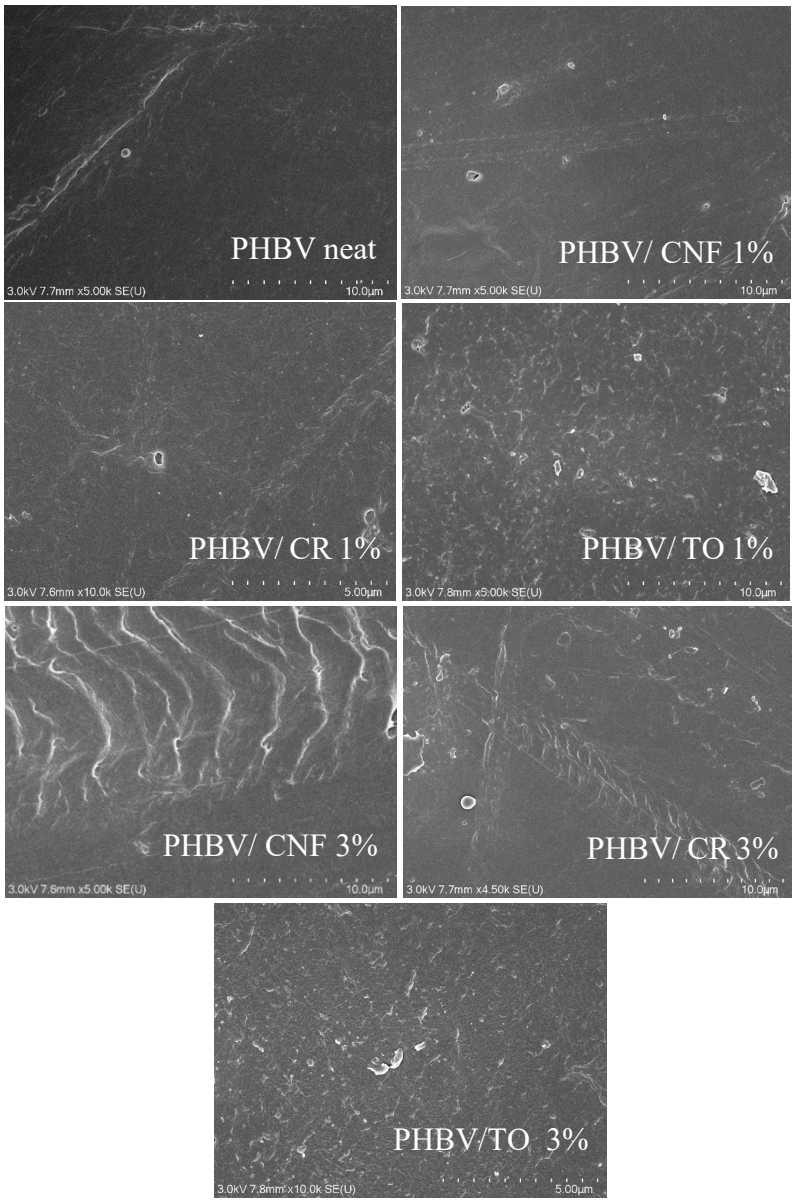

Figure 4. 16 : SEM images of neat PHBV and of composites with additions of 1% and 3% CNF, CR and TO cellulose.

The surface morphology of the PHBV film containing 3% CR cellulose (Figure 4.10 (f)) showed more prominent textural irregularities than the composite containing 1% CR cellulose. However, the PHBV composite film with 3% commercial CNF (Figure 4.10 (e)) showed moderate surface texturing, which did not significantly compromise the homogeneity of the material. This suggests that the CNF remained well-dispersed, indicating a reasonably favourable interaction with the PHBV matrix even at higher concentrations. In the composite containing 3% TO cellulose (Figure 4.10 (g)), the surfaced showed increased roughness and clear signs of agglomeration. This increase in

surface irregularities could indicate poor dispersion as the cellulose content increases, potentially impacting the composite's structural and functional performance. The increased hydrophilicity resulting from TEMPO oxidation due to added COOH groups may promote the formation of hydrogen bonds among TO cellulose fibres instead of integrating into the hydrophobic PHBV matrix. This effect may have been intensified by the rapid evaporation of the solvent during the casting process, which does not provide adequate time for the fibres to distribute evenly.

4.4.2.2 FTIR analysis

The surface chemical modifications of cellulose when incorporated into PHBV were analysed using FTIR spectroscopy. Figure 4.11 shows the FT-IR spectra of neat PHBV and PHBV composite films with 2% of CNF, CR and TO cellulose; this concentration was chosen as representative for the study. The bands observed at 2978 and 2935 cm^{-1} are attributed to anti-symmetric stretching of methyl and methylene groups of the PHBV chain (Dai et al. 2024). Other characteristic bands of PHBV, can be observed at 1723 cm^{-1} and 1282 cm^{-1} and are attributed to C-O stretching of the carbonyl ester (C=O) group and of PHBV, respectively. The absorption bands at 1451 and 1377 cm^{-1} are attributed to methylene (-CH2) and methyl (-CH3) groups, respectively (Masood et al. 2018). Additionally, absence of the characteristic peak of chloroform at 754 cm^{-1} confirms the complete evaporation of the solvent during the drying process of solvent casting (Malmir et al. 2017).

In the PHBV/cellulose composite films, only subtle variations are observed due to the low concentrations of cellulose fillers. Therefore, no significant changes in the characteristic absorption bands of the cellulose functional groups are detected, indicating that the primary structure of PHBV remains intact (Mármol et al. 2020). The consistency of the spectra suggests that the addition of cellulose does not result in significant chemical modification within the composite that are detectable by FTIR.

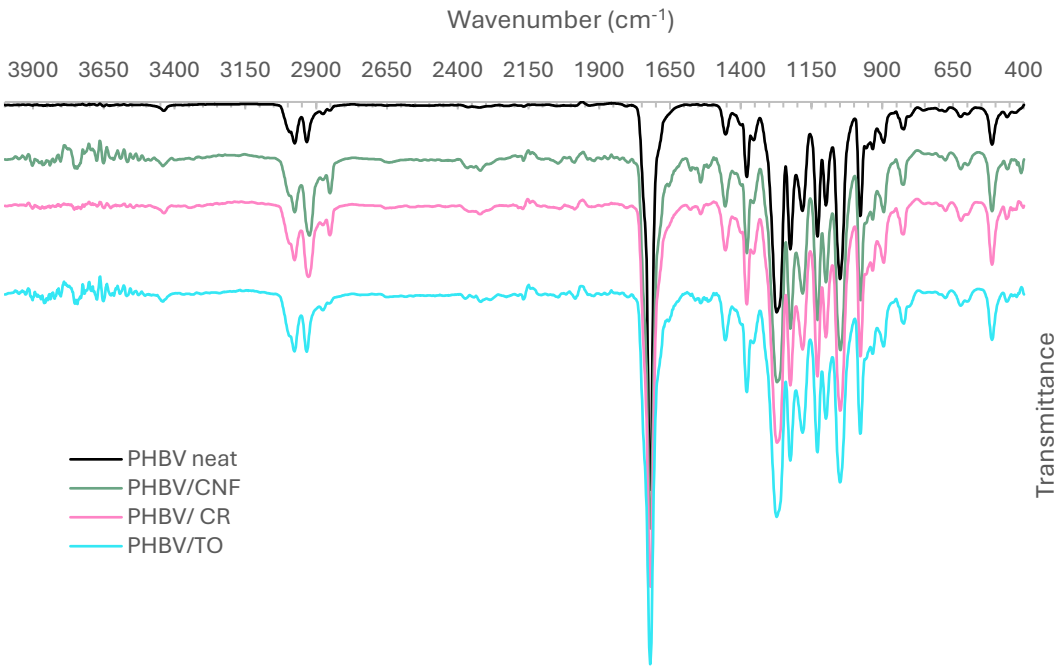

Figure 4. 17 : Representative FT-IR spectra of neat PHBV, and composite films with 2% of CNF, CR and TO cellulose.

4.4.2.3 Thermal Transitions and Crystallinity of PHBV composites by DSC

Crystallization properties of a composite demonstrate important characteristics to understand the physical properties of polymers (Zhang et al. 2019). Table 4.2 shows the thermal performance characteristic parameters of the PHBV composite films at different concentrations of nanocellulose material including cold crystallization temperature (T_c), melting temperature (T_{m2}), melting enthalpy ΔH_m, and crystallinity of the material (Debzi et al.). In this context, Tc refers to the temperature at which crystallization first occurs upon heating, indicating the polymer's processing stability. The Tm2 represents the decomposition temperature of the crystalline regions, providing insights into the polymer's thermal resistance. ΔHm quantifies the energy necessary to melt these regions, and indicates the purity and crystallinity, while Xc measures the proportion of crystalline material, important for understanding the polymer's mechanical properties (Menczel et al. 2009) .

Table 4. 2 : DSC second melting point Tm2, cooling temperature Tc, melting enthalpy ΔHm and crystallinity percentage of PHBV composites.

Sample	T_c (°C)	T_{m2} (°C)	ΔH_m(J/g)	X_c (%)
PHBV neat	90.2	169.4	79.2	54.0
PHBV/ CNF 1%	88.9	170.3	72.2	49.7
PHBV/CNF 2%	88.7	167.5	73.0	50.8
PHBV/ CNF 3%	94.0	171.5	74.9	52.6
PHBV/ CR 1%	86.1	173.4	71.5	49.3
PHBV/ CR 2%	86.9	169.9	67.8	47.2
PHBV/ CR 3%	91.0	170.1	68.7	48.3
PHBV/ TO 1%	87.4	170.2	66.0	45.5
PHBV/ TO 2%	90.7	169.3	68.6	47.7
PHBV/ TO 3%	92.3	171.6	73.9	52.0

Figure 4. 12 and Figure 4. 13 show the DSC first cooling and second heating curves of cellulose composite PHBV films compared with neat PHBV film, respectively. The cold crystallization temperature (T_c) of PHBV composites changed with the addition of CNF, CR, and TO cellulose. At concentration levels 1% and 2%, CNF and CR act as nucleating agents, slightly reducing T_c and facilitating earlier crystallization, a common phenomenon observed in composites obtained by solution casting method (Benini et al. 2017). However, the increase in T_c at higher concentrations (3% for CNF and CR, 2-3% for TO) indicates a shift in the crystallization mechanism. Although, a decrease in Tc might be expected for CR and TO cellulose at 3% concentrations due to the densely packed structure of algae cellulose and the introduction of additional COOH groups through TEMPO oxidation, this trend was not observed for CR and TO at 3%. Instead, the Tc increased. In particular, with the addition of 3% CNF, the composite showed the highest Tc, which was 4°C higher than that of the neat PHBV composite.

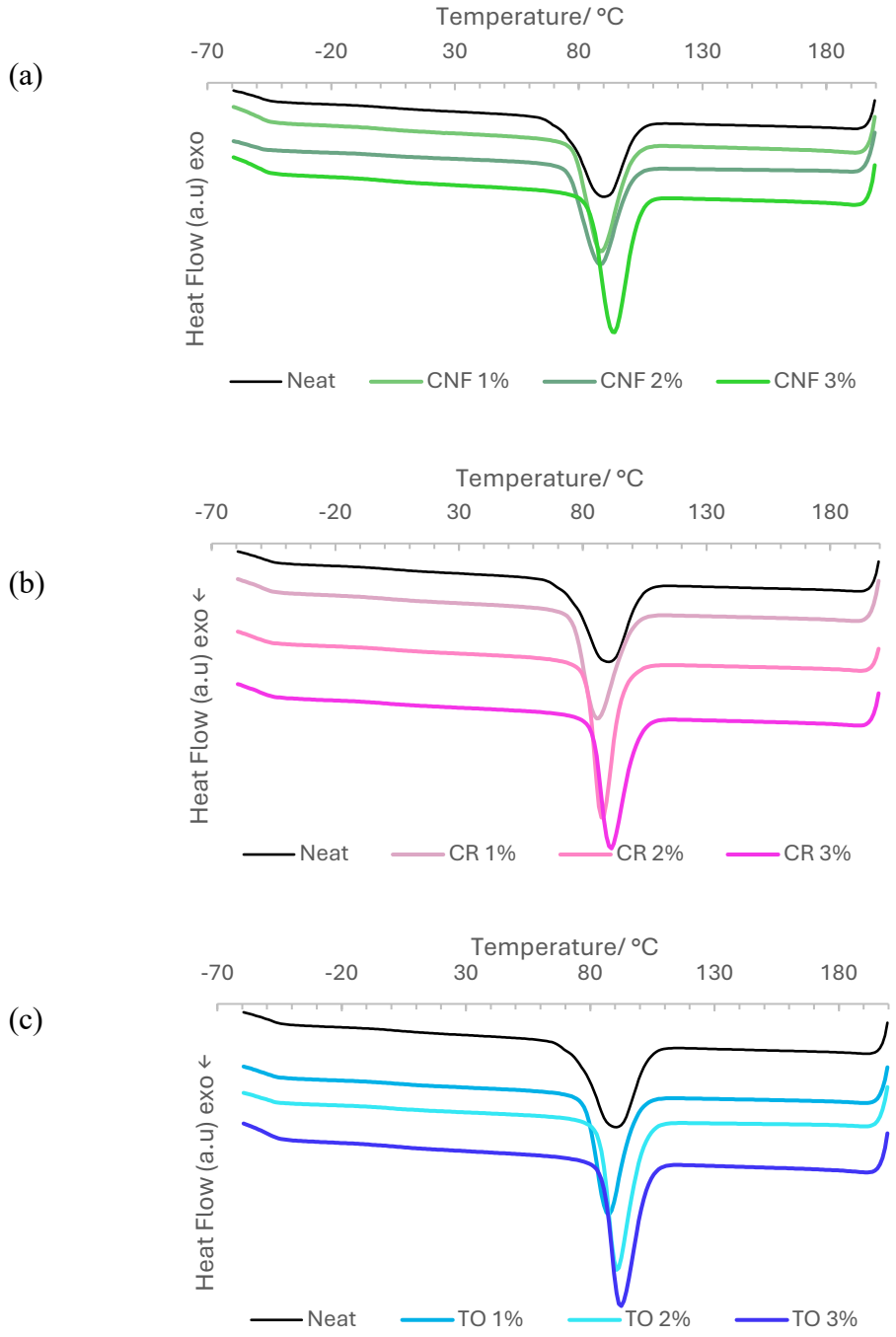

Figure 4. 18 : DSC first cooling curves of PHBV films with (a) CNF, (b) CR cellulose and (c) TO cellulose at 1-3% compared with neat PHBV film.

Thermal history was removed from the samples during the first heating cycle to ensure accurate measurement of melt temperature and melting enthalpy. The second melting temperature (T_{m2}) indicates the thermal stability of the crystalline phase. The melt temperatures in general showed a small increase with the addition of nanocellulose

compared to PHBV neat films consistent with the previous studies on PHBV/nanocellulose composites (Zhang et al. 2019). The composite material containing 1% CR cellulose exhibited the highest melting temperature (T_m), which increased to 173.4°C from 169.4°C observed for neat PHBV film. However, the observed melting temperatures showed slight variations within a narrow range, indicating no clear linear correlation with the cellulose concentration levels.

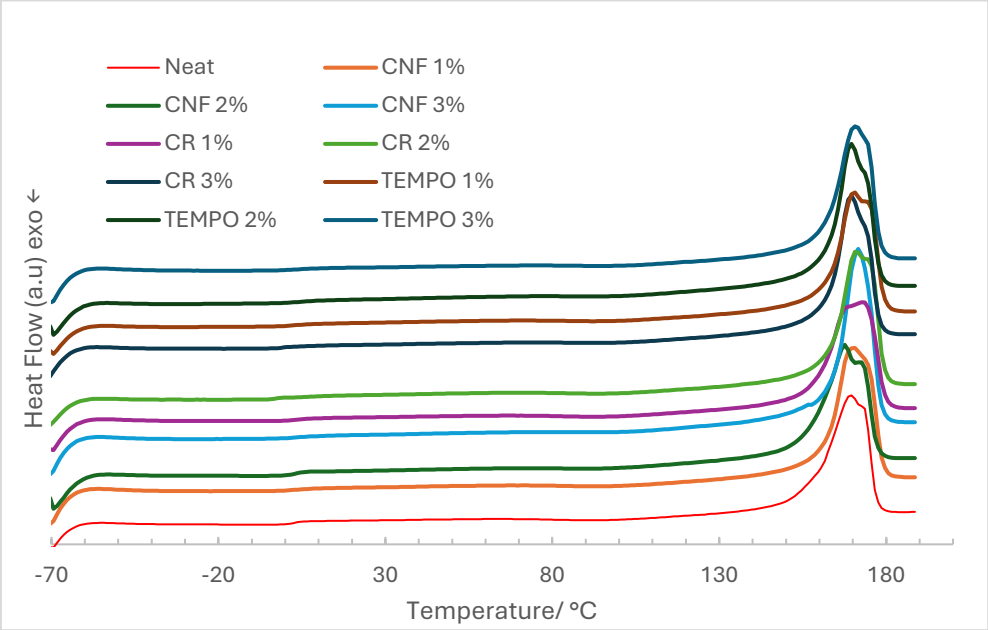

Figure 4. 19 : DSC second heating curves of neat PHBV, PHBV/CNF, PHBV/CR and PHBV/TO at 1-3% loading.

The melting enthalpy (ΔH_{m2}) indicates the amount of energy required to melt the crystalline regions of a polymer. The neat PHBV had the highest ΔH_{m2} of 79.2 J/g, suggesting a high degree of crystallinity. In general, with the addition of fillers, ΔH_m decreased, indicating that the fillers may have disrupted the crystalline structure of PHBV to some extent or affected the crystallization process. This trend is similar to that reported by Sanchez-Gracia *et al* for PHBV films incorporating purified cellulose fibres (Sanchez-Garcia et al. 2008) at higher loadings (at 5% and 10% (w/w) of the filler). However, the ΔH_m values of PHBV/cellulose composites reported in previous studies are lower (45- 48 J/g) than those found in this current study (Ashori et al. 2019; Benini et al. 2017). This could be due to various factors such as the purity, molecular weight of PHBV polymer, and sample preparation.

The calculated crystallinity percentages of all films slightly decreased with the addition of cellulose fillers compared to that of the PHBV neat films (54.0 %). Out of the nanocellulose composites, the Xc values were highest for the films with 3% addition of CNF (52.6 %) and TO cellulose (52.0%).

4.4.2.4 Mechanical Properties

The influence of the cellulose fibres on the mechanical properties of the samples were analysed by a tensile test. The effect of the cellulose fibres as a reinforcement filler was analysed based on the three parameters: Young's modulus (YM), reflecting the stiffness of the films; tensile strength (σ), indicating the strength, and tensile strain at break (ε), indicating the ductility of the composite films (Figure 4.14, Table 4.3).

Table 4. 3 : Mechanical properties of PHBV and Cellulose Nanofiber Composites in terms of Young's modulus (YM), tensile strength (σ), and tensile strain at break (ε)

Sample	YM (GPa)	σ (MPa)	ε (%)
PHBV neat	3.77 ± 0.27	39.86 ± 1.03	1.93 ± 0.19
PHBV/ CNF 1%	4.09 ± 0.26	42.20 ± 1.89	1.40 ± 0.13
PHBV/CNF 2%	3.70 ± 0.42	36.78 ± 0.47	1.12 ± 0.23
PHBV/ CNF 3%	3.44 ± 0.09	34.47 ± 2.01	1.24 ± 0.08
PHBV/ CR 1%	3.85 ± 0.68	40.02 ± 3.58	1.42 ± 0.14
PHBV/ CR 2%	3.91 ± 0.23	40.75 ± 1.95	1.58 ± 0.10
PHBV/ CR 3%	4.23 ± 0.20	42.50 ± 1.07	1.47 ± 0.10
PHBV/ TO 1%	3.28 ± 0.20	36.89 ± 0.68	1.78 ± 0.29
PHBV/ TO 2%	3.31 ± 0.33	33.46 ± 2.02	1.47 ± 0.24
PHBV/ TO 3%	3.40 ± 0.14	33.82 ± 2.25	1.39 ± 0.12

The Young's modulus values observed in this study for neat PHBV films are consistent with the values reported in literature (3.7 GPa) (Jost and Langowski 2015).

The highest increase observed was for the PHBV/CR cellulose composite with a 3% addition, showing a 12% increase compared to the neat film, suggesting an improved reinforcing effect. However, this increase was not statistically significant ($p= 0.4546$), suggesting that the reinforcing effect of CR cellulose at this concentration may vary due to the inconsistencies of the solvent casting method. (Ten et al. 2010) reported that adding 5% cellulose nano whiskers powder increased the YM by 77% compared to neat PHBV film. However, in this study, a subsequent reduction in YM was observed in composites containing 3% of CNF and TO cellulose relative to the PHBV neat film. Interestingly, a trend was observed of increasing stiffness of the composites with increasing filler concentration for the CR and TO composites.

The tensile strength of a composite material is mainly influenced by the interfacial adhesion between the reinforcing filler and the matrix (Ashori et al. 2019). In this study, the PHBV films with 1% addition of CNF had approximately 5.8% higher tensile strength than that of the neat PHBV film. However, at higher percentages of CNF tensile strength reduced. The PHBV/CR 3% composite exhibited the highest tensile strength which was 6.6 % higher than that of the PHBV neat film, although this difference is not statistically significant ($p= 0.9927$). All PHBV/TO composites had 7% lower tensile strength than the neat PHBV film.

The tensile strain of all of the PHBV composite films was lower than that of the neat PHBV film ($\varepsilon =1.93$, $Xc = 54.0\%$). In general, the elongation at break decreases with the addition of fillers, indicating that the composites become more brittle with cellulose agglomeration (Mármol et al. 2020; Zhang et al. 2019). This decrease in tensile strain can be attributed to the fillers disrupting the uniformity of the polymer matrix, which can lead to increased stress concentrations that make the material more prone to breaking under pressure.

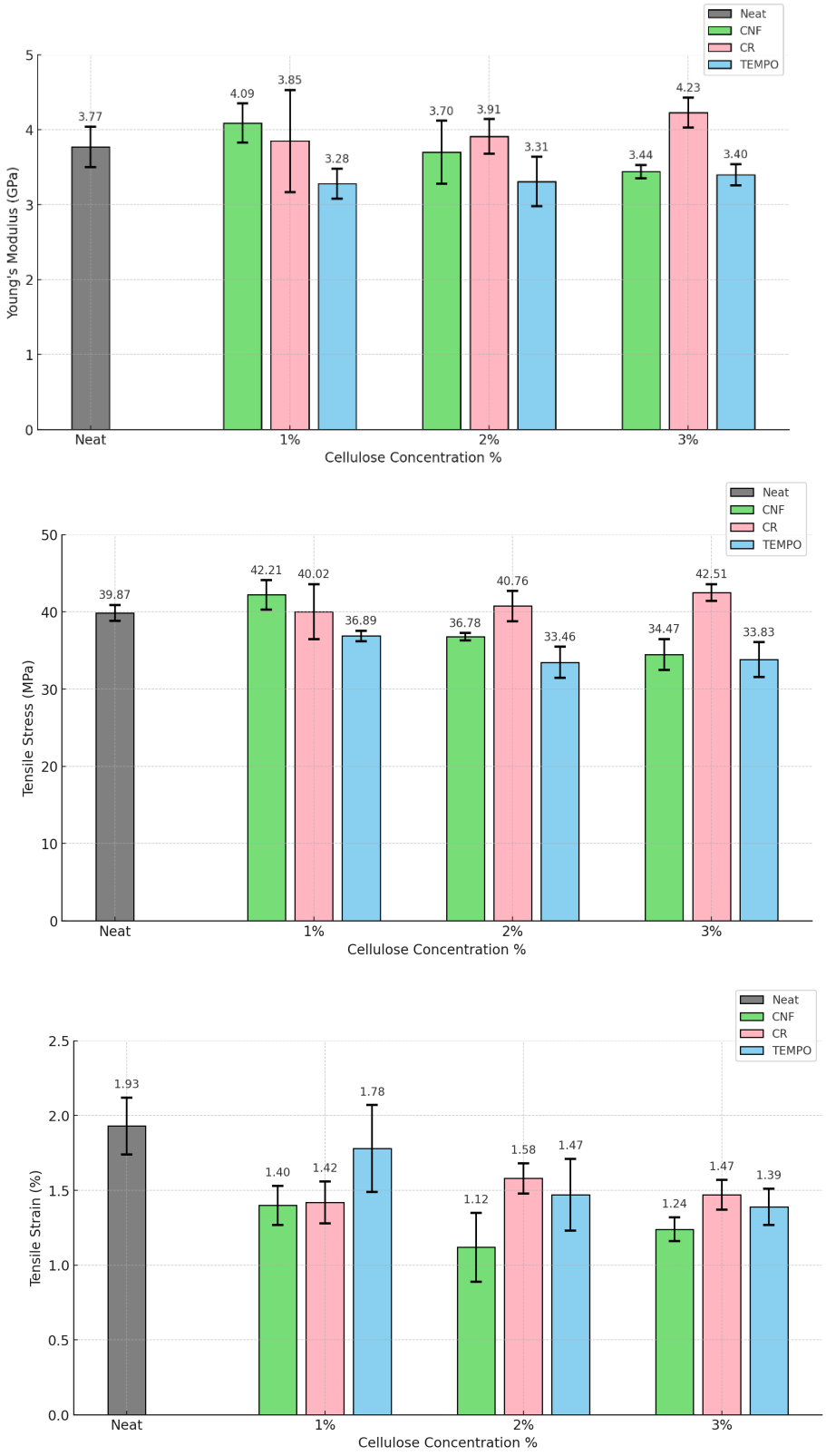

Figure 4. 20 : Mechanical Properties of PHBV and Cellulose Nanofiber Composites in terms of (a) Young's modulus, (b) tensile strength (σ), and (c) tensile strain at break (ε)

4.4.2.5 Thermogravimetric Analysis

Figure 4.15 shows the TGA and DTA curves demonstrating the thermal degradation properties of PHBV composite films. The onset degradation temperatures for these films are summarised in Table 4.4. The neat PHBV film begins its thermal degradation at an onset temperature of 243°C. This primary degradation of PHBV occurs due to ester bond cleavage within the polymer chain. With the addition of cellulose, there is an increase in onset temperatures for all composite films, indicative of enhanced thermal stability.

Algae cellulose, at a 3% concentration, increased the onset temperature by 22°C (9%) higher than that of the neat PHBV film. This improvement can be attributed to the high crystallinity index (92%) of the algae cellulose, suggesting that a well-ordered, crystalline structure contributes significantly to thermal resistance. In regard to crystalline structure, PHBV/CR composites had higher melting temperatures compared to neat PHBV films which correlates with their improved mechanical properties. This suggests that algae cellulose, in its natural unmodified state, works as a better reinforcing filler compared to TEMPO oxidized cellulose prepared following the protocol used in this study. Similarly, the composites containing CNF had enhanced thermal stability, evidenced by an onset temperature increase of 16°C at a CNF concentration of 3%. However, TEMPO cellulose composites did not show this pattern; as the 3% concentration decreased the onset temperature to 256°C from 262°C. This reduction may be likely due to agglomeration and decreased compatibility with the PHBV matrix at higher concentrations of TO cellulose.

Table 4. 4 : The onset degradation temperatures and temperatures of maximum degradation rate of the composite films

PHBV composite	Onset temperature (°C)	Temperature of maximum degradation rate (°C)
PHBV neat	243	257.5
PHBV/ CNF 1%	255	278.2
PHBV/ CNF 2%	256.7	275.2
PHBV/ CNF 3%	259.2	286.7
PHBV/ CR 1%	248.9	268.8
PHBV/ CR 2%	253.6	281.8
PHBV/ CR 3%	265.2	290.7
PHBV/ TO 1%	261.5	281.5
PHBV/ TO 2%	262.8	281.5
PHBV/ TO 3%	256.7	278.0

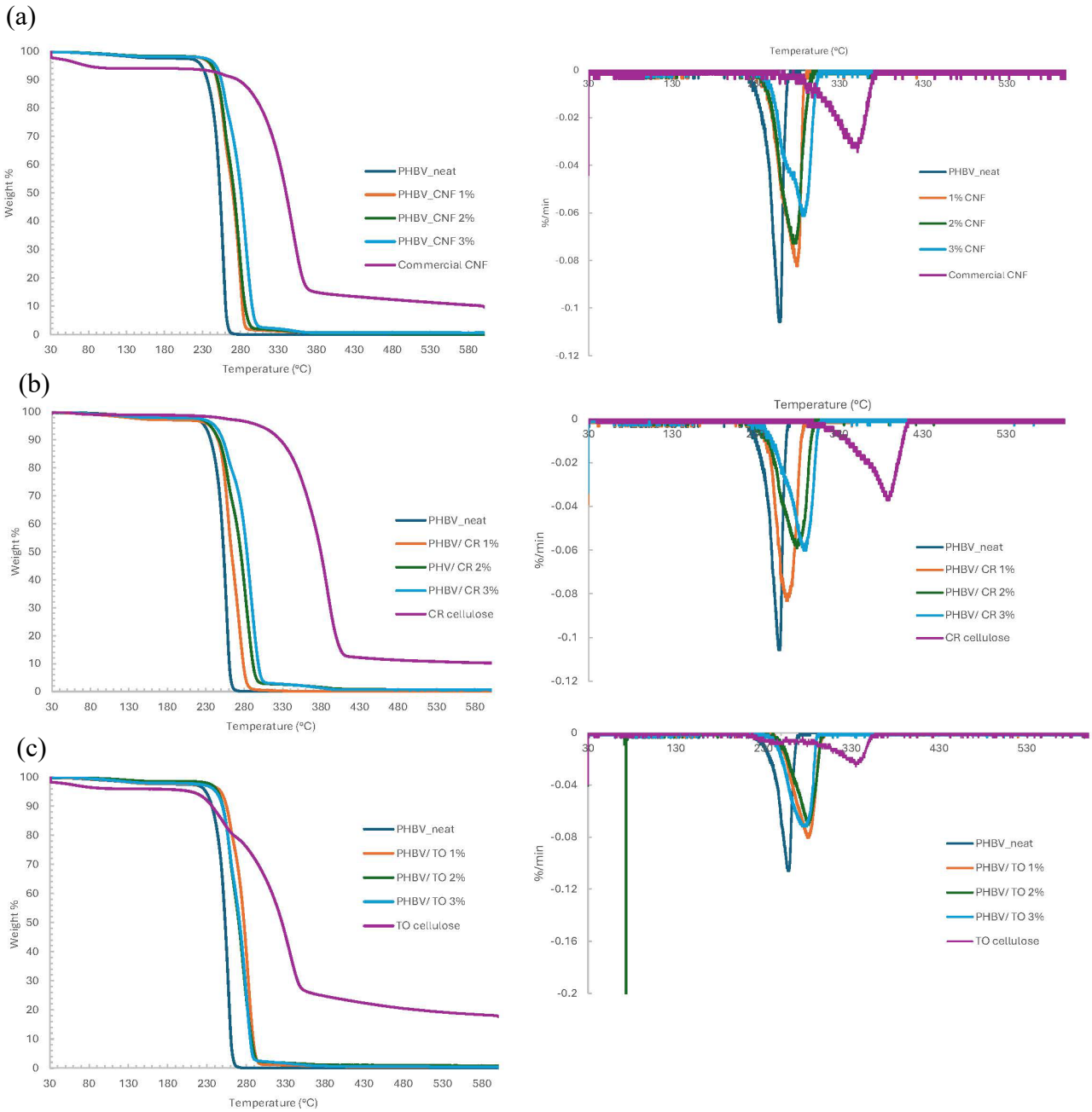

Figure 4. 21 : TGA and DTA curves demonstrating the thermal degradation properties of (a) PHBV/CNF (b) PHBV/CR and (c) PHBV/TO composite films at 1-3% addition in comparison to PHBV neat film.

4.5 Conclusion

This study demonstrates the successful extraction and utilization of cellulose nanofibers from a mixed freshwater filamentous macroalgae sample of *Rhizoclonium* sp. and *Cladophora* sp., grown in wastewater, and the impact on the thermal and mechanical properties of poly(3-hydroxybutyrate-co-3-hydroxyvalerate) films from reinforcing with macroalgae CNF. The cellulose was extracted using a sequential process involving bleaching, alkaline treatment, and acid hydrolysis, yielding approximately 15.6%. Algae cellulose demonstrated a high crystallinity index of 92% and thermal stability up to 350 °C. Subsequent TEMPO oxidation under neutral conditions produced CNFs with crystallinity of 87% and thermal stability, up to 240 °C.

The composite films were prepared using a solvent exchange method followed by a solvent casting method to disperse the CNFs within the PHBV matrix. This method involved initial dispersion of the cellulose in water, followed by acetone to remove residual water, and finally chloroform to integrate the nanocellulose with the dissolved PHBV. This approach was expected to significantly improve the uniformity of nano cellulose dispersion compared to traditional solvent casting methods.

Characterization of the PHBV composite films demonstrated improvements in their mechanical and thermal properties. Mechanical testing indicated that the addition of 3% algae cellulose resulted in a 6.6% increase in tensile strength compared to neat PHBV. The highest tensile modulus was observed in the 3% algae cellulose composite, showing a 12% increase over the neat film. DSC analysis demonstrated variations in crystallinity, with the 3% CNF composite exhibiting the highest crystallinity index of 52.6%. Moreover, thermogravimetric analysis showed enhanced thermal stability for the composite films, with the 3% algae cellulose composite increasing the onset degradation temperature by 22°C compared to neat PHBV.

This research highlights the potential of utilizing wastewater-grown macroalgae to produce high-quality nanocellulose, which can improve the mechanical and thermal properties of biodegradable PHBV composites. To further enhance the application of macroalgae CNF in thermoplastics, future research should explore alternative dispersion methods and surface modifications of algae CNF to improve compatibility with various

polymer matrices. Moreover, conducting extended biodegradability assessments of these composites under various conditions is important for validating their practical use and determining the degradation timeline. These PHBV films could potentially be utilized as packaging material for perishable goods, providing an environmentally friendly option that supports sustainability through their improved mechanical and thermal properties.

Chapter 5
General Discussion

5.1 Summary of Thesis

The overall objective of this thesis was to utilise the residual macroalgae biomass generated by small-scale wastewater treatment plants particularly in rural areas of New Zealand following bioremediation. The aim was, to recover wastewater nutrient resources as bioproducts, thereby contributing to a circular economy and to some extent provide a revenue stream from wastewater treatment. By transforming waste resources into valuable bioproducts, this research also contributes to reducing environmental pollution, minimizing waste discharge, and promoting sustainable resource management. Specifically, this thesis investigated the potential of using freshwater macroalgae biomass produced by high rate filamentous algal pond wastewater bioremediation as a substrate from valuable products such as cellulose and subsequently produce cellulose nanofibers for use in PHBV biodegradable polymer as a reinforcement filler.

This thesis has successfully met its established objectives stated under section 1.5.1, significantly advancing the knowledge and application of wastewater grown macroalgae-derived bioproducts.

Objective 1: A New Biorefinery Process for Safe Handling of Biomass and Dual Product Extraction:

Chapter 2 successfully addressed the first objective by investigating a two-step cascading biorefinery process. Freshwater filamentous macroalgae biomass of *Oedogonium calcareum*, that had been cultivated during primary wastewater treatment, was used to extract valuable bio-based products; a biostimulant extract and cellulose. The biostimulant extraction process also provided effective disinfection of the algal biomass, eliminating the indicators of human pathogens *E. coli* and F-specific RNA bacteriophage, making it safe for further use. This process produced a biostimulant extract comprising

proteins, free amino acids, the phytohormone phenylacetic acid (an auxin-like growth promoter), fatty acids, and minerals that enhance plant growth. The residual biomass following biostimulant extraction was used to extract high-quality cellulose that exhibits properties suitable for application in biodegradable polymers. Comprehensive characterization and analysis has shown that the extracted cellulose had high purity, moderate crystallinity, and thermal stability up to 260 °C, demonstrating similar characteristics to commercial MCC.

Objective 2: Freshwater Macroalgae-Derived Cellulose: Bridging the Knowledge Gap:

Chapter 3 addressed a significant gap in the literature by focusing on the extraction of cellulose from freshwater macroalgae produced as a by-product of bioremediation, which has been little studied compared to extraction of cellulose from marine macroalgae. This chapter focused on the extraction and characterisation of cellulose from four freshwater macroalgae species that commonly grow in wastewater treatment high rate filamentous algae ponds: *Rhizoclonium* sp., *Zygnema* sp., *Oedogonium* sp., and *Stigeoclonium* sp.. The extraction process employed a sequence of bleaching, alkali, and acid hydrolysis treatments and the extracted cellulose was analysed and compared in terms of yield, thermal properties, crystallinity, and morphologic structure. Furthermore, the findings of Objective 2 laid the foundation to choose a suitable algal species for subsequent use in the production of CNF for integration into PHBV polymer to produce composite materials.

Objective 3: Macroalgae-derived Cellulose Nanofiber (CNF) Production:

Chapter 4 initially focused on the production and characterization of cellulose nanofibers (CNF) from a mixed algal culture of *Rhizoclonium* sp. and *Cladophora* sp. for the production and characterization of cellulose nanofibers (CNF). Given that *Rhizoclonium* and *Cladophora* cellulose naturally coexist and have cellulose extracts with similar characteristics, as demonstrated in Chapter 3, this chapter investigated the production of macroalgae CNF using the TEMPO oxidation method under neutral conditions. This method was specifically chosen because it avoids producing by-products that could

compromise the thermal stability and water dispersion ability of the CNF. The TEMPO-oxidized CNFs exhibited high crystallinity and thermal stability. Further analysis using scanning electron microscopy (SEM) revealed the CNFs' structural attributes, such as well-defined nanofibers and high crystallinity index making them suitable for reinforcement applications.

Objective 4: Biocomposite Development:

The fourth research objective, focusing on the development and characterisation of biocomposite materials was also addressed in Chapter 4. The incorporation of unmodified algae cellulose, TEMPO-oxidized algae CNF and commercial CNF into poly(3-hydroxybutyrate-co-3-hydroxyvalerate) (PHBV) was analysed. A detailed study was conducted to evaluate the impact of these cellulose materials on the mechanical and thermal properties of PHBV composites. Composite films were prepared using a solvent exchange method, significantly enhancing the dispersion of CNF within the PHBV matrix and thereby improving mechanical properties, including tensile strength and modulus. These films, prepared using TEMPO-oxidized algae cellulose and unmodified algae cellulose, were compared against composites made with commercial CNF. The resulting films exhibited varied mechanical and thermal properties, dependent on the concentration and type of cellulose material used and could potentially be utilized as environmentally friendly packaging materials.

5.2 Implications of Research Findings

This research on the development of a new biorefinery process (Chapter 2) for the use of the algae biomass by-product from wastewater treatment using filamentous algae has identified a practical and innovative approach to recover nutrients into high value bio-products that would significantly enhance the sustainability of wastewater treatment.

Safe and Cost-Effective Disinfection of Algal Biomass:

The hot alkaline extraction method used in this study presents a feasible and cost-effective method for biostimulant extraction that simultaneously disinfects the remaining algal biomass. By effectively disinfecting the algal biomass directly within the wastewater

treatment facilities, this method would ensure that the biomass is safe for further applications, reducing the risks associated with pathogenic contaminants from the wastewater.

Enhancement of Alge Biorefinery Systems:

The study shows that the biostimulant extraction process, followed by the drying of the biomass, did not compromise the quality of the subsequently extracted cellulose. This finding is important for biorefinery operations as it allows for the sequential production of multiple valuable products from a single biomass input, enhancing overall process efficiency. The subsequent cellulose extraction from the disinfected algae biomass would likely be done in a specialised facility, therefore, the drying step post-biostimulant extraction could facilitate easier and more efficient transport of the biomass.

Economic and Environmental Benefits:

By enabling the recovery of valuable bio-based products from wastewater-grown macroalgae, this integrated process could off-set the cost of small-scale wastewater treatment. While cost assessments studies have not been conducted, the ability to produce valuable by-products (biostimulants and high-quality cellulose) could off-set operation costs and promote the adoption of sustainable wastewater treatment using macroalgae. Moreover, this approach uses fewer resources compared to other methods for disinfecting the biomass, resulting in lower maintenance costs. The use of disinfected residual macroalgae produced after extracting the biostimulant as a resource aligns with circular economy principles by turning waste into valuable resources.

Potential Applications in Material Science:

The macroalgal cellulose extract had high purity, moderately high crystallinity, and thermal stability up to 260°C. These characteristics make it suitable as a biodegradable filler in bio-composite materials. This opens up new avenues for the use of algal biomass produced during wastewater treatment. The algae-derived cellulose has potential as an

alternative source of cellulose in the materials industry such as cellulose-based foams and packaging with good barrier properties.

The findings from Chapter 3 provide important insights for the field of sustainable material sciences from freshwater macroalgae used in bioremediation.

Filling a Significant Research Gap:

The study significantly contributes to the limited literature on cellulose derived from freshwater macroalgae grown in wastewater remediation systems. By characterizing the cellulose extracted from four commonly used freshwater macroalgae, this research provides foundational insights into the unique properties of freshwater macroalgae-derived cellulose. Notably, cellulose was extracted using the same method across all species, thereby confirming that the observed differences in cellulose properties are due to species-specific characteristics, not variations in processing. Furthermore, this chapter demonstrated the distinct variations between macroalgae-derived cellulose compared to plant-derived cellulose (MCC), contributing valuable insights to the research gap in this area. This is particularly important given the limited full characterization studies available for freshwater macroalgae, compared to more commonly studied marine species.

Superior Properties of Rhizoclonium Cellulose:

Rhizoclonium cellulose demonstrated remarkably high crystallinity (92%) and thermal stability (up to 345 °C), surpassing that of commercially available plant-derived cellulose nanofibers (CNF). Moreover, *Rhizoclonium* cellulose showed similar characteristics to *Cladophora* cellulose which has been previously used to reinforce thermoplastics. These unique characteristics position *Rhizoclonium* as an excellent candidate for reinforcing bioplastics, offering a sustainable alternative to traditional synthetic fibres used in composite materials.

Sustainable Material Development and Implications for Bioplastics:

The findings from Chapter 3 provide valuable insights into the potential of macroalgae-derived cellulose for use in PHBV composites and its impact on thermal and mechanical properties such as tensile strength and modulus. Additionally, the integration of macroalgal cellulose into PHBV has been shown to enhance thermal stability, increasing the degradation temperature of the composites, which is crucial for processing and application in high temperature settings. These improvements demonstrate the efficacy of using sustainable biobased materials to improve the performance of biodegradable plastics.

Utilization of Mixed Algae Cultures:

By successfully utilizing a mixed culture of *Rhizoclonium* and *Cladophora*, which naturally coexist in wastewater treatment ponds, this research highlights the feasibility of using non-monocultured algae biomass for nanocellulose production. The characterization of cellulose from this mixed culture demonstrated similar XRD patterns and thermal stability to those of monoculture biomass of these species, confirming that these properties are not compromised when moving from pure culture to mixed-species culture. This broadens the scope for sourcing of raw algal biomass, making the process more applicable to real-world applications.

Implications for Nanocellulose Applications:

Wastewater-grown algae is an underutilized biomass in industrial settings, offering significant potential. Utilizing waste algae biomass reduces environmental impact while providing a cost-effective approach to produce high-quality nanocellulose, advancing material science. The successful incorporation of algae-derived cellulose nanofibers (CNF) into PHBV composites and the comprehensive analysis of their mechanical and thermal properties provides foundational work for future practical applications of macroalgal biomass from wastewater treatment.

Implications for Industrial Operations:

Demonstrating the effective use of mixed algae biomass in producing high-quality CNF that can be integrated into commercial polymers paves the way for scaling up this technology. The findings of chapter 4 have relevance for industries that could focus on sustainable material solutions to utilize readily available wastewater algae. This approach offers substantial economic benefits by converting waste into valuable bioproducts, reducing operational costs and creating new revenue streams. Additionally, the environmental impact is significant, as this method contributes to the reduction of pollutants and the carbon footprint of treatment facilities. These advancements could also lead to significant socioeconomic benefits by creating new industries and job opportunities in sustainable practices, aligning with worldwide efforts to enhance environmental sustainability and economic strength.

Sustainable Composite Material Development:

This research demonstrates the potential of utilizing eco-friendly reinforcement fillers such as algae-derived nanocellulose in enhancing the properties of composites made from the biodegradable polymer; PHBV. The findings of this study could encourage the thermoplastic industry to explore biodegradable alternatives that maintain the material properties required for applications, particularly targeting packaging material for perishable goods.

5.3 Recommendations for Future Work

The thesis has laid a foundation for the sustainable utilisation of wastewater-grown freshwater macroalgal biomass by producing valuable bio-based products (such as cellulose and biostimulant), macro-algae derived nanocellulose (CNF) and incorporating macroalgae-CNF into PHBV bioplastic.

Future research should focus on conducting detailed plant assays to assess the growth-promoting activity of the *O. calcareum* biostimulant analysing the seed germination rate and growth in terms of root length, shoot length, plant height etc. This would involve evaluating its efficacy to improve the production of various plant species under controlled conditions to confirm its commercial viability as a biostimulant.

Additionally, it is essential to conduct stability studies to determine the longevity and effectiveness of the biostimulant over time in different storage conditions. This will help assess the biostimulant's viability as a commercial product complying in accordance with the European Union Fertilising Products Regulation (EU) 2019/1009. This will ensure that the biostimulant meets all necessary regulatory requirements for commercial distribution.

Moreover, pilot-scale studies should be conducted to evaluate the operational feasibility and scalability of incorporating the biorefinery process into established small-scale wastewater treatment plants (WWTPs). This would involve scaling up the production process and assessing the economic and environmental impacts of the scale-up.

This research assessed the quality of cellulose of four macroalgae species that are commonly found in wastewater treatment filamentous algae high rate algal ponds. However, future work needs to include cellulose from other freshwater macroalgae species found in diverse freshwater habitats (rivers and lakes) such as *Prasiola* sp., *Lemanea* sp., and *Spirogyra* sp. This will help to build a comprehensive database of macroalgae-derived cellulose characterization, which would be helpful to select species for specific material applications.

Moreover, the reasons why cellulose varies between macroalgae species are not well understood. Therefore, investigating the genetic factors that influence cellulose production in different algae species will be useful understand cellulose biosynthesis. This could provide insights into the biochemical mechanisms responsible for variations in cellulose quality and yield, leading to potential genetic research.

Investigating the chemical modification of algae cellulose, such as esterification, methylation, and acetylation, should be a future focus to enhance its compatibility with PHBV and other polymers. This could significantly improve the mechanical properties and expand the range of potential applications for the composites.

Further research should explore alternative processing methods like melt compounding, which may provide better integration of nanocellulose into polymers, thereby improving the uniformity and properties of the composite materials.

Additionally, examining the impact of the addition of algae-derived CNF to other biopolymers such as thermoplastic starch, and agar would assess its versatility and effectiveness as a reinforcing agent. Such studies could lead to the development of new composite materials with enhanced properties for a wide range of applications.

Conducting comprehensive biodegradability assessments of the developed biocomposite materials would be crucial. This would help understand their decomposition time periods, quantify the sustainability benefits, and identify areas for improvement.

5.4 Concluding Remarks

This thesis has successfully explored the potential of using freshwater macroalgae biomass produced as a by-product of wastewater bioremediation to produce biostimulants and cellulose and the subsequent production of high-quality cellulose nanofibers (CNF). These CNFs were then incorporated into biodegradable polymers, specifically PHBV, to enhance their mechanical and thermal properties, demonstrating the practical applicability of wastewater algae-derived materials in sustainable material development.

The interconnected studies conducted as part of this thesis collectively demonstrate the versatility and value of wastewater grown macroalgae as a sustainable resource. This research applies chemistry principles to make significant contributions to the field of chemistry environmental science and material science by effectively disinfecting and utilising algae biomass in biorefinery processes, as well as through the production and application of algae-derived CNFs in PHBV biocomposites. These advancements also enhance practical environmental approaches, bridging academic research with real-world applications. Each chapter addressed specific current research gaps and also laid the foundation for future work that can expand these findings into commercial and environmental applications.

The integration of these processes into existing systems, such as small-scale high rate filamentous algal pond wastewater treatment plants, highlights the potential for real-world application, offering a dual benefit of waste treatment and valuable product recovery. This aligns with the principles of a circular economy, where wastewater resources are recovered for beneficial re-use, providing a two-product biorefinery model for future innovation in sustainable manufacturing processes.

In conclusion, the work presented in this thesis demonstrates a promising pathway for the use of wastewater-derived macroalgae through extraction of valuable bio-based products. The findings from this thesis pave the way for future research while highlighting the potential for expanding the scope of bio-based products derived from macroalgae to meet the increasing demands for sustainable and environmentally friendly materials.

References

Al-Haik MY, Aldajah S, Siddique W, Kabir MM, Haik Y (2022) Mechanical and thermal characterization of polypropylene-reinforced nanocrystalline cellulose nanocomposites. Journal of Thermoplastic Composite Materials 35:680-691

Alam SN, Khalid Z, Guldhe A, Singh B, Korstad J (2021) Harvesting and pretreatment techniques of aquatic macrophytes and macroalgae for production of biofuels. Environmental Sustainability 4:299-316

Aloui H, Khwaldia K, Hamdi M, Fortunati E, Kenny JM, Buonocore GG, Lavorgna M (2016) Synergistic Effect of Halloysite and Cellulose Nanocrystals on the Functional Properties of PVA Based Nanocomposites. ACS Sustainable Chemistry & Engineering 4:794-800 doi:10.1021/acssuschemeng.5b00806

Amara C, El Mahdi A, Medimagh R, Khwaldia K (2021) Nanocellulose-based composites for packaging applications. Current Opinion in Green and Sustainable Chemistry 31:100512

Ashori A, Jonoobi M, Ayrilmis N, Shahreki A, Fashapoyeh MA (2019) Preparation and characterization of polyhydroxybutyrate-co-valerate (PHBV) as green composites using nano reinforcements. International journal of biological macromolecules 136:1119-1124

Atalla RH, Whitmore RE, Vanderhart DL (1985) A highly crystalline cellulose from Rhizoclonium hieroglyphicum. Biopolymers 24:421-423 doi:https://doi.org/10.1002/bip.360240209

Bajpai P (2016) Chapter 3 - Pulp and Paper Production Processes and Energy Overview. In: Bajpai P (ed) Pulp and Paper Industry. Elsevier, Amsterdam, pp 15-49

Barbot YN, Al-Ghaili H, Benz R (2016) A Review on the Valorization of Macroalgal Wastes for Biomethane Production. Marine drugs 14:120 doi:10.3390/md14060120

Bartošová A, Blinová L, Gerulová K (2015) Characterisation of polysacharides and lipids from selected green algae species by FTIR-ATR spectroscopy. Research Papers Faculty of Materials Science and Technology Slovak University of Technology 23:97-102

Benini KC, Cioffi MOH, Voorwald HJC (2017) PHBV/cellulose nanofibrils composites obtained by solution casting and electrospinning process. Matéria (Rio de Janeiro) 22:e11837

Berglund B, Dienus O, Sokolova E, Berglind E, Matussek A, Pettersson T, Lindgren P-E (2017) Occurrence and removal efficiency of parasitic protozoa in Swedish wastewater treatment plants. Science of The Total Environment 598:821-827 doi:https://doi.org/10.1016/j.scitotenv.2017.04.015

Bhaladhare S, Das D (2022) Cellulose: A fascinating biopolymer for hydrogel synthesis. Journal of Materials Chemistry B

Bhong M, Khan TK, Devade K, Krishna BV, Sura S, Eftikhaar H, Thethi HP, Gupta N (2023) Review of composite materials and applications. Materials Today: Proceedings

Bogolitsyn K, Ovchinnikov D, Kaplitsin P, Druzhinina A, Parshina A, Shul′ gina E, Semushina M, Aleshina L (2017) Isolation and structural characterization of cellulose from arctic brown algae. Chemistry of Natural Compounds 53:533-537

Börjesson M, Westman G (2015) Crystalline nanocellulose—preparation, modification, and properties. Cellulose-fundamental aspects and current trends

Boskovic BO, Stolojan V, Khan RUA, Haq S, Silva SRP (2002) Large-area synthesis of carbon nanofibres at room temperature. Nature Materials 1:165-168 doi:10.1038/nmat755

Brigham C (2018) Chapter 3.22 - Biopolymers: Biodegradable Alternatives to Traditional Plastics. In: Török B, Dransfield T (eds) Green Chemistry. Elsevier, pp 753-770

Chahal C, van den Akker B, Young F, Franco C, Blackbeard J, Monis P (2016) Chapter Two - Pathogen and Particle Associations in Wastewater: Significance and Implications for Treatment and Disinfection Processes. In: Sariaslani S, Michael Gadd G (eds) Advances in Applied Microbiology, vol 97. Academic Press, pp 63-119. doi:https://doi.org/10.1016/bs.aambs.2016.08.001

Chaker A, Alila S, Mutjé P, Vilar MR, Boufi S (2013) Key role of the hemicellulose content and the cell morphology on the nanofibrillation effectiveness of cellulose pulps. Cellulose 20:2863-2875 doi:10.1007/s10570-013-0036-y

Chen Z, Aziz T, Sun H, Ullah A, Ali A, Cheng L, Ullah R, Khan FU (2023) Advances and applications of cellulose bio-composites in biodegradable materials. Journal of Polymers and the Environment 31:2273-2284

Cheremisinoff NP, Rosenfeld PE (2010) Chapter 6 - Sources of air emissions from pulp and paper mills. In: Cheremisinoff NP, Rosenfeld PE (eds) Handbook of Pollution Prevention and Cleaner Production. William Andrew Publishing, Oxford, pp 179-259

Chitbanyong K, Pitiphatharaworachot S, Pisutpiched S, Khantayanuwong S, Puangsin B (2018) Characterization of bamboo nanocellulose prepared by TEMPO-mediated oxidation. BioResources 13:4440-4454

Ciolacu D, Popa V (2010) Cellulose allomorphs - Overview and perspectives. In: Cellulose: Structure and Properties, Derivatives and Industrial Uses. pp 1-38

Clarke K, Gorley R (2015) Getting started with PRIMER v7. PRIMER-E: Plymouth, Plymouth Marine Laboratory 20

Cook SD (2019) An historical review of phenylacetic acid. Plant and Cell Physiology 60:243-254

Dai Z, Li B, He M, Li J, Zou X, Wang Y, Shan Y (2024) Biodegradable and high-performance composites of poly (butylene adipate-co-terephthalate) with PHBV chain-functionalized nanocellulose. Progress in Organic Coatings 187:108136

de Amorim JDP, de Souza KC, Duarte CR, da Silva Duarte I, de Assis Sales Ribeiro F, Silva GS, de Farias PMA, Stingl A, Costa AFS, Vinhas GM (2020) Plant and bacterial nanocellulose: Production, properties and applications in medicine, food, cosmetics, electronics and engineering. A review. Environmental Chemistry Letters 18:851-869

Debzi EM, Chanzy H, Sugiyama J, Tekely P, Excoffier G (1991) The Iα →Iβ transformation of highly crystalline cellulose by annealing in various mediums. Macromolecules 24:6816-6822 doi:10.1021/ma00026a002

10.1021/ma00026a002</p>

Department of Internal Affairs (2018) Three water review, cost estimates for upgrading wastewater treatment plants to meet objectives of the NPS freshwater. https://www.dia.govt.nz/Three-waters-review

Ding Q, Han W, Li X, Jiang Y, Zhao C (2020) New insights into the autofluorescence properties of cellulose/nanocellulose. Scientific Reports 10:21387 doi:10.1038/s41598-020-78480-2

Dos Santos RM, Neto WPF, Silvério HA, Martins DF, Dantas NO, Pasquini D (2013) Cellulose nanocrystals from pineapple leaf, a new approach for the reuse of this agro-waste. Industrial Crops and Products 50:707-714

Du H, Liu W, Zhang M, Si C, Zhang X, Li B (2019) Cellulose nanocrystals and cellulose nanofibrils based hydrogels for biomedical applications. Carbohydrate polymers 209:130-144

Dziergowska K, Wełna M, Szymczycha-Madeja A, Chęcmanowski J, Michalak I (2021) Valorization of Cladophora glomerata biomass and obtained bioproducts into biostimulants of plant growth and as sorbents (biosorbents) of metal ions. Molecules 26:6917

Environment Mft (2017) A guide to the national policy statement for freshwater management 2014.

Eshaq FS, Ali MN, Mohd MK (2010) Spirogyra biomass a renewable source for biofuel (bioethanol) Production. International Journal of Engineering Science and Technology 2:7045-7054

Espinosa E, Filgueira D, Rodríguez A, Chinga-Carrasco G (2019) Nanocellulose-Based Inks—Effect of Alginate Content on the Water Absorption of 3D Printed Constructs. Bioengineering 6 doi:10.3390/bioengineering6030065

Fang Z, Li B, Liu Y, Zhu J, Li G, Hou G, Zhou J, Qiu X (2020) Critical role of degree of polymerization of cellulose in super-strong nanocellulose films. Matter 2:1000-1014

Faradilla RHF, Lee G, Rawal A, Hutomo T, Stenzel MH, Arcot J (2016) Nanocellulose characteristics from the inner and outer layer of banana pseudo-stem prepared by TEMPO-mediated oxidation. Cellulose 23:3023-3037 doi:10.1007/s10570-016-1025-8

Faria-Tischer PCS, Tischer CA, Heux L, Denmat SL, Picart C, Sierakowski M-R, Putaux J-L (2015) Preparation of cellulose II and IIII films by allomorphic conversion of bacterial cellulose I pellicles. Materials Science and Engineering: C 51:167-173 doi:https://doi.org/10.1016/j.msec.2015.02.025

Fernandes Diniz JMB, Gil MH, Castro JAAM (2004) Hornification—its origin and interpretation in wood pulps. Wood Science and Technology 37:489-494 doi:10.1007/s00226-003-0216-2

Festucci-Buselli RA, Otoni WC, Joshi CP (2007) Structure, organization, and functions of cellulose synthase complexes in higher plants. Brazilian Journal of Plant Physiology 19:1-13

Flores-Rojas E, Schnabel D, Justo-Cabrera E, Solorza-Feria O, Poggi-Varaldo HM, Breton-Deval L (2021) Using Nano Zero-Valent Iron Supported on Diatomite to Remove Acid Blue Dye: Synthesis, Characterization, and Toxicology Test. Sustainability 13:13899

Foley PM, Beach ES, Zimmerman JB (2011) Algae as a source of renewable chemicals: opportunities and challenges. Green Chemistry 13:1399-1405

Frank BP, Durkin DP, Caudill ER, Zhu L, White DH, Curry ML, Pedersen JA, Fairbrother DH (2018) Impact of silanization on the structure, dispersion properties, and biodegradability of nanocellulose as a nanocomposite filler. ACS Applied Nano Materials 1:7025-7038

Freile-Pelegrín Y, Chávez-Quintal C, Caamal-Fuentes E, Vázquez-Delfín E, Madera-Santana T, Robledo D (2020) Valorization of the filamentous seaweed Chaetomorpha gracilis (Cladophoraceae, Chlorophyta) from an IMTA system. Journal of Applied Phycology 32:2295-2306 doi:10.1007/s10811-020-02066-8

French AD, Santiago Cintrón M (2013) Cellulose polymorphy, crystallite size, and the Segal Crystallinity Index. Cellulose 20:583-588

French AD (2014) Idealized powder diffraction patterns for cellulose polymorphs. Cellulose 21:885-896 doi:10.1007/s10570-013-0030-4

Fukuzumi H, Saito T, Iwata T, Kumamoto Y, Isogai A (2009) Transparent and high gas barrier films of cellulose nanofibers prepared by TEMPO-mediated oxidation. Biomacromolecules 10:162-165

Fukuzumi H, Saito T, Okita Y, Isogai A (2010) Thermal stabilization of TEMPO-oxidized cellulose. Polymer Degradation and Stability 95:1502-1508 doi:https://doi.org/10.1016/j.polymdegradstab.2010.06.015

Gan P, Sam S, Abdullah MFb, Omar MF (2020) Thermal properties of nanocellulose‐reinforced composites: A review. Journal of Applied Polymer Science 137:48544

Gauss C, Pickering KL (2023) A new method for producing polylactic acid biocomposites for 3D printing with improved tensile and thermo-mechanical performance using grafted nanofibrillated cellulose. Additive Manufacturing 61:103346

Gautam SP, Bundela PS, Pandey AK, Jamaluddin J, Awasthi MK, Sarsaiya S (2010) A review on systematic study of cellulose. Journal of Applied and Natural Science 2:330-343 doi:10.31018/jans.v2i2.143

Ge S, Madill M, Champagne P (2018) Use of freshwater macroalgae Spirogyra sp. for the treatment of municipal wastewaters and biomass production for biofuel applications. Biomass and Bioenergy 111:213-223 doi:https://doi.org/10.1016/j.biombioe.2017.03.014

George J, Sabapathi SN (2015) Cellulose nanocrystals: Synthesis, functional properties, and applications. Nanotechnology, Science and Applications 8:45-54 doi:10.2147/NSA.S64386

Glasson CRK, Sims IM, Carnachan SM, Nys Rd, Magnusson M (2017) A cascading biorefinery process targeting sulfated polysaccharides (ulvan) from Ulva ohnoi. Algal Research 27:383-391 doi:https://doi.org/10.1016/j.algal.2017.07.001

Gong J, Li J, Xu J, Xiang Z, Mo L (2017) Research on cellulose nanocrystals produced from cellulose sources with various polymorphs. RSC Adv 7:33486-33493 doi:10.1039/C7RA06222B

Grayburn W, Holbrook G, Tatara R, Rosentrater K (2013) Harvesting, oil extraction, and conversion of local filamentous algae growing in wastewater into biodiesel. International Journal of Energy and Environment (Print) 4

Gu Y, Somerville C (2010) Cellulose synthase interacting protein: a new factor in cellulose synthesis. Plant signaling & behavior 5:1571-1574 doi:10.4161/psb.5.12.13621

Gubitosi M, Nosrati P, Koder Hamid M, Kuczera S, Behrens MA, Johansson EG, Olsson U Stable, metastable and unstable cellulose solutions. Royal Society Open Science 4:170487 doi:10.1098/rsos.170487

Habibi Y, Lucia LA, Rojas OJ (2010) Cellulose Nanocrystals: Chemistry, Self-Assembly, and Applications. Chemical Reviews 110:3479-3500 doi:10.1021/cr900339w

Halib N, Amin M, Ahmad I (2012) Physicochemical properties and characterization of nata de coco from local food industries as a source of cellulose. Sains Malaysiana 41:205-211

Hariz HB, Lawton RJ, Craggs RJ (2023a) Nutrient uptake and biomass productivity performance comparison among freshwater filamentous algae species on mesocosm-scale FANS under ambient summer and winter conditions. Ecological Engineering 189:106910

Hariz HB, Lawton RJ, Craggs RJ (2023b) Novel assay for attached Filamentous algae productivity and nutrient removal. Journal of Applied Phycology 35:251-264

Henriksson G, Lennholm H (2009) Cellulose and carbohydrate chemistry. Wood chemistry and biotechnology 1:71-101

Henriksson M, Henriksson G, Berglund L, Lindström T (2007) An environmentally friendly method for enzyme-assisted preparation of microfibrillated cellulose

(MFC) nanofibers. European Polymer Journal 43:3434-3441 doi:10.1016/j.eurpolymj.2007.05.038
Hernández-Herrera RM, Santacruz-Ruvalcaba F, Ruiz-López MA, Norrie J, Hernández-Carmona G (2014) Effect of liquid seaweed extracts on growth of tomato seedlings (Solanum lycopersicum L.). Journal of applied phycology 26:619-628
Higgins H, Stewart C, Harrington K (1961) Infrared spectra of cellulose and related polysaccharides. Journal of polymer science 51:59-84
Honjo G, Watanabe M (1958) Examination of Cellulose Fibre by the Low-Temperature Specimen Method of Electron Diffraction and Electron Microscopy. Nature 181:326-328 doi:10.1038/181326a0
Horikawa Y, Sugiyama J (2009) Localization of Crystalline Allomorphs in Cellulose Microfibril. Biomacromolecules 10:2235-2239 doi:10.1021/bm900413k
Huang L, Zhang X, Xu M, Chen J, Shi Y, Huang C, Wang S, An S, Li C (2018) Preparation and mechanical properties of modified nanocellulose/PLA composites from cassava residue. Aip Advances 8
Huang Y, Meng F, Liu R, Yu Y, Yu W (2019) Morphology and supramolecular structure characterization of cellulose isolated from heat-treated moso bamboo. Cellulose 26:7067-7078
Ilyas R, Atikah M Production of nanocellulose from sustainable algae marine biomass. In: Seminar on Advanced Bio-and Mineral based Natural Fibre Composites (SBMC2021); Institute of Tropical Forestry and Forest Product (INTROP), Universiti Putra Malaysia: Serdang, Malaysia, 2021.
Imai T, Sugiyama J, Itoh T, Horii F (1999) Almost Pure Iα Cellulose in the Cell Wall of Glaucocystis. Journal of Structural Biology 127:248-257 doi:https://doi.org/10.1006/jsbi.1999.4160
Ioelovich M (2021) Preparation, characterization and application of amorphized cellulose—A review. Polymers 13:4313
Isogai A, Saito T, Fukuzumi H (2011) TEMPO-oxidized cellulose nanofibers. Nanoscale 3:71-85 doi:10.1039/C0NR00583E
Isogai A, Hänninen T, Fujisawa S, Saito T (2018) Review: Catalytic oxidation of cellulose with nitroxyl radicals under aqueous conditions. Progress in Polymer Science 86:122-148 doi:https://doi.org/10.1016/j.progpolymsci.2018.07.007
Isogai A, Bergström L (2018) Preparation of cellulose nanofibers using green and sustainable chemistry. Current Opinion in Green and Sustainable Chemistry 12:15-21
Iwamoto S, Nakagaito A, Yano H (2007) Nano-fibrillation of pulp fibers for the processing of transparent nanocomposites. Applied Physics A 89:461-466
Janardhnan S, Sain MM (2006) Isolation of cellulose microfibrils–an enzymatic approach. Bioresources 1:176-188
Jayasooriya N, Magnusson M, Gavin C, Gauss C, Craggs R, Battershill CN, Glasson CRK (2024) Quality of cellulose and biostimulant extracts from Oedogonium calcareum cultivated during primary wastewater treatment. Bioresource Technology:130850 doi:https://doi.org/10.1016/j.biortech.2024.130850
Jmel MA, Anders N, Ben Messaoud G, Marzouki MN, Spiess A, Smaali I (2019) The stranded macroalga Ulva lactuca as a new alternative source of cellulose: Extraction, physicochemical and rheological characterization. J Cleaner Prod 234:1421-1427 doi:https://doi.org/10.1016/j.jclepro.2019.06.225
Jonjaroen V, Ummartyotin S, Chittapun S (2020) Algal cellulose as a reinforcement in rigid polyurethane foam. Algal Research 51:102057 doi:https://doi.org/10.1016/j.algal.2020.102057

Jost V, Langowski H-C (2015) Effect of different plasticisers on the mechanical and barrier properties of extruded cast PHBV films. European Polymer Journal 68:302-312 doi:https://doi.org/10.1016/j.eurpolymj.2015.04.012

Jun D, Guomin Z, Mingzhu P, Leilei Z, Dagang L, Rui Z (2017) Crystallization and mechanical properties of reinforced PHBV composites using melt compounding: Effect of CNCs and CNFs. Carbohydrate polymers 168:255-262

Kalia S, Boufi S, Celli A, Kango S (2014) Nanofibrillated cellulose: surface modification and potential applications. Colloid and Polymer Science 292:5-31

Kapoore RV, Wood EE, Llewellyn CA (2021) Algae biostimulants: A critical look at microalgal biostimulants for sustainable agricultural practices. Biotechnology Advances 49:107754

Kargarzadeh H, Ioelovich M, Ahmad I, Thomas S, Dufresne A (2017) Methods for Extraction of Nanocellulose from Various Sources. In. pp 1-49

Kerr N (1995) Advantages and Limitations of the Ninhydrin Test for Analysis of Historic Wool Fibers. MRS Online Proceedings Library 352:233-244 doi:10.1557/PROC-352-233

Keshri J (2018) Present Status and Development of Algal Pulp for Hand-Made Paper Making Technology: A Review. Advances in Plants & Agriculture Research 8 doi:10.15406/apar.2018.08.00284

Keskin G, Kızıl G, Bechelany M, Pochat-Bohatier C, Öner M (2017) Potential of polyhydroxyalkanoate (PHA) polymers family as substitutes of petroleum based polymers for packaging applications and solutions brought by their composites to form barrier materials. Pure and Applied Chemistry 89:1841-1848

Khalil HPSA, Davoudpour Y, Saurabh CK, Hossain MS, Adnan AS, Dungani R, Paridah MT, Sarker MZI, Fazita MRN, Syakir MI, Haafiz MKM (2016) A review on nanocellulosic fibres as new material for sustainable packaging: Process and applications. Renew Sust Energ Rev 64:823-836 doi:https://doi.org/10.1016/j.rser.2016.06.072

Khammee P, Ramaraj R, Whangchai N, Bhuyar P, Unpaprom Y (2020) The immobilization of yeast for fermentation of macroalgae Rhizoclonium sp. for efficient conversion into bioethanol. Biomass Conversion and Biorefinery doi:10.1007/s13399-020-00786-y

Kian LK, Jawaid M, Ariffin H, Alothman OY (2017) Isolation and characterization of microcrystalline cellulose from roselle fibers. International Journal of Biological Macromolecules 103:931-940

Kidgell JT, de Nys R, Hu Y, Paul NA, Roberts DA (2014) Bioremediation of a complex industrial effluent by biosorbents derived from freshwater macroalgae. PLoS One 9:e94706-e94706 doi:10.1371/journal.pone.0094706

Koga H, Nogi M, Komoda N, Nge TT, Sugahara T, Suganuma K (2014) Uniformly connected conductive networks on cellulose nanofiber paper for transparent paper electronics. NPG Asia Materials 6:e93-e93 doi:10.1038/am.2014.9

Kong I, Tshai KY, Hoque ME (2015) Manufacturing of Natural Fibre-Reinforced Polymer Composites by Solvent Casting Method. In: Salit MS, Jawaid M, Yusoff NB, Hoque ME (eds) Manufacturing of Natural Fibre Reinforced Polymer Composites. Springer International Publishing, Cham, pp 331-349

Koyama M, Sugiyama J, Itoh T (1997) Systematic survey on crystalline features of algal celluloses. Cellulose 4:147-160 doi:10.1023/A:1018427604670

Koyanagi J, Sato M (2019) 8 - Time and temperature dependence of transverse tensile failure of unidirectional carbon fiber-reinforced polymer matrix composites. In: Guedes RM (ed) Creep and Fatigue in Polymer Matrix Composites (Second Edition). Woodhead Publishing, pp 253-268

Kulshreshtha AK (1979) 2—A review of the literature on the formation of cellulose IV, its structure, and its significance in the technology of rayon manufacture. The Journal of The Textile Institute 70:13-18 doi:10.1080/00405007908631510
La Barre S, S. Bates S, Neveux N, Bolton JJ, Bruhn A, Roberts DA, Ras M (2018) The Bioremediation Potential of Seaweeds: Recycling Nitrogen, Phosphorus, and Other Waste Products. Blue Biotechnology:217-239 doi:10.1002/9783527801718.ch7
Lacerda TM, Zambon MD, Frollini E (2013) Effect of acid concentration and pulp properties on hydrolysis reactions of mercerized sisal. Carbohydrate Polymers 93:347-356 doi:https://doi.org/10.1016/j.carbpol.2012.10.039
Laurenson S, Bolan N, Horne D, Vogeler I, Lowe H, HortResearch B The sustainable management of sewage wastewater irrigation to pasture. In: New Zealand Land Treatment Collective: Proceedings for the 2007 Annual Conference, 2007.
Lavanya D, Kulkarni P, Dixit M, Raavi PK, Krishna LNV (2011) Sources of cellulose and their applications- A review. International Journal of Drug Formulation and Research 2:19-38
Lawton RJ, de Nys R, Paul NA (2013) Selecting Reliable and Robust Freshwater Macroalgae for Biomass Applications. PLoS One 8:e64168 doi:10.1371/journal.pone.0064168
Lawton RJ, Cole AJ, Roberts DA, Paul NA, Nys Rd (2017) The industrial ecology of freshwater macroalgae for biomass applications. Algal Research 24:486-491 doi:https://doi.org/10.1016/j.algal.2016.08.019
Lawton RJ, Glasson CRK, Novis PM, Sutherland JE, Magnusson ME (2021) Productivity and municipal wastewater nutrient bioremediation performance of new filamentous green macroalgal cultivars. Journal of Applied Phycology 33:4137-4148 doi:10.1007/s10811-021-02595-w
Le Gars M, Roger P, Belgacem N, Bras J (2020) Role of solvent exchange in dispersion of cellulose nanocrystals and their esterification using fatty acids as solvents. Cellulose 27:4319-4336 doi:10.1007/s10570-020-03101-0
Lee H, Mani S (2017) Mechanical pretreatment of cellulose pulp to produce cellulose nanofibrils using a dry grinding method. Industrial crops and products 104:179-187
Lemire KA, Rodriguez YY, McIntosh MT (2016) Alkaline hydrolysis to remove potentially infectious viral RNA contaminants from DNA. Virology Journal 13:88 doi:10.1186/s12985-016-0552-0
Levanič J, Šenk VP, Nadrah P, Poljanšek I, Oven P, Haapala A (2020) Analyzing TEMPO-Oxidized Cellulose Fiber Morphology: New Insights into Optimization of the Oxidation Process and Nanocellulose Dispersion Quality. ACS Sustainable Chemistry & Engineering 8:17752-17762 doi:10.1021/acssuschemeng.0c05989
Lewandowska S, Marczewski K, Kozak M, Ohkama-Ohtsu N, Łabowska M, Detyna J, Michalak I (2022) Impact of freshwater macroalga (Cladophora glomerata) extract on the yield and morphological responses of Glycine max (L.) Merr. Agriculture 12:685
Liu S, Low ZX, Xie Z, Wang H (2021a) TEMPO‐Oxidized Cellulose Nanofibers: A Renewable Nanomaterial for Environmental and Energy Applications. Advanced Materials Technologies 6:2001180
Liu Y, Ahmed S, Sameen DE, Wang Y, Lu R, Dai J, Li S, Qin W (2021b) A review of cellulose and its derivatives in biopolymer-based for food packaging application. Trends in Food Science & Technology 112:532-546
Lo Faro E, Menozzi C, Licciardello F, Fava P (2021) Improvement of Paper Resistance against Moisture and Oil by Coating with Poly (-3-hydroxybutyrate-co-3-hydroxyvalerate)(PHBV) and Polycaprolactone (PCL). Applied Sciences 11:8058

Lyu Y, Ye H, Zhao Z, Tian J, Chen L (2020) Exploring the cost of wastewater treatment in a chemical industrial Park: Model development and application. Resources, Conservation and Recycling 155:104663 doi:https://doi.org/10.1016/j.resconrec.2019.104663

Magnusson M, Carl C, Mata L, Nys Rd, Paul NA (2016) Seaweed salt from Ulva: A novel first step in a cascading biorefinery model. Algal Research 16:308-316 doi:https://doi.org/10.1016/j.algal.2016.03.018

Malmir S, Montero B, Rico M, Barral L, Bouza R (2017) Morphology, thermal and barrier properties of biodegradable films of poly (3-hydroxybutyrate-co-3-hydroxyvalerate) containing cellulose nanocrystals. Composites Part A: Applied Science and Manufacturing 93:41-48

Manns D, Deutschle AL, Saake B, Meyer AS (2014) Methodology for quantitative determination of the carbohydrate composition of brown seaweeds (Laminariaceae). RSC Adv 4:25736-25746

Mariano M, El Kissi N, Dufresne A (2014) Cellulose nanocrystals and related nanocomposites: Review of some properties and challenges. Journal of Polymer Science Part B: Polymer Physics 52:791-806

Mármol G, Gauss C, Fangueiro R (2020) Potential of cellulose microfibers for PHA and PLA biopolymers reinforcement. Molecules 25:4653

Masarin F, Paz Cedeno FR, Chavez E, Oliveira L, Gelli V, Monti R (2016) Chemical analysis and biorefinery of red algae Kappaphycus alvarezii for efficient production of glucose from residue of carrageenan extraction process. Biotechnology for Biofuels 9 doi:10.1186/s13068-016-0535-9

Masood F, Aziz M, Haider H, Shakil O, Yasin T, Hameed A (2018) Biodegradation of gamma irradiated poly-3-hydroxybutyrate/sepiolite nanocomposites. International Biodeterioration & Biodegradation 126:1-9

Menczel JD, Judovits L, Prime RB, Bair HE, Reading M, Swier S (2009) Differential scanning calorimetry (DSC). Thermal analysis of polymers: Fundamentals and applications:7-239

Mihhels K, Yousefi N, Blomster J, Solala I, Solhi L, Kontturi E (2023) Assessment of the Alga Cladophora glomerata as a Source for Cellulose Nanocrystals. Biomacromolecules 24:4672-4679 doi:10.1021/acs.biomac.3c00380

Mihranyan A, Piñas A, Karmhag R, Strømme M, Ek R (2004a) Moisture sorption by cellulose powders of varying crystallinity. 269:433-442 doi:10.1016/j.ijpharm.2003.09.030

Mihranyan A, Andersson S-B, Ek R (2004b) Sorption of nicotine to cellulose powders. European Journal of Pharmaceutical Sciences 22:279-286 doi:10.1016/j.ejps.2004.03.012

Mihranyan A (2010) Cellulose from Cladophorales Green Algae : From Environmental Problem to High-Tech Composite Materials. doi:10.1002/app

Mihranyan A (2011) Cellulose from cladophorales green algae: From environmental problem to high-tech composite materials. Journal of Applied Polymer Science 119:2449-2460 doi:10.1002/app.32959

Miri NE, Achaby ME, Fihri A, Larzek M, Zahouily M, Abdelouahdi K, Barakat A, Solhy A (2016) Synergistic effect of cellulose nanocrystals/graphene oxide nanosheets as functional hybrid nanofiller for enhancing properties of PVA nanocomposites. Carbohydrate Polymers 137:239-248 doi:https://doi.org/10.1016/j.carbpol.2015.10.072

Mondragon G, Peña C, González A, Eceiza A, Arbelaiz A (2014) Bionanocomposites based on gelatin matrix and nanocellulose. European Polymer Journal 62 doi:10.1016/j.eurpolymj.2014.11.003

Moon RJ, Martini A, Nairn J, Simonsen J, Youngblood J (2011) Cellulose nanomaterials review: structure, properties and nanocomposites. Chem Soc Rev 40:3941-3994 doi:10.1039/C0CS00108B

Mungmai L, Jiranusornkul S, Peerapornpisal Y, Sirithunyalug B, Leelapornpisid P (2014) Extraction, characterization and biological activities of extracts from freshwater macroalga [Rhizoclonium hieroglyphicum (C. Agardh) Kützing] cultivated in Northern Thailand. Chiang Mai J Sci 41:14-26

Nakamura K, Hatakeyama T, Hatakeyama H (1981) Studies on bound water of cellulose by differential scanning calorimetry. Text Res J 51:607-613

Nam S, French AD, Condon BD, Concha M (2016) Segal crystallinity index revisited by the simulation of X-ray diffraction patterns of cotton cellulose Iβ and cellulose II. Carbohydrate Polymers 135:1-9 doi:https://doi.org/10.1016/j.carbpol.2015.08.035

Nasir M, Hashim R, Sulaiman O, Asim M (2017) Nanocellulose: Preparation methods and applications. In: Cellulose-reinforced nanofibre composites. Elsevier, pp 261-276

National Institute of Water and Atmospheric Research (2019) Quick-guide to common filamentous algae New Zealand fresh waters. National Institute of Water and Atmospheric Research (NIWA),

Nechyporchuk O, Belgacem MN, Bras J (2016) Production of cellulose nanofibrils: A review of recent advances. Industrial Crops and Products 93:2-25 doi:10.1016/j.indcrop.2016.02.016

Netramai S, Kijchavengkul T, Kittipinyovath P (2016) Pulp and Paper Production. In: Reference Module in Food Science. Elsevier,

Neveux N, Yuen A, Jazrawi C, Magnusson M, Haynes B, Masters A, Montoya A, Paul N, Maschmeyer T, de Nys R (2013) Biocrude yield and productivity from the hydrothermal liquefaction of marine and freshwater green macroalgae. Bioresource technology 155C:334-341 doi:10.1016/j.biortech.2013.12.083

Neveux N, Magnusson M, Mata L, Whelan A, de Nys R, Paul NA (2016) The treatment of municipal wastewater by the macroalga Oedogonium sp. and its potential for the production of biocrude. Algal Research 13:284-292 doi:10.1016/j.algal.2015.12.010

Neveux N, Bolton JJ, Bruhn A, Roberts DA, Ras M (2018) The Bioremediation Potential of Seaweeds: Recycling Nitrogen, Phosphorus, and Other Waste Products. In: Blue Biotechnology. pp 217-239. doi:https://doi.org/10.1002/9783527801718.ch7

Neveux N, Nugroho AA, Roberts DA, Vucko MJ, de Nys R (2020) Selecting extraction conditions for the production of liquid biostimulants from the freshwater macroalga Oedogonium intermedium. Journal of Applied Phycology 32:539-551 doi:10.1007/s10811-019-01925-3

Nishiyama Y, Langan P, Chanzy H (2002) Crystal structure and hydrogen-bonding system in cellulose Iβ from synchrotron X-ray and neutron fiber diffraction. Journal of the American Chemical Society 124:9074-9082

Nishiyama Y, Sugiyama J, Chanzy H, Langan P (2003) Crystal structure and hydrogen bonding system in cellulose Iα from synchrotron X-ray and neutron fiber diffraction. Journal of the American Chemical Society 125:14300-14306

Nogi M, Kim C, Sugahara T, Inui T, Takahashi T, Suganuma K (2013) High thermal stability of optical transparency in cellulose nanofiber paper. Applied Physics Letters 102:181911 doi:10.1063/1.4804361

Nutautaitė M, Vilienė V, Racevičiūtė-Stupelienė A, Bliznikas S, Karosienė J, Koreivienė J (2021) Freshwater Cladophora glomerata biomass as promising protein and

other essential nutrients source for high quality and more sustainable feed production. Agriculture 11:582
NZ government Water New Zealand.
Obaidat RM, Tashtoush BM, Bayan MF, Al Bustami RT, Alnaief M (2015) Drying Using Supercritical Fluid Technology as a Potential Method for Preparation of Chitosan Aerogel Microparticles. AAPS PharmSciTech 16:1235-1244 doi:10.1208/s12249-015-0312-2
Oechsle A-L, Lewis L, Hamad WY, Hatzikiriakos SG, MacLachlan MJ (2018) CO2-Switchable Cellulose Nanocrystal Hydrogels. Chemistry of Materials 30:376-385 doi:10.1021/acs.chemmater.7b03939
Oh SY, Yoo DI, Shin Y, Seo G (2005) FTIR analysis of cellulose treated with sodium hydroxide and carbon dioxide. Carbohydrate Research 340:417-428 doi:https://doi.org/10.1016/j.carres.2004.11.027
Okita Y, Saito T, Isogai A (2010) Entire surface oxidation of various cellulose microfibrils by TEMPO-mediated oxidation. Biomacromolecules 6:1696-1700
Onyianta AJ, O'Rourke D, Sun D, Popescu C-M, Dorris M (2020) High aspect ratio cellulose nanofibrils from macroalgae Laminaria hyperborea cellulose extract via a zero-waste low energy process. Cellulose 27:7997-8010 doi:10.1007/s10570-020-03223-5
Pal N, Dubey P, Gopinath P, Pal K (2017) Combined effect of cellulose nanocrystal and reduced graphene oxide into poly-lactic acid matrix nanocomposite as a scaffold and its anti-bacterial activity. International Journal of Biological Macromolecules 95:94-105 doi:https://doi.org/10.1016/j.ijbiomac.2016.11.041
Panaitescu DM, Nicolae CA, Gabor AR, Trusca R (2020) Thermal and mechanical properties of poly(3-hydroxybutyrate) reinforced with cellulose fibers from wood waste. Industrial Crops and Products 145:112071 doi:https://doi.org/10.1016/j.indcrop.2019.112071
Paniz OG, Pereira CMP, Pacheco BS, Wolke SI, Maron GK, Mansilla A, Colepicolo P, Orlandi MO, Osorio AG, Carreño NLV (2020) Cellulosic material obtained from Antarctic algae biomass. Cellulose 27:113-126 doi:10.1007/s10570-019-02794-2
Park S, Baker JO, Himmel ME, Parilla PA, Johnson DK (2010) Cellulose crystallinity index: measurement techniques and their impact on interpreting cellulase performance. Biotechnology for biofuels 3:1-10
Peciulyte A, Karlström K, Larsson PT, Olsson L (2015) Impact of the supramolecular structure of cellulose on the efficiency of enzymatic hydrolysis. Biotechnology for Biofuels 8:56 doi:10.1186/s13068-015-0236-9
Peng Y, Gardner DJ, Han Y (2012) Drying cellulose nanofibrils: in search of a suitable method. Cellulose 19:91-102 doi:10.1007/s10570-011-9630-z
Periyasamy AP, Militky J (2020) Sustainability in regenerated textile fibers. Sustainability in the Textile and Apparel Industries: Sourcing Synthetic and Novel Alternative Raw Materials:63-95
Piotrowski MJ, Graham LE, Graham JM (2020) Temperate-zone cultivation of Oedogonium in municipal wastewater effluent to produce cellulose and oxygen. Journal of Industrial Microbiology and Biotechnology 47:251-262 doi:10.1007/s10295-020-02260-0
Postma PR, Cerezo-Chinarro O, Akkerman RJ, Olivieri G, Wijffels RH, Brandenburg WA, Eppink MHM (2018) Biorefinery of the macroalgae Ulva lactuca: extraction of proteins and carbohydrates by mild disintegration. Journal of Applied Phycology 30:1281-1293 doi:10.1007/s10811-017-1319-8
Pracella M, Haque MM-U, Puglia D (2014) Morphology and properties tuning of PLA/cellulose nanocrystals bio-nanocomposites by means of reactive

functionalization and blending with PVAc. Polymer 55:3720-3728 doi:https://doi.org/10.1016/j.polymer.2014.06.071
Prakash Menon M, Selvakumar R, Suresh kumar P, Ramakrishna S (2017) Extraction and modification of cellulose nanofibers derived from biomass for environmental application. RSC Adv 7:42750-42773 doi:10.1039/C7RA06713E
Prasad V, Alliyankal Vijayakumar A, Jose T, George SC (2024) A Comprehensive Review of Sustainability in Natural-Fiber-Reinforced Polymers. Sustainability 16:1223
Prepas EE, Charette T (2003) 9.08 - Worldwide Eutrophication of Water Bodies: Causes, Concerns, Controls. In: Holland HD, Turekian KK (eds) Treatise on Geochemistry. Pergamon, Oxford, pp 311-331
Quiroz-Castañeda RE, Folch-Mallol JL (2013) Hydrolysis of biomass mediated by cellulases for the production of sugars. Sustainable degradation of lignocellulosic biomass techniques, applications and commercialization InTech:119-155
Quiroz-Castañeda RE (2013) Hydrolysis of Biomass Mediated by Cellulases for the Production of Sugars. In: da Silva JLF-MEDAKCEDSS (ed). IntechOpen, Rijeka, pp Ch.-6
Rajasulochana P, Preethy V (2016) Comparison on efficiency of various techniques in treatment of waste and sewage water – A comprehensive review. Resource-Efficient Technologies 2:175-184 doi:https://doi.org/10.1016/j.reffit.2016.09.004
Ramachandra TV, Hebbale D (2020) Bioethanol from macroalgae: Prospects and challenges. Renew Sust Energ Rev 117:109479 doi:https://doi.org/10.1016/j.rser.2019.109479
Rawlinson C, Kamphuis LG, Gummer JPA, Singh KB, Trengove RD (2015) A rapid method for profiling of volatile and semi-volatile phytohormones using methyl chloroformate derivatisation and GC–MS. Metabolomics 11:1922-1933 doi:10.1007/s11306-015-0837-0
Ray D (2002) New Zealand Municipal Wastewater Monitoring Guidelines.
Ren J-L, Sun R-C (2010) Hemicelluloses. Cereal straw as a resource for sustainable biomaterials and biofuels 1:73-130
Rivera-Briso AL, Serrano-Aroca Á (2018) Poly (3-Hydroxybutyrate-co-3-Hydroxyvalerate): Enhancement strategies for advanced applications. Polymers 10:732
Roesijadi G, Jones SB, Snowden-Swan LJ, Zhu Y (2010) Macroalgae as a biomass feedstock: a preliminary analysis. Pacific Northwest National Lab.(PNNL), Richland, WA (United States),
Rozaklis T, Ramsay S, Whitfield P, Ranieri E, Hopwood J, Meikle P (2002) Determination of Oligosaccharides in Pompe Disease by Electrospray Ionization Tandem Mass Spectrometry. Clinical chemistry 48:131-139 doi:10.1093/clinchem/48.1.131
Sadeghifar H, Filpponen I, Clarke SP, Brougham DF, Argyropoulos DS (2011) Production of cellulose nanocrystals using hydrobromic acid and click reactions on their surface. J Mater Sci 46:7344-7355 doi:10.1007/s10853-011-5696-0
Sainorudin MH, Mohammad M, Kadir NHA, Abdullah NA, Yaakob Z (2018) Characterization of several microcrystalline cellulose (Mcc)-based agricultural wastes via x-ray diffraction method. Solid state phenomena 280:340-345
Saito T, Isogai A (2004) TEMPO-mediated oxidation of native cellulose. The effect of oxidation conditions on chemical and crystal structures of the water-insoluble fractions. Biomacromolecules 5:1983-1989
Saito T, Nishiyama Y, Putaux J-L, Vignon M, Isogai A (2006) Homogeneous suspensions of individualized microfibrils from TEMPO-catalyzed oxidation of native cellulose. Biomacromolecules 7:1687-1691

Saito T, Hirota M, Tamura N, Kimura S, Fukuzumi H, Heux L, Isogai A (2009) Individualization of Nano-Sized Plant Cellulose Fibrils by Direct Surface Carboxylation Using TEMPO Catalyst under Neutral Conditions. Biomacromolecules 10:1992-1996 doi:10.1021/bm900414t

Samiee S, Ahmadzadeh H, Hosseini M, Lyon S (2019) Algae as a source of microcrystalline cellulose. In: Advanced bioprocessing for alternative fuels, biobased chemicals, and bioproducts. Elsevier, pp 331-350

Samyn P, Pappa M, Lama S, Vandamme D (2022) Algae for Nanocellulose Production. In: Bioprospecting Algae for Nanosized Materials. Springer, pp 293-343

Sanchez-Garcia M, Gimenez E, Lagaron J (2008) Morphology and barrier properties of solvent cast composites of thermoplastic biopolymers and purified cellulose fibers. Carbohydrate Polymers 71:235-244

Saxena IM, Brown RM, Jr. (2005) Cellulose biosynthesis: current views and evolving concepts. Annals of botany 96:9-21 doi:10.1093/aob/mci155

Sebeia N, Jabli M, Ghith A, Elghoul Y, Alminderej FM (2019) Production of cellulose from Aegagropila Linnaei macro-algae: Chemical modification, characterization and application for the bio-sorptionof cationic and anionic dyes from water. International journal of biological macromolecules 135:152-162

Seddiqi H, Oliaei E, Honarkar H, Jin J, Geonzon LC, Bacabac RG, Klein-Nulend J (2021) Cellulose and its derivatives: towards biomedical applications. Cellulose 28:1893-1931 doi:10.1007/s10570-020-03674-w

Segal L, Creely JJ, Martin Jr A, Conrad C (1959) An empirical method for estimating the degree of crystallinity of native cellulose using the X-ray diffractometer. Text Res J 29:786-794

Segneanu AE, Orbeci C, Lazau C, Sfirloaga P, Vlazan P, Bandas C, Grozescu I (2013) Waste water treatment methods. Water Treat:53-80

Siddhanta AK, Prasad K, Meena R, Prasad G, Mehta GK, Chhatbar MU, Oza MD, Kumar S, Sanandiya ND (2009) Profiling of cellulose content in Indian seaweed species. Bioresour Technol 100:6669-6673 doi:10.1016/j.biortech.2009.07.047

Siddhanta AK, Chhatbar MU, Mehta GK, Sanandiya ND, Kumar S, Oza MD, Prasad K, Meena R (2011) The cellulose contents of Indian seaweeds. Journal of Applied Phycology 23:919-923 doi:10.1007/s10811-010-9599-2

Siddhanta AK, Kumar S, Mehta GK, Chhatbar MU, Oza MD, Sanandiya ND, Chejara DR, Godiya CB, Kondaveeti S (2013) Cellulose Contents of Some Abundant Indian Seaweed Species. Natural Product Communications 8:1934578X1300800423 doi:10.1177/1934578X1300800423

Siqueira G, Bras J, Dufresne A (2010) Cellulosic Bionanocomposites: A Review of Preparation, Properties and Applications. Polymers 2 doi:10.3390/polym2040728

Somord K, Somord K, Suwantong O, Thanomsilp C, Peijs T, Soykeabkaew N (2018) Self-reinforced poly (lactic acid) nanocomposites with integrated bacterial cellulose and its surface modification. Nanocomposites 4:102-111

Srithep Y, Ellingham T, Peng J, Sabo R, Clemons C, Turng L-S, Pilla S (2013) Melt compounding of poly (3-hydroxybutyrate-co-3-hydroxyvalerate)/nanofibrillated cellulose nanocomposites. Polymer Degradation and Stability 98:1439-1449

Starcher B (2001) A ninhydrin-based assay to quantitate the total protein content of tissue samples. Analytical biochemistry 292:125-129

Stepanova M, Korzhikova-Vlakh E (2022) Modification of cellulose micro-and nanomaterials to improve properties of aliphatic polyesters/cellulose composites: A review. Polymers 14:1477

Stirk WA, Bálint P, Vambe M, Kulkarni MG, van Staden J, Ördög V (2021) Effect of storage on plant biostimulant and bioactive properties of freeze-dried Chlorella vulgaris biomass. Journal of Applied Phycology 33:3797-3806

Sturcová A, His I, Apperley D, Sugiyama J, Jarvis M (2004) Structural Details of Crystalline Cellulose from Higher Plants. Biomacromolecules 5:1333-1339 doi:10.1021/bm034517p

Sucaldito MR, Camacho DH (2017) Characteristics of unique HBr-hydrolyzed cellulose nanocrystals from freshwater green algae (Cladophora rupestris) and its reinforcement in starch-based film. Carbohydrate Polymers 169:315-323 doi:10.1016/j.carbpol.2017.04.031

Sunasee R, Hemraz UD, Ckless K (2016) Cellulose nanocrystals: a versatile nanoplatform for emerging biomedical applications. Expert Opinion on Drug Delivery 13:1243-1256 doi:10.1080/17425247.2016.1182491

Sunesh NP, Suyambulingam I, Divakaran D, Siengchin S (2024) Isolation of microcrystalline cellulose from Valoniopsis pachynema green macroalgae: physicochemical, thermal, morphological, and mechanical characterization for biofilm applications. Waste Biomass Valorization 15:1247-1266

Sunich S (2016) Taupo District Land Treatment Scheme.

Suryanegara L, Yano H Manufacture of Nanocomposites Based On Microfibrillated Cellulose and Polylactic Acid. In: 2014 International Conference on Physics and its Applications (ICOPIA-14), 2014. Atlantis Press, pp 103-109

Sutherland DL, Park J, Heubeck S, Ralph PJ, Craggs RJ (2020) Size matters – Microalgae production and nutrient removal in wastewater treatment high rate algal ponds of three different sizes. Algal Research 45:101734 doi:https://doi.org/10.1016/j.algal.2019.101734

Tanaka R, Saito T, Isogai A (2012) Cellulose nanofibrils prepared from softwood cellulose by TEMPO/NaClO/NaClO2 systems in water at pH 4.8 or 6.8. International Journal of Biological Macromolecules 51:228-234

Tarchevsky IA, Marchenko GN (1991) Morphological Structure of Cellulose. In: Cellulose: Biosynthesis and Structure. Springer Berlin Heidelberg, Berlin, Heidelberg, pp 270-287

Tarchoun AF, Trache D, Klapötke TM, Chelouche S, Derradji M, Bessa W, Mezroua A (2019) A promising energetic polymer from Posidonia oceanica brown algae: synthesis, characterization, and kinetic modeling. Macromolecular Chemistry and Physics 220:1900358

Tebaldi ML, Maia ALC, Poletto F, de Andrade FV, Soares DCF (2019) Poly (-3-hydroxybutyrate-co-3-hydroxyvalerate)(PHBV): Current advances in synthesis methodologies, antitumor applications and biocompatibility. J Drug Delivery Sci Technol 51:115-126

Teboho M, Sefadi J, Sadiku R, John M, Mochane M, Mtibe A (2018) Thermoplastic Processing of PLA/Cellulose Nanomaterials Composites. Polymers 10:1363 doi:10.3390/polym10121363

Ten E, Turtle J, Bahr D, Jiang L, Wolcott M (2010) Thermal and mechanical properties of poly(3-hydroxybutyrate-co-3-hydroxyvalerate)/cellulose nanowhiskers composites. Polymer 51:2652-2660 doi:https://doi.org/10.1016/j.polymer.2010.04.007

Thi Thanh Hop T, Thi Mai D, Duc Cong T, Thi Y. Nhi T, Duc Loi V, Thi Mai Huong N, Trinh Tung N (2022) A comprehensive study on preparation of nanocellulose from bleached wood pulps by TEMPO-mediated oxidation. Results in Chemistry 4:100540 doi:https://doi.org/10.1016/j.rechem.2022.100540

Thomas B, Raj MC, B AK, H RM, Joy J, Moores A, Drisko GL, Sanchez C (2018) Nanocellulose, a Versatile Green Platform: From Biosources to Materials and Their Applications. Chemical Reviews 118:11575-11625 doi:10.1021/acs.chemrev.7b00627

Tomic N, Djekic I, Hofland G, Smigic N, Udovicki B, Rajkovic A (2020) Comparison of Supercritical CO(2)-Drying, Freeze-Drying and Frying on Sensory Properties of Beetroot. Foods (Basel, Switzerland) 9:1201 doi:10.3390/foods9091201

Trache D, Tarchoun AF, Derradji M, Hamidon TS, Masruchin N, Brosse N, Hussin MH (2020) Nanocellulose: From Fundamentals to Advanced Applications. Frontiers in chemistry 8:392-392 doi:10.3389/fchem.2020.00392

Trifol J, van Drongelen M, Clegg F, Plackett D, Szabo P, Daugaard AE (2019) Impact of thermal processing or solvent casting upon crystallization of PLA nanocellulose and/or nanoclay composites. Journal of Applied Polymer Science 136:47486 doi:https://doi.org/10.1002/app.47486

Trivedi N, Baghel RS, Bothwell J, Gupta V, Reddy CRK, Lali AM, Jha B (2016) An integrated process for the extraction of fuel and chemicals from marine macroalgal biomass. Scientific Reports 6:30728 doi:10.1038/srep30728

Ubando AT, Felix CB, Chen W-H (2020) Biorefineries in circular bioeconomy: A comprehensive review. Bioresource Technology 299:122585 doi:https://doi.org/10.1016/j.biortech.2019.122585

US Environmental Protection Agency (2001) Male-specific (F+) and somatic coliphage in water by single agar layer (SAL) procedure. Method

Vadiveloo A, Nwoba EG, Moheimani NR (2019) Viability of combining microalgae and macroalgae cultures for treating anaerobically digested piggery effluent. Journal of Environmental Sciences 82:132-144

Viikari L, Suurnäkki A, Grönqvist S, Raaska L, Ragauskas A (2009) Forest Products: Biotechnology in Pulp and Paper Processing. In: Schaechter M (ed) Encyclopedia of Microbiology (Third Edition). Third Edition edn. Academic Press, Oxford, pp 80-94

Vucko MJ, Cole AJ, Moorhead JA, Pit J, de Nys R (2017) The freshwater macroalga Oedogonium intermedium can meet the nutritional requirements of the herbivorous fish Ancistrus cirrhosus. Algal Research 27:21-31 doi:https://doi.org/10.1016/j.algal.2017.08.020

Wada M, Okano T, Sugiyama J (2001) Allomorphs of native crystalline cellulose I evaluated by two equatoriald-spacings. Journal of Wood Science 47:124-128 doi:10.1007/BF00780560

Wada M, Okano T (2001) Localization of Iα and Iβ phases in algal cellulose revealed by acid treatments. Cellulose 8:183-188 doi:10.1023/A:1013196220602

Wada M, Kondo T, Okano T (2003) Thermally Induced Crystal Transformation from Cellulose Iα to Iβ. Polymer Journal 35:155-159 doi:10.1295/polymj.35.155

Wada M, Chanzy H, Nishiyama Y, Langan P (2004) Cellulose IIII Crystal Structure and Hydrogen Bonding by Synchrotron X-ray and Neutron Fiber Diffraction. Macromolecules 37:8548-8555 doi:10.1021/ma0485585

Wahib SA, Da'na DA, Al-Ghouti MA (2022) Insight into the extraction and characterization of cellulose nanocrystals from date pits. Arabian J Chem 15:103650 doi:https://doi.org/10.1016/j.arabjc.2021.103650

Wahid F, Khan T, Hussain Z, Ullah H (2018) 30 - Nanocomposite scaffolds for tissue engineering; properties, preparation and applications. In: Inamuddin, Asiri AM, Mohammad A (eds) Applications of Nanocomposite Materials in Drug Delivery. Woodhead Publishing Series in Biomaterials. Woodhead Publishing, pp 701-735

Wahlström N, Edlund U, Pavia H, Toth G, Jaworski A, Pell AJ, Choong FX, Shirani H, Nilsson KPR, Richter-Dahlfors A (2020) Cellulose from the green macroalgae Ulva lactuca: isolation, characterization, optotracing, and production of cellulose nanofibrils. Cellulose 27:3707-3725 doi:10.1007/s10570-020-03029-5

Wang J, Gardner DJ, Stark NM, Bousfield DW, Tajvidi M, Cai Z (2018) Moisture and oxygen barrier properties of cellulose nanomaterial-based films. ACS Sustainable Chemistry & Engineering 6:49-70

Warwick C, Guerreiro A, Soares A (2013) Sensing and analysis of soluble phosphates in environmental samples: A review. Biosensors and Bioelectronics 41:1-11 doi:https://doi.org/10.1016/j.bios.2012.07.012

Wiercigroch E, Szafraniec E, Czamara K, Pacia MZ, Majzner K, Kochan K, Kaczor A, Baranska M, Malek K (2017) Raman and infrared spectroscopy of carbohydrates: A review. Spectrochim Acta, Part A 185:317-335 doi:https://doi.org/10.1016/j.saa.2017.05.045

Windeisen E, Wegener G (2012) 10.15 - Lignin as Building Unit for Polymers. In: Matyjaszewski K, Möller M (eds) Polymer Science: A Comprehensive Reference. Elsevier, Amsterdam, pp 255-265

Wu C-N, Saito T, Fujisawa S, Fukuzumi H, Isogai A (2012) Ultrastrong and High Gas-Barrier Nanocellulose/Clay-Layered Composites. Biomacromolecules 13:1927-1932 doi:10.1021/bm300465d

Xiang Z, Gao W, Chen L, Lan W, Zhu JY, Runge T (2016) A comparison of cellulose nanofibrils produced from Cladophora glomerata algae and bleached eucalyptus pulp. Cellulose 23:493-503 doi:10.1007/s10570-015-0840-7

Xie H, Du H, Yang X, Si C (2018) Recent strategies in preparation of cellulose nanocrystals and cellulose nanofibrils derived from raw cellulose materials. Int J Polym Sci 2018

Xie J, Hse C-Y, Cornelis F, Hu T, Qi J, Shupe TF (2016) Isolation and characterization of cellulose nanofibers from bamboo using microwave liquefaction combined with chemical treatment and ultrasonication. Carbohydrate polymers 151:725-734

Xu X, Liu F, Jiang L, Zhu JY, Haagenson D, Wiesenborn D (2013) Cellulose Nanocrystals vs. Cellulose Nanofibrils: A Comparative Study on Their Microstructures and Effects as Polymer Reinforcing Agents. ACS Applied Materials & Interfaces 6 doi:10.1021/am302624t

Xue J, Song F, Yin X-w, Wang X-l, Wang Y-z (2015) Let It Shine: A Transparent and Photoluminescent Foldable Nanocellulose/Quantum Dot Paper. ACS Applied Materials & Interfaces 7:10076-10079 doi:10.1021/acsami.5b02011

Yang Q, Zhao D, Liu Q (2020) Connections between amino acid metabolisms in plants: lysine as an example. Frontiers in Plant Science 11:928

Yildirim N, Shaler S (2017) A Study on Thermal and Nanomechanical Performance of Cellulose Nanomaterials (CNs). Materials (Basel, Switzerland) 10:718 doi:10.3390/ma10070718

Young RA, Kundrot R, Tillman DA (2003) Pulp and Paper. In: Meyers RA (ed) Encyclopedia of Physical Science and Technology (Third Edition). Academic Press, New York, pp 249-265

Yu H-y, Qin Z-y, Zhe Z (2011) Cellulose nanocrystals as green fillers to improve crystallization and hydrophilic property of poly (3-hydroxybutyrate-co-3-hydroxyvalerate). Progress in Natural Science: Materials International 21:478-484

Zanchetta E, Damergi E, Patel B, Borgmeyer T, Pick H, Pulgarin A, Ludwig C (2021) Algal cellulose, production and potential use in plastics: Challenges and opportunities. Algal Research 56:102288 doi:https://doi.org/10.1016/j.algal.2021.102288

Zeng J, Hu F, Cheng Z, Wang B, Chen K (2021) Isolation and rheological characterization of cellulose nanofibrils (CNFs) produced by microfluidic homogenization, ball-milling, grinding and refining. Cellulose 28:3389-3408

Zhang B, Huang C, Zhao H, Wang J, Yin C, Zhang L, Zhao Y (2019) Effects of cellulose nanocrystals and cellulose nanofibers on the structure and properties of polyhydroxybutyrate nanocomposites. Polymers 11:2063

Zhou S, Nyholm L, Strømme M, Wang Z (2019) Cladophora Cellulose: Unique Biopolymer Nanofibrils for Emerging Energy, Environmental, and Life Science Applications. Accounts of Chemical Research 52:2232-2243 doi:10.1021/acs.accounts.9b00215

Zhu Z, Sathitsuksanoh N, Zhang Y-HP (2009) Direct quantitative determination of adsorbed cellulase on lignocellulosic biomass with its application to study cellulase desorption for potential recycling. Analyst 134:2267-2272

Zimmermann M, Borsoi C, Lavoratti A, Zanini M, Zattera A, Santana R (2016) Drying techniques applied to cellulose nanofibers. Journal of Reinforced Plastics and Composites 35 doi:10.1177/0731684415626286

Zollmann M, Robin A, Prabhu M, Polikovsky M, Gillis A, Greiserman S, Golberg A (2019) Green technology in green macroalgal biorefineries. Phycologia 58:516-534 doi:10.1080/00318884.2019.1640516

Zrimec MB, Malta E, Dunbar MB, Cerar A, Reinhardt R, Mihelič R (2022) Wastewater Cultivated Macroalgae as a Bio-resource in Agriculture. Sustainable Global Resources Of Seaweeds Volume 1:435-449

Zugenmaier P (2008) Cellulose. In: Crystalline Cellulose and Derivatives: Characterization and Structures. Springer Berlin Heidelberg, Berlin, Heidelberg, pp 101-174

Appendix

Appendix A : Chapter 2

Biostimulant Analysis:

Enumeration of fRNA bacteriophage and E-coli in treated biomass

Methods:

Enumeration of fRNA bacteriophage was by USEPA-a (2001) Method 1602: Male-specific (F+) coliphage in Water by Single Agar Layer (SAL) procedure. *E.coli* was enumerated using Brilliance *E.coli* / Coliform Selective Medium (OXOID), using a pour-plate method. All samples were tested in triplicate. In brief, to extract any *E. coli* or fRNA bacteriophage from the sample, triplicate 10g sub-samples were weighed into 100ml schott bottles, 100ml of ¼-strength Ringers, (OXOID), solution was added, and the samples were sonicated for one-minute, sonicating probe, SONICS Vibracell. The sample was transferred to centrifuge tubes, centrifuged at 4°C for 10 minutes at 3000rpm. The supernatant was poured / squeezed off into a sterile 250ml schott bottle. The pH was adjusted, as the three samples were between 11.48 to 11.84. These were adjusted to 7.5±0.2. Samples were then analysed using the SAL or pour plating onto Brilliance *E.coli* / Coliform Selective Medium (Oxoid), in triplicate. Positive and negative controls were run as well as a spiked control for fRNA bacteriophage at 10 plaque-forming unit (pfu) per mL.

Results:

*Escherichia col*i and fRNA bacteriophage were not detected in any of the samples subjected to biostimulant production.

Table A 1 : FRNA bacteriophage (PFU/100 mL) test results for treated biomass

	Parameter	Result	Units	Detection limit
Positive control	fRNA bacteriophage according to USEPA method 1602	15	PFU/100mL	<1 PFU per 100 mL
Spiked control	fRNA bacteriophage according to USEPA method 1602	0	PFU/100mL	<1 PFU per 100 mL
Trial 1	fRNA bacteriophage according to USEPA method 1602	0	PFU/100mL	<1 PFU per 100 mL

Trial 2	fRNA bacteriophage according to USEPA method 1602	0	PFU/100mL	<1 PFU per 100 mL
Trail 3	fRNA bacteriophage according to USEPA method 1602	0	PFU/100mL	<1 PFU per 100 mL

USEPA-a (2001) Method 1602: Male-specific (F+) and somatic coliphage in Water by Single Agar Layer (SAL) procedure. Washington, DC: Office of Water USEPA

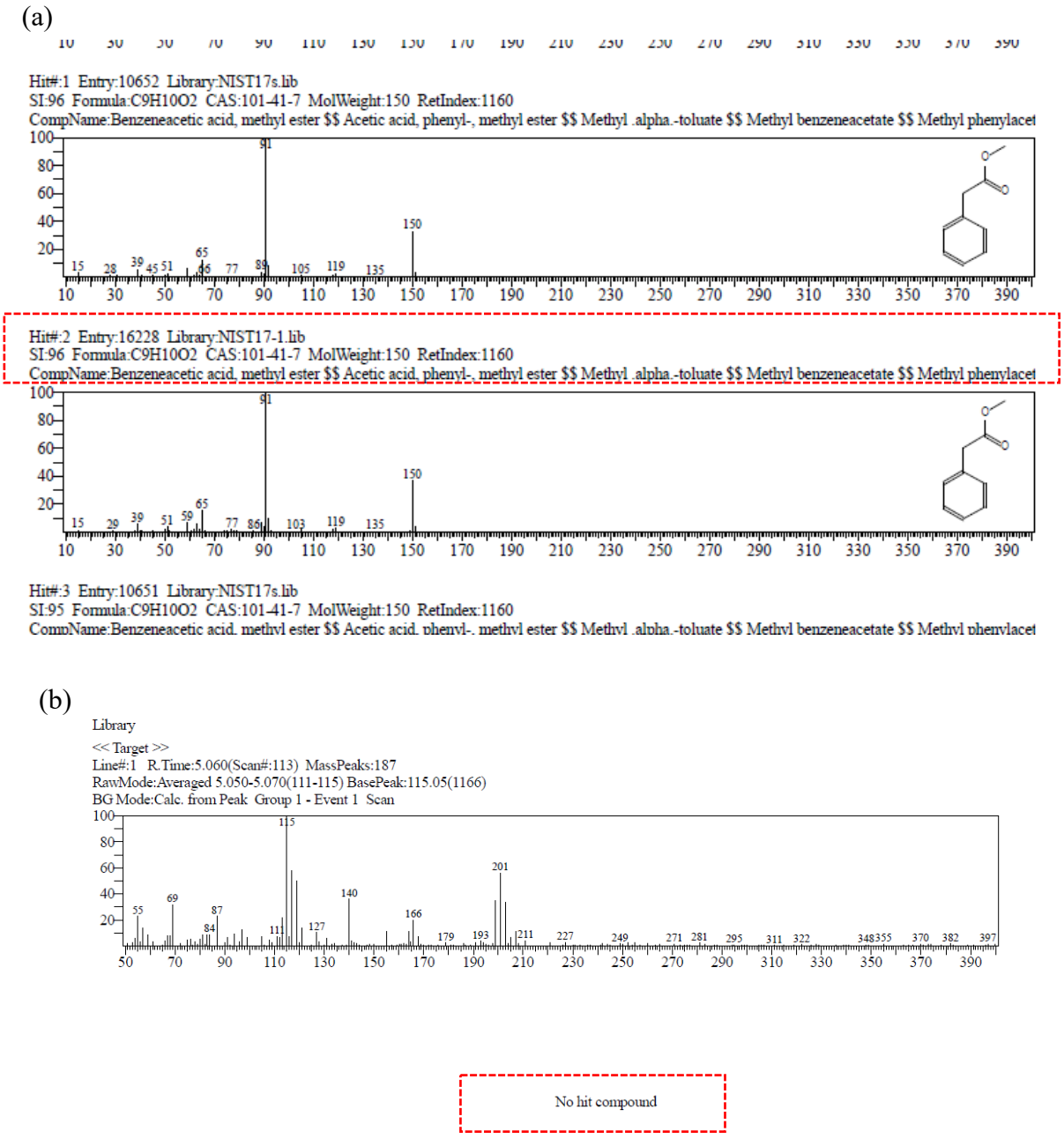

Figure A 1 : Example of NIST Library Mass Spectral Matching Results: (a) Compound Identification Examples with Similarity Indices (b) No-Hit compound

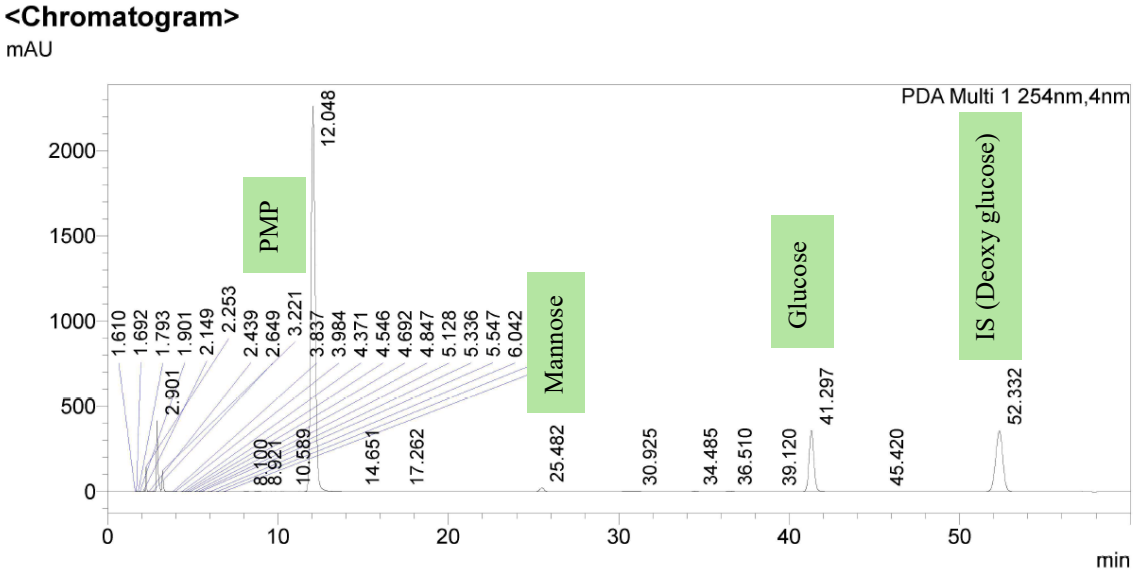

Figure A 2 : Representative HPLC chromatograph of *O.calcareum* cellulose demonstrating peak retention times for mannose, glucose and the internal standard (IS)

Table A 2 : Amino acids, fatty acids and other compounds detected in the biostimulant above 85 similarity index (GC-MS solution NIST 17 library).

Compound name	**Retention time**	**% of total peak area of the identified compounds in the bio stimulant**	**Similarity index**	**Class**
L-Serine	5.71	10.2	88	Amino acid
Benzeneacetic acid	6.34	0.5	91	Auxin
β-Alanine	6.82	0.5	88	Amino acid
L-Valine	7.37	3.1	97	Amino acid
L-Leucine,	8.44	3.8	95	Amino acid
d-Proline	9.09	4.7	89	Amino acid
L-Proline	9.1	4.8	89	Amino acid
Nonanoic acid	9.74	2.1	91	Fatty acid
L-Aspartic acid	9.8	1.0	91	Amino acid
Octanedioic acid	9.87	3.2	94	Fatty acid
Citric acid	10.15	8.2	95	-
Nonanedioic acid/Azelaic acid	11.14	7.0	86	Fatty acid
Ala-Ala	12.14	0.9	87	Peptide
Decanedioic acid/ Sebacic acid	12.32	1.1	87	Fatty acid
L-Phenylalanine	13.1	4.7	90	Amino acid
L-Phenylalanine	13.11	5.7	90	Amino acid
Methyl tetradecanoate	13.24	2.7	92	Fatty acid
l-Alanine	14.13	2.0	88	Amino acid
l-Alanyl-l-leucine	14.23	3.2	85	Amino acid
l-Isoleucylglycine	14.6	1.3	88	Amino acid/peptide sub class
l-Prolylglycine	14.66	0.9	85	Amino acid
l-Alanyl-l-proline	15.02	3.8	87	Peptide
11,14,17-Eicosatrienoic acid	15.11	4.4	89	Fatty acid
9,12,15-Octadecatrienoic	17.1	8.2	89	Fatty acid

acid/Linolenic acid				
12-Octadecenoic acid methyl ester	17.15	4.3	85	Fatty acid
l-Prolylglycine	17.4	2.0	89	Ethyl ester
Phytol $$ 2-Hexadecen-1-ol	17.72	1.8	89	Long chain primary fatty alcohol
Methyl parinarate	19.41	4.2	88	Fatty acid

Table A 3 : Full compositional analysis of the biostimulant

Parameter	Unit	Condition of the biomass	
		Fresh	Freeze-dried
Total dissolved solids	TDS % (w/v)	1.12 ± 0.3	0.98 ± 0.35
	(mg/L) ppm	11243.33	9822.22
Free amino acids (FAA)	µg/mL	15.61	21.97
Protein	µg/mL	44.79	48.03
Carbon	% of dry weight	10.98	11.4
Nitrogen	% of dry weight	1.38	1.48
Sulfur	% of dry weight	0.01	0.01
Ash	% of dry weight	41.95	41.27
Metals (Descending order)	ppm (mg/Kg)		
39 K	ppm	1660.01	1650.1
31 P	ppm	43.63	48.63
34 S	ppm	24.8	27.71
43 Ca	ppm	9.65	6.71
23 Na	ppm	9.26	9.15
44 Ca	ppm	8.51	6.33
24 Mg	ppm	5.57	4.58
56 Fe	ppm	3.02	3.19
205 Tl	ppm	1.82	1.18
75 As	ppm	0.45	0.47
68 Zn	ppm	0.39	0.45
55 Mn	ppm	0.3	0.45
27 Al	ppm	0.25	0.19
111 Cd	ppm	0.25	0.18
63 Cu	ppm	0.1	0.13
66 Zn	ppm	0.1	0.13

59 Co	ppm	0.01	0.02
60 Ni	ppm	0.01	0.01
51 V	ppm	0	0
52 Cr	ppm	0	0
53 Cr	ppm	0	0
78 Se	ppm	0	0.01
82 Se	ppm	0	0
88 Sr	ppm	0	0
137 Ba	ppm	0	0
206 Pb	ppm	0	0
207 Pb	ppm	0	0
208 Pb	ppm	0	0
238 U	ppm	0	0

Table A 4 : Crystallinity Index of cellulose fractions

Treatment	Crystallinity Index %	SD (±)
T1	57.95	0.56
T2	61.06	0.83
T3	60.82	1.32
T4	65.42	0.27
T6	59.97	1.27
T7	60.82	0.08
T8	61.02	1.18
MCC	76.12	-

Table A 5 : Decomposition temperatures and percentage of char remaining at 600 ºC of cellulose over 3 harvests

Treatment	Decomposition temperature (ºC)	Percentages of char at 600 ºC (ºC)
T1	271.0	16.1 ± 1.7
T2	277.2	23.2 ± 2.1
T3	275.5	23.4 ± 2.8
T4	272.3	17.3 ± 1.7
T6	283.8	17.0 ± 3.69
T7	274.7	20.2 ± 0.78
T8	288.3	18.3 ± 2.6

Table A 6 : Results of permutational analyses of variance (PERMANOVAs) testing the effects of biomass condition (fresh or freeze-dried) on % C, N, ash, FAA, protein (Bovine serum albumin) of the biostimulant and the effects of biomass condition, biostimulant extraction and drying process after biostimulant extraction on % cellulose yield, C, H, N, ash, glucose, mannose and crystallinity index by XRD of the cellulose fractions. (Factor/source abbreviations are as follows: Co- Biomass condition (freeze dried/ fresh), Ex- Extraction of biostimulant (yes/no), Dr- Drying process after biostimulant extraction (oven dry/wet))

Parameter	Source	Degree of freedom	Sum of squares	Mean sum of squares	F value by permutation	P(perm)	Unique perms	η2 (%)
C%-biostimulant	Co	1	2.0417	2.0417	1.986	0.2946	10	-
	Res	4	4.1121	1.028				
	Total	5	6.1537					
N % - biostimulant	Co	1	0.10323	0.1032	1.4212	0.2966	10	-
	Res	4	0.29053	0.07263				
	Total	5	0.39376					
A s h % - biostimulant	Co	1	2.9681	2.9681	0.13103	0.6909	10	-
	Res	4	90.609	22.652				
	Total	5	93.577					
FAA%-	Co	1	87.913	87.913	4.9337	0.0056	163	33.03

biostimulant	Res	10	178.19	17.819				
	Total	11	266.1					
Protein %-	Co	1	31.493	31.493	1.0182	0.3368	170	-
biostimulant	Res	10	309.3	30.93				
	Total	11	340.8					
Cellulose yield %	Co	1	0.006309	0.006309	0.26061	0.614	996	-
	Ex	1	2.22E-03	2.22E-03	0.000917	0.973	997	-
	Dr	1	0.0026645	0.0026645	0.11006	0.742	997	-
	CoxEx	1	2.408E-04	2.408E-04	0.0009947	0.976	997	-
	CoxDr	1	0.018723	0.018723	0.77336	0.378	994	-
	ExxDr	1	0.0048	0.0048	0.19827	0.684	996	-
	Res	14	0.33894	0.02421				
	Total	20	0.38121					
C%-cellulose	Co	1	7.0533	7.0533	6.7313	0.0233	9833	25.63
	Ex	1	0.49207	0.49207	0.46961	0.5142	9834	-
	Dr	1	0.35021	0.35021	0.33422	0.5634	9802	-
	CoxEx	1	0.51668	0.51668	0.49308	0.4933	9837	-
	CoxDr	1	0.65801	0.65801	0.62796	0.4431	9838	-
	ExxDr	1	1.1041	1.1041	1.0537	0.3182	9831	-
	Res	14	14.67	1.0478				
	Total	20	27.509					
H%-cellulose	Co	1	0.18253	0.18253	8.4749	0.0113	9742	26.92
	Ex	1	0.022533	0.022533	1.0462	0.3206	9726	-
	Dr	1	0.022533	0.022533	1.0462	0.3316	9744	-
	CoxEx	1	0.025208	0.025208	1.1704	0.2946	9661	-
	CoxDr	1	0.023408	0.023408	1.0868	0.3074	9689	-
	ExxDr	1	0.033075	0.033075	1.5357	0.2295	9722	-
	Res	14	0.30153	0.021538				
	Total	20	0.67783	Total				
N%-cellulose	Co	1	0.17521	0.17521	7.4091	0.0178	9660	31.38
	Ex	1	0.013333	0.013333	0.56383	0.4651	9653	-
	Dr	1	0.072075	0.072075	3.0479	0.1055	9686	-
	CoxEx	1	0.040833	0.040833	1.7267	0.2238	9672	-
	CoxDr	1	0.042008	0.042008	1.7764	0.2053	9685	-
	ExxDr	1	0.1083	0.1083	4.5797	0.0489	9668	-
	Res	14	0.33107	0.023648				
	Total	20	0.55818					
Ash%-	Co	1	0.0070083	0.0070083	1.0951	0.3185	8882	-
cellulose	Ex	1	0.034133	0.034133	5.3333	0.0343	8936	21.76
	Dr	1	0.011408	0.011408	1.7826	0.2012	8863	-

	CoxEx	1	0.044408	0.044408	6.9388	0.0165	8842	28.31
	CoxDr	1	0.038533	0.038533	6.0208	0.0268	8912	24.56
	ExxDr	1	0.014008	0.014008	2.1888	0.1598	8958	-
	Res	14	0.0896	0.0064				
	Total	20	0.15683					
Glucose w/w%-	Co	1	15.187	15.187	1.2114	0.2978	9820	-
cellulose	Ex	1	3.1621	3.1621	0.2522	0.6361	9832	-
	Dr	1	3.876	3.876	0.3091	0.5833	9850	-
	CoxEx	1	2.176	2.176	0.1735	0.684	9839	-
	CoxDr	1	3.7969	3.7969	0.3028	0.5925	9847	-
	ExxDr	1	18.625	18.625	1.4856	0.2398	9835	-
	Res	14	175.52	12.537				
	Total	20	265.28					
Mannose w/w%-	Co	1	0.0004200	0.0004200	0.1487	0.7166	9843	-
cellulose	Ex	1	0.016502	0.0165	5.8416	0.0244	9857	25.04
	Dr	1	0.005376	0.0053	1.9032	0.1925	9812	-
	CoxEx	1	0.001026	0.0010268	0.3636	0.5736	9812	-
	CoxDr	1	0.005808	0.005808	2.056	0.1676	9833	-
	ExxDr	1	0.011285	0.011285	3.9949	0.0603	9839	-
	Res	14	0.039549	0.0028249				
	Total	20	0.065882					
Crystallinity index%-	Co	1	4.2257	4.2257	2.2308	0.1548	9834	-
cellulose	Ex	1	21.174	21.174	11.178	0.0052	9830	18.17
	Dr	1	7.7327	7.7327	4.0821	0.0671	9859	-
	CoxEx	1	3.0517	3.0517	1.611	0.2236	9849	-
	CoxDr	1	14.553	14.553	7.6828	0.0151	9814	12.49
	ExxDr	1	1.9095	1.9095	1.008	0.3297	9824	-
	Res	14	26.52	1.8943				
	Total	20	116.48					

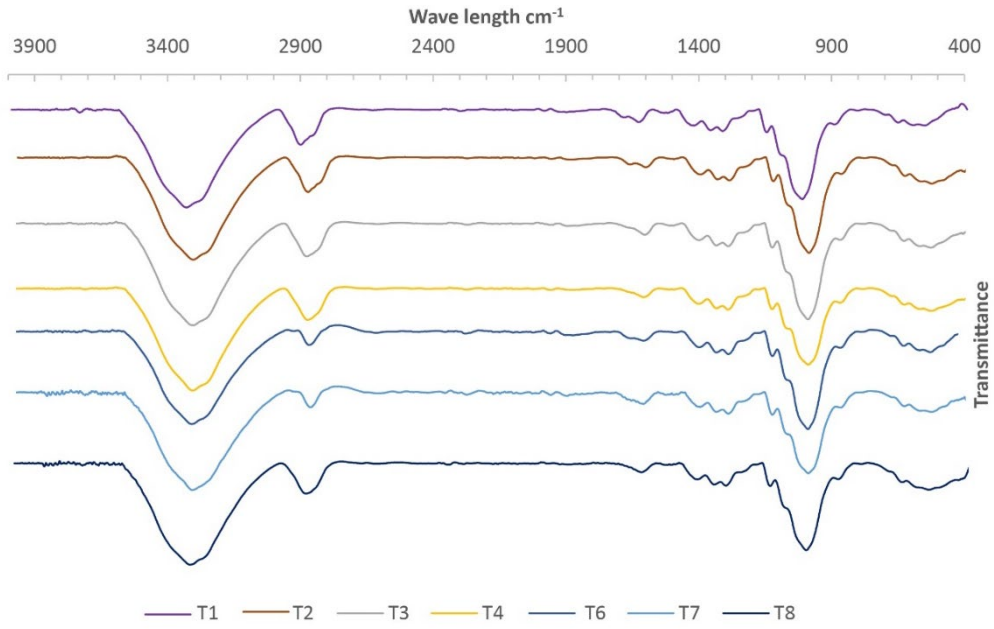

Figure A 3 : Representative FTIR spectra of *O.calcareum* cellulose from 3 harvests

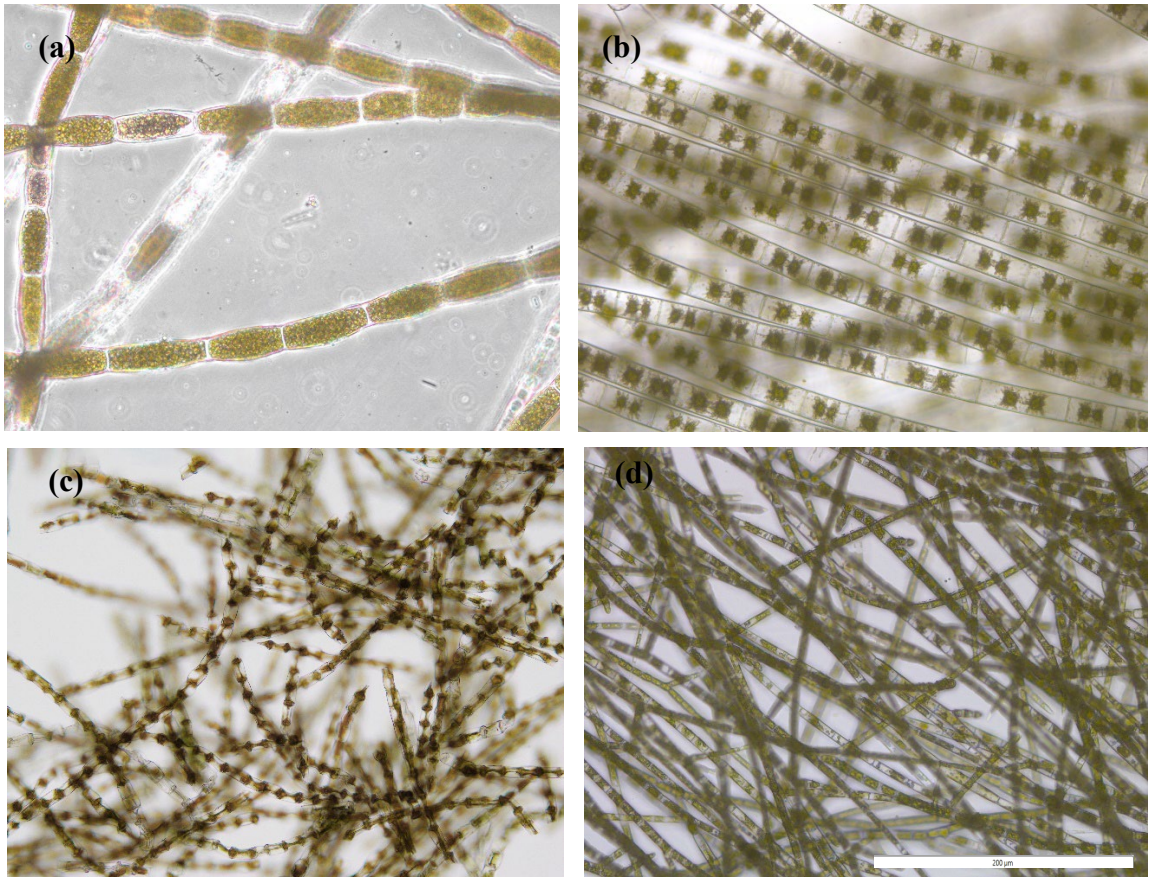

Figure B. 1: Microscopic images (provided by National Institute of Water and Atmospheric Research (NIWA), Hamilton, New Zealand) of filamentous algae used in this study (200 µm scale bar) (a) *Rhizoclonium* (b) *Zygnema* (c) *Oedogonium* (d) *Stigeoclonium*

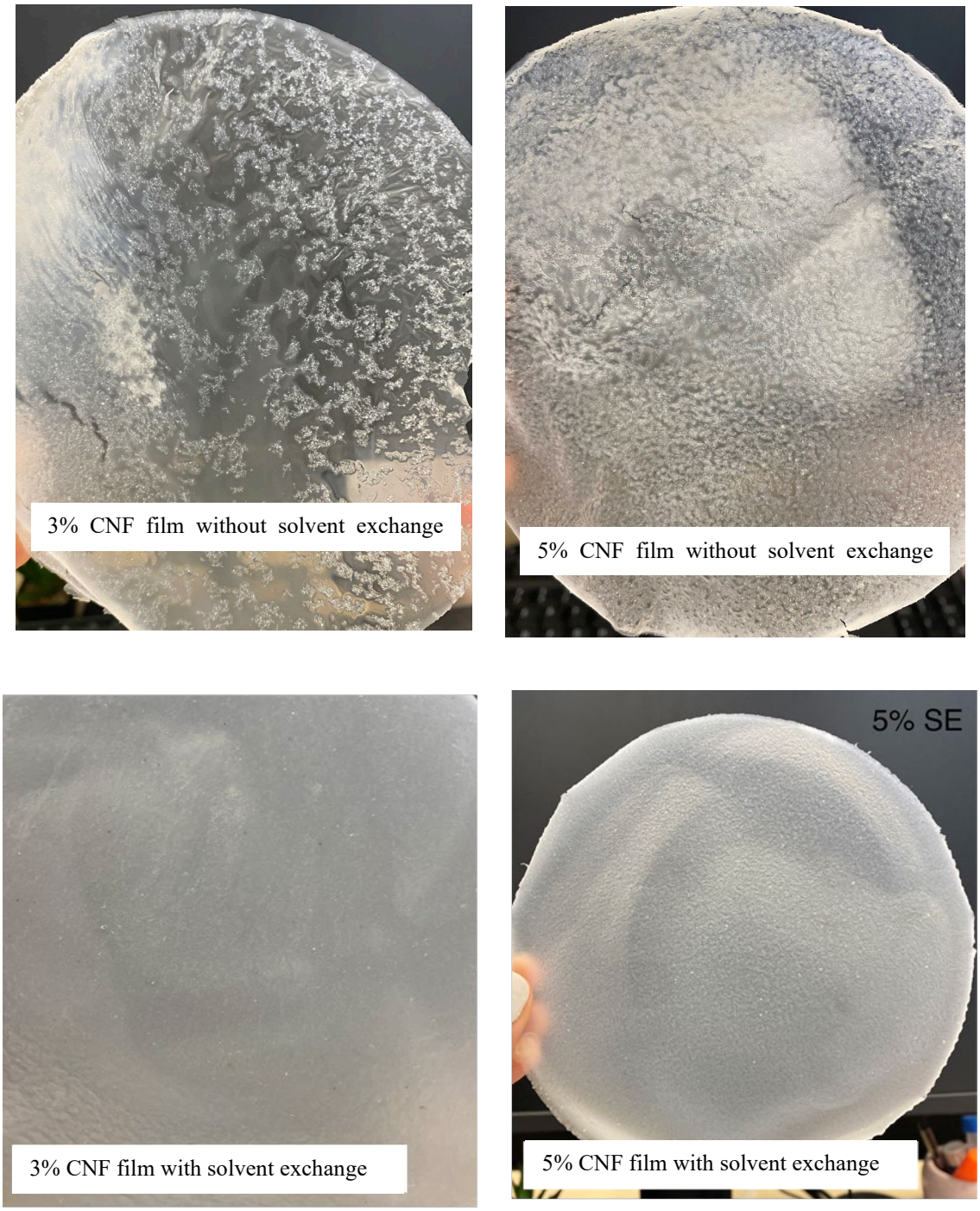

Figure C. 1 PHB films with 3% and 5% addition of CNF with and without following solvent exchange method

Statistical Analysis by Primer7

Pairwise comparison of Young's modulus:

Group factor: Tensile strain
Number of permutations: 9999

Number of groups: 10
Number of samples: 50

DEVIATIONS FROM CENTROID
F: 3.2195 df1: 9 df2: 40
P(perm): 0.0375

Table C. 1 *PAIRWISE COMPARISONS for Young's modulus*

Groups	t	P(perm)
(PHBV neat,CNF 1)	0.14896	0.8718
(PHBV neat,CNF 2)	0.57489	0.8268
(PHBV neat,CNF 3)	2.4132	0.0585
(PHBV neat,CR 1)	2.2031	0.0512
(PHBV neat,CR 2)	0.48008	0.6756
(PHBV neat,CR 3)	0.9089	0.4546
(PHBV neat,TO 1)	0.76581	0.4192
(PHBV neat,TO 2)	0.43167	0.7423
(PHBV neat,TO 3)	1.6342	0.1375
(CNF 1,CNF 2)	0.66212	0.7975
(CNF 1,CNF 3)	2.1753	0.0724
(CNF 1,CR 1)	2.2772	0.0559
(CNF 1,CR 2)	0.3229	0.7944
(CNF 1,CR 3)	0.74441	0.5823
(CNF 1,TO 1)	0.56595	0.6485
(CNF 1,TO 2)	0.55263	0.5972
(CNF 1,TO 3)	1.4303	0.1748
(CNF 2,CNF 3)	1.7768	0.1067
(CNF 2,CR 1)	1.3747	0.3379
(CNF 2,CR 2)	0.86029	0.67
(CNF 2,CR 3)	1.107	0.5459

(CNF 2,TO 1)	1.0013	0.7821
(CNF 2,TO 2)	0.24532	0.8854
(CNF 2,TO 3)	1.4504	0.3126
(CNF 3,CR 1)	3.3633	0.0259
(CNF 3,CR 2)	1.872	0.112
(CNF 3,CR 3)	1.3569	0.3279
(CNF 3,TO 1)	3.0417	0.0254
(CNF 3,TO 2)	2.2887	0.0354
(CNF 3,TO 3)	1.0285	0.3287
(CR 1,CR 2)	2.4685	0.051
(CR 1,CR 3)	2.6959	0.0306
(CR 1,TO 1)	2.6688	0.0459
(CR 1,TO 2)	1.8126	0.0985
(CR 1,TO 3)	3.0529	0.0346
(CR 2,CR 3)	0.43129	0.66
(CR 2,TO 1)	0.17584	0.867
(CR 2,TO 2)	0.83284	0.4273
(CR 2,TO 3)	1.1023	0.318
(CR 3,TO 1)	0.37155	0.7209
(CR 3,TO 2)	1.1849	0.2377
(CR 3,TO 3)	0.60846	0.6039
(TO 1,TO 2)	1.0806	0.3023
(TO 1,TO 3)	1.4075	0.1906
(TO 2,TO 3)	1.7428	0.1037

Table C. 2 *MEANS AND STANDARD ERRORS*

Group	Size	Average	SE
PHBV neat	5	0.24395	0.063804
CNF 1	5	0.2304	0.06485
CNF 2	5	0.33134	0.13796
CNF 3	5	0.084216	0.01762
CR 1	5	0.62002	0.15833
CR 2	5	0.20181	0.060294
CR 3	5	0.16586	0.057536
TO 1	5	0.18997	0.029972
TO 2	5	0.2911	0.08866

TO 3	5	0.12479	0.035299

Sums of squares type: Type III (partial)

Fixed effects sum to zero for mixed terms

Permutation method: Unrestricted permutation of raw data

Number of permutations: 9999

Factors

Name Abbrev. Type Levels

Tensile strain Te Fixed 10

Table C. 3 PERMANOVA table of results of Young's Modulus

Source	df	SS	MS	Pseudo-F	P(perm)	Unique perms
Te	9	5.2119	0.5791	4.2228	0.0007	9941
Res	40	5.4855	0.13714			
Total	49	10.697				

Details of the expected mean squares (EMS) for the model

Source EMS

Te 1*V(Res) + 5*S(Te)

Res 1*V(Res)

Construction of Pseudo-F ratio(s) from mean squares

Source Numerator Denominator Num.df Den.df

Te 1*Te 1*Res 9 40

Estimates of components of variation

Source Estimate Sq.root

S(Te) 0.088393 0.29731

V(Res) 0.13714 0.37032

Tensile stress:

Group factor: Tensile Stress

Number of permutations: 9999

Number of groups: 10

Number of samples: 50

DEVIATIONS FROM CENTROID

F: 9.8681 df1: 9 df2: 40

P(perm): 0.0004

Table C. 4 *PAIRWISE COMPARISONS for Tensile stress*

Groups	t	P(perm)
(PHBV neat,CNF 1)	1.5663	0.1494
(PHBV neat,CNF 2)	1.8675	0.0883
(PHBV neat,CNF 3)	2.292	0.0377
(PHBV neat,CR 1)	4.1776	0.0082
(PHBV neat,CR 2)	2.6431	0.0518
(PHBV neat,CR 3)	0.021817	0.9927
(PHBV neat,TO 1)	0.97895	0.2788
(PHBV neat,TO 2)	0.9363	0.65
(PHBV neat,TO 3)	0.84174	0.5349
(CNF 1,CNF 2)	2.8636	0.0227
(CNF 1,CNF 3)	0.36866	0.7797
(CNF 1,CR 1)	3.5561	0.0256
(CNF 1,CR 2)	0.38265	0.6862
(CNF 1,CR 3)	1.5016	0.1603
(CNF 1,TO 1)	2.3344	0.0459
(CNF 1,TO 2)	0.16217	0.8989
(CNF 1,TO 3)	0.086048	0.8588
(CNF 2,CNF 3)	3.9933	0.0084
(CNF 2,CR 1)	4.565	0.0083
(CNF 2,CR 2)	4.9042	0.008
(CNF 2,CR 3)	1.7194	0.1224
(CNF 2,TO 1)	1.6263	0.2972
(CNF 2,TO 2)	1.7524	0.1102
(CNF 2,TO 3)	1.5044	0.2559
(CNF 3,CR 1)	3.4682	0.0234
(CNF 3,CR 2)	0.021062	0.9521
(CNF 3,CR 3)	2.1794	0.0827
(CNF 3,TO 1)	3.389	0.0157
(CNF 3,TO 2)	0.44906	0.6774
(CNF 3,TO 3)	0.3262	0.7685

(CR 1,CR 2)	3.5117	0.0232
(CR 1,CR 3)	4.1571	0.0088
(CR 1,TO 1)	4.3993	0.0082
(CR 1,TO 2)	3.4686	0.0244
(CR 1,TO 3)	3.3081	0.0225
(CR 2,CR 3)	2.4777	0.0302
(CR 2,TO 1)	4.2073	0.0062
(CR 2,TO 2)	0.45689	0.6242
(CR 2,TO 3)	0.32592	0.7594
(CR 3,TO 1)	0.90796	0.3889
(CR 3,TO 2)	0.90964	0.6395
(CR 3,TO 3)	0.8225	0.7001
(TO 1,TO 2)	1.3788	0.2421
(TO 1,TO 3)	1.1944	0.4197
(TO 2,TO 3)	0.047583	0.9462

Table C. 5 *MEANS AND STANDARD ERRORS*

Group	Size	Average	SE
PHBV neat	5	0.92878	0.24615
CNF 1	5	1.714	0.43668
CNF 2	5	0.41354	0.12461
CNF 3	5	1.9218	0.35654
CR 1	5	7.2245	1.4868
CR 2	5	1.9122	0.27904
CR 3	5	0.93687	0.27769
TO 1	5	0.66993	0.096576
TO 2	5	1.586	0.65733
TO 3	5	1.6353	0.80251

Factors

Name	Abbrev.	Type	Levels
Tensile Stress	Te	Fixed	10

Table C. 6 PERMANOVA table of results of Tensile stress

Source	df	SS	MS	Pseudo-F	P(perm)	Unique perms
Te	9	531.31	59.034	5.5295	0.0001	9934

Res	40	427.05	10.676
Total	49	958.36	

Details of the expected mean squares (EMS) for the model

Source	EMS
Te	1*V(Res) + 5*S(Te)
Res	1*V(Res)

Construction of Pseudo-F ratio(s) from mean squares

Source	Numerator	Denominator	Num.df	Den.df
Te	1*Te	1*Res	9	40

Estimates of components of variation

Source	Estimate	Sq.root
S(Te)	9.6716	3.1099
V(Res)	10.676	3.2674

Elongation at break

Number of groups: 10

Number of samples: 50

DEVIATIONS FROM CENTROID

F: 2.2819 df1: 9 df2: 40

P(perm): 0.1086

Table C. 7 *PAIRWISE COMPARISONS for Elongation at break*

Groups	t	P(perm)
(PHBV neat,CNF 1)	0.60759	0.4991
(PHBV neat,CNF 2)	1.0056	0.3978
(PHBV neat,CNF 3)	1.5879	0.2005
(PHBV neat,CR 1)	0.55019	0.5465
(PHBV neat,CR 2)	1.2265	0.2356
(PHBV neat,CR 3)	1.1994	0.2789
(PHBV neat,TO 1)	1.2468	0.2511
(PHBV neat,TO 2)	0.40624	0.5778
(PHBV neat,TO 3)	0.99058	0.518
(CNF 1,CNF 2)	2.2263	0.0646
(CNF 1,CNF 3)	1.5579	0.166
(CNF 1,CR 1)	0.017583	0.9845
(CNF 1,CR 2)	0.95807	0.4195
(CNF 1,CR 3)	0.92293	0.422
(CNF 1,TO 1)	2.0323	0.0575
(CNF 1,TO 2)	0.9506	0.3802
(CNF 1,TO 3)	0.61763	0.6036
(CNF 2,CNF 3)	3.5142	0.0157
(CNF 2,CR 1)	1.9486	0.0945
(CNF 2,CR 2)	2.8283	0.0481
(CNF 2,CR 3)	2.8505	0.0328
(CNF 2,TO 1)	0.51563	0.6312
(CNF 2,TO 2)	0.362	0.7254
(CNF 2,TO 3)	2.4657	0.1959
(CNF 3,CR 1)	1.323	0.3511
(CNF 3,CR 2)	0.38089	0.6552
(CNF 3,CR 3)	0.4726	0.6845
(CNF 3,TO 1)	2.8859	0.0271

(CNF 3,TO 2)	1.7171	0.1556
(CNF 3,TO 3)	0.65392	0.5899
(CR 1,CR 2)	0.85191	0.5117
(CR 1,CR 3)	0.81364	0.4283
(CR 1,TO 1)	1.9042	0.0984
(CR 1,TO 2)	0.8956	0.3753
(CR 1,TO 3)	0.56067	0.5983
(CR 2,CR 3)	0.066646	0.9903
(CR 2,TO 1)	2.5142	0.0321
(CR 2,TO 2)	1.4392	0.1906
(CR 2,TO 3)	0.26291	0.6501
(CR 3,TO 1)	2.5069	0.0411
(CR 3,TO 2)	1.4165	0.2303
(CR 3,TO 3)	0.20712	0.8568
(TO 1,TO 2)	0.70167	0.4435
(TO 1,TO 3)	2.2828	0.0754
(TO 2,TO 3)	1.2499	0.2163

Table C. 8 *MEANS AND STANDARD ERRORS*

Group	Size	Average	SE
PHBV neat	5	0.1592	0.05422
CNF 1	5	0.1224	0.026992
CNF 2	5	0.2256	0.037685
CNF 3	5	0.0632	0.026748
CR 1	5	0.1232	0.036626
CR 2	5	0.08	0.035071
CR 3	5	0.0832	0.032794
TO 1	5	0.264	0.064234

Factors

Name	Abbrev.	Type	Levels
Elongation at Break/ Tensile strain	El	Fixed	10

Table C. 9 PERMANOVA table of results of Elongation at break

Source	df	SS	MS	Pseudo-F	P(perm)	Unique perms
El	9	2.5319	0.28133	6.995	0.001	983
Res	40	1.6087	0.040218			
Total	49	4.1407				

Details of the expected mean squares (EMS) for the model

El	1*V(Res) + 5*S(El)
Res	1*V(Res)

Construction of Pseudo-F ratio(s) from mean squares

Source	Numerator	Denominator	Num.df	Den.df
El	1*El	1*Res	9	40

Estimates of components of variation

Source	Estimate	Sq.root
S(El)	0.048222	0.21959
V(Res)	0.040218	0.20054

THE UNIVERSITY OF WAIKATO
Te Whare Wānanga o Waikato

Co-Authorship Form

School of Graduate Research
The University of Waikato
Private Bag 3105
Hamilton 3240, New Zealand
Phone +64 7 838 5096
Email: SGR@waikato.ac.nz
Website: http://www.waikato.ac.nz/students/research-degree

This form is to accompany the submission of any PhD that contains research reported in published or unpublished co-authored work. **Please include one copy of this form for each co-authored work.** Completed forms should be included in your appendices for all the copies of your thesis submitted for examination and library deposit (including digital deposit).

Please indicate the chapter/section/pages of this thesis that are extracted from a co-authored work and give the title and publication details or details of submission of the co-authored work.

Chapter 2: Quality of cellulose and biostimulant extracts from Oedogonium calcareum cultivated during primary wastewater treatment. (Pg 53-72)

Nature of contribution by PhD candidate	Project Lead, Data collection, Data analysis, Manuscript preparation, Design and Execution of experiments, visualization/data presentation
Extent of contribution by PhD candidate (%)	70 %

CO-AUTHORS

Name	Nature of Contribution
Prof Christopher Battershill	Manuscript preparation and consultation
Dr Rupert Craggs	Manuscript preparation and consultation
Dr Chanelle Gavin	Manuscript preparation and consultation
Dr Christian Gauss	Manuscript preparation and consultation
A Prof Marie Magnusson	Manuscript preparation and consultation
Dr Christopher Glasson	Manuscript preparation and consultation

Certification by Co-Authors

The undersigned hereby certify that:

- the above statement correctly reflects the nature and extent of the PhD candidate's contribution to this work, and the nature of the contribution of each of the co-authors; and
- that the candidate wrote all or the majority of the text.

Name	Signature	Date
Prof Christopher Battershill		8/8/2024
Dr Rupert Craggs		25/07/2024
Dr Chanelle Gavin		26/07/2024
Dr Christian Gauss		26/07/2024
A Prof Marie Magnusson		08/08/2024
Dr Christopher Glasson		8/08/2024

THE UNIVERSITY OF WAIKATO
Te Whare Wānanga o Waikato

Co-Authorship Form

School of Graduate Research
The University of Waikato
Private Bag 3105
Hamilton 3240, New Zealand
Phone +64 7 838 5096
Email: SGR@waikato.ac.nz
Website: http://www.waikato.ac.nz/students/research-degree

This form is to accompany the submission of any PhD that contains research reported in published or unpublished co-authored work. **Please include one copy of this form for each co-authored work.** Completed forms should be included in your appendices for all the copies of your thesis submitted for examination and library deposit (including digital deposit).

Please indicate the chapter/section/pages of this thesis that are extracted from a co-authored work and give the title and publication details or details of submission of the co-authored work.

Chapter 3: Extraction and characterization of cellulose from four selected freshwater macroalgae species grown in a phycoremediation process. (Pg 73-92)

Nature of contribution by PhD candidate	Project Lead, Data collection, Data analysis, Manuscript preparation, Design and Execution of experiments, visualization/data presentation
Extent of contribution by PhD candidate (%)	70 %

CO-AUTHORS

Name	Nature of Contribution
Prof Christopher Battershill	Manuscript preparation and Consulation
Dr Rupert Craggs	Manuscript preparation and Consulation
Dr Chanelle Gavin	Manuscript preparation and Consulation
Dr Christian Gauss	Manuscript preparation and Consulation
A Prof Marie Magnusson	Manuscript preparation and Consulation
Dr Christopher Glasson	Manuscript preparation and Consulation

Certification by Co-Authors

The undersigned hereby certify that:

- the above statement correctly reflects the nature and extent of the PhD candidate's contribution to this work, and the nature of the contribution of each of the co-authors; and
- that the candidate wrote all or the majority of the text.

Name	Signature	Date
Prof Christopher Battershill		8/8/2024
Dr Rupert Craggs		25/07/2024
Dr Chanelle Gavin		26/07/2024
Dr Christian Gauss		26/07/2024
A Prof Marie Magnusson		08/08/2024
Dr Christopher Glasson		8/08/2024

THE UNIVERSITY OF WAIKATO
Te Whare Wānanga o Waikato

Co-Authorship Form

School of Graduate Research
The University of Waikato
Private Bag 3105
Hamilton 3240, New Zealand
Phone +64 7 838 5096
Email: SGR@waikato.ac.nz
Website: http://www.waikato.ac.nz/students/research-degree

This form is to accompany the submission of any PhD that contains research reported in published or unpublished co-authored work. **Please include one copy of this form for each co-authored work.** Completed forms should be included in your appendices for all the copies of your thesis submitted for examination and library deposit (including digital deposit).

Please indicate the chapter/section/pages of this thesis that are extracted from a co-authored work and give the title and publication details or details of submission of the co-authored work.

Chapter 4. Preparation and Characterization of Poly(3-hydroxybutyrate-co-3-hydroxyvalerate) PHBV composite films with Cellulose Nanofibers from Freshwater Green Algae (Cladophora sp and Rhizoclonium sp) grown in primary effluent. (Pg 93-129)

Nature of contribution by PhD candidate	Project Lead. Research design. Data collection. Data analysis. Manuscript preparation. Design and Execution of experiments. visualization/data presentation
Extent of contribution by PhD candidate (%)	75%

CO-AUTHORS

Name	Nature of Contribution
Prof Christopher Battershill	Manuscript preparation and Consulation
Dr Rupert Craggs	Manuscript preparation and Consulation
Dr Chanelle Gavin	Manuscript preparation and Consulation
Dr Christian Gauss	Manuscript preparation and Consulation
Dr Christopher Glasson	Consultation

Certification by Co-Authors

The undersigned hereby certify that:

- the above statement correctly reflects the nature and extent of the PhD candidate's contribution to this work, and the nature of the contribution of each of the co-authors; and
- that the candidate wrote all or the majority of the text.

Name	Signature	Date
Prof Christopher Battershill		31/7/2024
Dr Rupert Craggs		25/07/2024
Dr Chanelle Gavin		26/07/2024
Dr Christian Gauss		26/07/2024
Dr Christopher Glasson		8/08/2024